2016

PPAP2B EXPRESSION LIMITS LESION FORMATION IN MURINE MODELS OF ATHEROSCLEROSIS

Paul A. Mueller
University of Kentucky, muellerp@ohsu.edu
Digital Object Identifier: http://dx.doi.org/10.13023/ETD.2016.299

STUDENT AGREEMENT:

I represent that my thesis or dissertation and abstract are my original work. Proper attribution has been given to all outside sources. I understand that I am solely responsible for obtaining any needed copyright permissions. I have obtained needed written permission statement(s) from the owner(s) of each third-party copyrighted matter to be included in my work, allowing electronic distribution (if such use is not permitted by the fair use doctrine) which will be submitted to UKnowledge as Additional File.

I hereby grant to The University of Kentucky and its agents the irrevocable, non-exclusive, and royalty-free license to archive and make accessible my work in whole or in part in all forms of media, now or hereafter known. I agree that the document mentioned above may be made available immediately for worldwide access unless an embargo applies.

I retain all other ownership rights to the copyright of my work. I also retain the right to use in future works (such as articles or books) all or part of my work. I understand that I am free to register the copyright to my work.

REVIEW, APPROVAL AND ACCEPTANCE

The document mentioned above has been reviewed and accepted by the student's advisor, on behalf of the advisory committee, and by the Director of Graduate Studies (DGS), on behalf of the program; we verify that this is the final, approved version of the student's thesis including all changes required by the advisory committee. The undersigned agree to abide by the statements above.

Paul A. Mueller, Student

Dr. Susan Smyth, Major Professor

Dr. Bret Smith, Director of Graduate Studies

PPAP2B EXPRESSION LIMITS LESION FORMATION IN MURINE MODELS OF ATHEROSCLEROSIS

DISSERTATION

A dissertation submitted in partial fulfillment of the
requirements for the degree of Doctor of Philosophy in the
College of Medicine
at the University of Kentucky

By
Paul Anthony Mueller

Lexington, Kentucky

Co-Directors: Dr. Susan Smyth, Professor of Internal Medicine
And: Dr. Steve Estus, Professor of Physiology

Lexington, Kentucky

2016

ABSTRACT OF DISSERTATION

PPAP2B EXPRESSION LIMITS THE DEVELOPMENT OF LESION FORMATION IN MURINE MODELS OF ATHEROSCLEROSIS

Coronary artery disease (CAD) is the leading cause of death in both men and women worldwide and is defined as a narrowing of the coronary arteries due to accumulation of atherosclerotic plaques. Genome-wide association studies have identified risk loci within the gene *PPAP2B* that confers increased risk of developing CAD. Evidence suggests these aforementioned SNPs are regulating *PPAP2B* expression in a *cis*-manner through the interruption of transcription factor binding sites. PPAP2B encodes the lipid phosphate phosphatase 3 enzyme that plays a key role in degrading bioactive lysophosphatidic acid (LPA). LPA has a plethora of effects on vascular tissue and is implicated in increasing inflammation and exacerbating the development of atherosclerotic lesions in mice. Interestingly, PPAP2B expression is increased in murine models of atherosclerosis and both global and smooth muscle cell-specific deletion increases the development of lesions compared to control mice. LPP3-deficient mice with increased atherosclerosis show significant increases in LPA accumulation in their proximal aorta as well as increased expression of inflammatory markers and positive staining for leukocyte marker CD68. Globally deficient mice also show substantial increases in ICAM-1 staining in their aortic root lesions relative to controls. Preliminary evidence also suggests that total LPA content, and specifically unsaturated LPA species, increase in the atherogenic LDL-C fractions of plasma in hyperlipidemic mice prone to developing atherosclerosis. Taken together, these data suggest that as CAD develops, LPA accumulates in atherosclerotic plaques, and the intrinsic mechanism of defense is to upregulate LPP3 through transcription factor-mediated effects on PPAP2B; however, individuals harboring the previously mentioned risk alleles are unable to increase PPAP2B expression and thus experience unchecked inflammation and exacerbated development of atherosclerosis.

KEYWORDS: Lipid phosphate phosphatase 3 (LPP3), Lysophosphatidic acid (LPA), genome-wide association studies (GWAS), inflammation, low density lipoproteins (LDL-C), coronary artery disease (CAD)

Paul A. Mueller

Student Signature

May 1, 2016

Date

PPAP2B EXPRESSION LIMITS LESION FORMATION IN MURINE MODELS OF ATHEROSCLEROSIS

By

Paul Anthony Mueller

Susan S. Smyth
Co-Director of Dissertation

Steve Estus
Co-Director of Dissertation

Bret Smith
Director of Graduate Studies

May 1, 2016
Date

ACKNOWLEDGEMENTS

First and foremost I would like to thank my mentor Dr. Susan Smyth for her guidance and support over the course of my studies at the University of Kentucky. Her mentorship has been integral to my development as an independent scientist. Dr. Smyth's patience and her passion for both quality and impactful research exemplify the role of a physician-scientist and I consider myself extremely fortunate for the opportunity to have her as my doctoral advisor all these years. I would also like to extend my gratitude to Dr. Andrew Morris who has provided his expertise, guidance and bravado throughout the years as well.

Additionally, I would like to thank my Dissertation Committee members, Dr. Alan Daugherty, Dr. Steve Estus, and Dr. Stefan Stamm for their advice and intellectual guidance on my thesis project over the last several years. I also want to thank Dr. Elizabeth Debski for agreeing to be my outside examiner.

I thank my teaching mentor and friend, Dr. Dexter Speck, for giving me so much of his time and expertise in my training. I truly enjoyed my training and practice in teaching physiology and, aside from my research, consider it a true passion in my life.

My development as a scientist was not attributed to my mentors and committee members alone and so I extend my thanks to all of the Smyth and Morris lab members, both past and present, for their patience and support over the years. I wish to extend my gratitude to members of the Cardiovascular Research Department including the Daugherty lab and the Temel lab for their help and training that was essential in the development of my thesis.

I thank all of the friends I have made throughout my time at the University of Kentucky, both in and out of research, for providing me with countless laughs and keeping me both humble and grounded.

Lastly, I would like to thank my family for their support, encouragement, and unending curiosity as to when I would finish my graduate education at the University of Kentucky. To my father Steve, my mother Debbie, and my brothers Bryan and Andy for always providing me with love and laughter.

Table of Contents

List of Figures

List of Tables

Chapter 1: Introduction

Since 1921 cardiovascular disease (CVD) is the leading cause of death of both men and women worldwide. From 2003 to 2013 death rates attributable to CVD declined 28.8% with the actual number of deaths per year dropping 11.7% in the United States[1]. These declines in death rates and total death toll are a display of progress, but it is important to note that in 2013 30.8% of all 2,596,993 deaths in the United States are still attributed to CVD [2]. Needless to say, in spite of declining rates of disease, CVD remains a significant burden on the United States and accounts for an estimated $316.6 billion burden annually [2]. With an estimated 15.5 million Americans over the age of 20 that suffer from CAD [3] there has been a focus on understanding not only the vascular pathophysiology, but also the factors that predispose an individual to an increased risk of disease. Bioactive lipids have taken a spotlight in the regulation and modulation of vascular pathophysiology. This chapter will discuss one such bioactive lipid, Lysophosphatidic acid (LPA), and its role in regulating vascular pathology. LPA, and its regulators autotaxin (ATX) and lipid phosphate phosphatase 3 (LPP3), play integral roles in components of vascular physiology and pathophysiology that are key steps in the development and progression of CAD. This chapter will discuss in detail the burden and specific mechanisms of CAD pathology and break down tissue-specific contributions to disease progression. Identifying risk factors contributing to CAD is essential to its prevention and treatment; as such, advances in genome-wide sequencing to identify genomic loci conferring risk of disease has become a rapidly developing field. Genome-wide association studies (GWAS) will be described in addition to a specific locus in the gene *PPAP2B* which confers increased risk of disease [4]. *PPAP2B* encodes the LPA-degrading protein LPP3 which has been implicated in both embryonic development and vascular disease. LPP3 structure and function will also be

described in detail. The aim herein is to illustrate a role for LPA and its regulators in the pathophysiology of CAD.

Lysophosphatidic Acid[1]

LPA is a bioactive lysophospholipid composed of a phosphate molecule bound to a glycerol backbone, which bears a variable length fatty acid chain (Figure 1.1). LPA is found in all eukaryotic tissues in low concentrations and its activity is dependent on its binding to one of six known extracellular G protein-coupled receptors (GPCRs) termed LPA receptor 1 – 6 (LPA1 – LPA6) which are differentially expressed throughout various tissues and cells [5-9]. Any given LPA receptor is capable of activating at least 2 of the 4 known g-protein complexes eliciting a variety of cell responses ranging from cytoskeletal rearrangement, migration, proliferation, survival and mild platelet activation [10-15]. In fact, the lysophospholipid was first identified in 1963 as a regulator of blood pressure mediating effects through smooth muscle cell function [16, 17]. LPA can be generated via two pathways: 1) lysophospholipase D activity of ATX hydrolysis of lysophosphotidylcholine and 2) phospholipase A2-mediated deacylation of phosphatidic acid leads to LPA production [18]. Pathways for production will be described in section “LPA Biosynthesis”. Degradation of LPA can occur through the actions of a family of membrane-bound proteins termed lipid phosphate phosphatases (LPPs), which are discussed in more detail in section “*PPAP2B* Encodes Lipid Phosphate Phosphatase 3”.

[1] *Portions of this section were taken from Mueller et al. [15]. Some additions and modifications to the text and figures have been made for clarity of information.*

LPA Receptor Signaling

The receptors for LPA are widely distributed on blood and vascular cells. In preclinical animal models, targeting the LPA receptors genetically and pharmacologically suggest that they may contribute to vascular injury and inflammatory responses, as well as endothelial barrier function and vascular stability. Single and multiple deletions of LPA receptors in mice produce differing vascular phenotypes. Deficiency of *Lpar1*, which results in 50% neonatal lethality, gives rise to the development of spontaneous frontal lobe hematomas [19]. This suggests a role for LPA1 in stabilization of vessels, as no defect in hemostasis has been observed in these animals. In experimental arterial injury models, LPA1 regulates the development of intimal hyperplasia, a complex response involving inflammation and smooth muscle cell proliferation and migration. LPA1 may influence the vascular remodeling response via the Gα12/Gα13 pathway that couples to RhoGEF to activate RhoA, given the similarities in development on intimal hyperplasia after injury in the *Lpar1*$^{-/-}$ mice [10] and those lacking the Gα12/Gα13 and Rho pathways [20] in smooth muscle cells. The lack of LPA1 disrupts the endothelial barrier and results in increased vascular permeability in response to inflammatory stimuli in the lung [21] and the skin [22]. Conversely, LPA1 antagonists prevent inflammation in response to peritoneal injection of lipopolysaccharide [23]. Whether either a defect in smooth muscle or endothelial cell function accounts for the bleeding observed in the *Lpar1*$^{-/-}$ mice remains unknown. Knockout of both *Lpa1* and *Lpa2* increases the incidence of prefrontal hematomas [24], impairs the response to vascular injury [10], and results in the development of pulmonary hypertension with age [25]; the latter phenotype is not observed in mice with deficiency of either of the receptors alone. Together, these results suggest some redundancy or overlap between the 2 receptor systems. Likewise, LPA1 and LPA3 antagonists, Ki16425, reduce arterial remodeling elicited by denudation injury [11] in mice, perhaps due to attenuated signaling through both Gα12/Gα13 and Gq/G11 signaling pathways, which appear to

regulate vascular remodeling antagonistically. *Lpar4*-deficient mice display a genetic background-dependent defect in formation of vasculature. On the C57Bl/6 background, the mice develop hemorrhage and edema due to a maturation defect from lack of smooth muscle cell and pericyte recruitment to vessels [26]. Additionally, LPA signaling through RAGE may also affect SMC function [27]. As described in more detail below, studies in zebrafish also support a role for several of the canonical LPA receptors in blood vessel formation

LPA Biosynthesis

LPA is present in many biologic fluids, including plasma, ascites, and bronchoalveolar lavage fluid. In the circulation, LPA turns over rapidly [28] and therefore must be maintained by constant production. Certain conditions, such as acute coronary syndromes [29, 30] and chronic liver disease [31] are associated with higher levels of plasma LPA. Whether this is due to increased production or reduced clearance or both is currently not known. As mentioned before there are several pathways that can generate LPA. The secreted lysophospholipase D ATX generates extracellular LPA by hydrolysis of lysophosphatidylcholine (LPC) [32-34]. ATX is an ecto-nucleotide pyrophosphatase/phospho-diesterase family member (encoded by *ENPP2* in humans and *Enpp2* in mice) that is synthesized as a pre-proenzyme and undergoes sequential signal peptide removal and proprotein convertase cleavage before being secreted from cells. Of five functional isoforms (ATXα, ATXβ, ATXγ, ATXδ, and ATXε) generated through alternative splicing, ATXβ is the most abundant and appears to account for most of the lysophospholipase D activity in plasma. The cellular source(s) of plasma ATX are incompletely understood, however, adipocytes likely secrete a substantial portion [35]. ATX is also stored in platelets and released during their activation [34, 36]. Circulating ATX is rapidly taken up by scavenger receptors of liver sinusoidal endothelial cells, the

same class of receptors capable of clearing formylated and maleyted BSA, and then degraded in the liver [37]. Thus, much like hormones, including insulin, ATX is largely removed from the circulation during first passage through the liver. While ATX is normally a major source of plasma LPA levels [28, 38], other minor pathways may contribute to increases in LPA in certain situations, such as in the setting of acute myocardial infarction [29, 30, 39].

Autotaxin's Role in Vascular Development

Studies of organisms that lack or express catalytically-inactive ATX have shed light on its role, and by inference, the role of LPA signaling, in vascular biology. ATX expression is required for normal vascular development in mice. *Enpp2*-deficient mice [40, 41] die between embryonic days 9.5–10.5 with blood vessel formation defects in the yolk sac and embryo. In the absence of ATX, initial blood vessel formation appears normal, but vessels fail to mature, suggesting that ATX is critical for extension and stabilization of blood vessels but perhaps not for the initial endothelial cell differentiation and migration. The phenotype of *Enpp2*$^{-/-}$ mice resembles that observed in Gα13 knockout embryos, which would be consistent with ATX-generated LPA signaling through Gα13-coupled receptors. To date, no single or multiple LPA receptor knock-out mice have fully recapitulated the phenotype observed in embryos lacking ATX or Gα13. However, mice expressing a functionally inactive ATX (T210A) also die embryonically [42], indicating that the catalytic activity of ATX, and likely LPA synthesis, is essential for vascular development. *Enpp2*-heterozygous mice are viable and express half of normal levels of ATX and LPA. However, they are hyper-responsive to hypoxia-induced vasoconstriction and remodeling, and prone to develop pulmonary hypertension [25]. Knockdown of ATX in zebrafish embryos by morpholino antisense oligonucleotides also causes aberrant vascular connections with normal initial sprouting; interestingly, while knockdown of each single LPA receptor by

morpholino antisense oligonucleotides show little phenotype, attenuating LPA1 and LPA4 signaling recapitulated the ATX knockdown vascular defects [43].

As described above, ATX and LPA-signaling contributes to the development of embryonic vasculature in multiple species and LPA-receptor signaling affects vEC- and SMC-function in mature mice. LPA is also implicated in the development and progression of CAD. Levels of vessel-associated LPA increase during progression of atherosclerosis [44, 45] and are substantially higher in advanced lesions [46]. Cholesterol feeding influences levels and distribution of plasma LPA in rabbits [47]. Additionally, feeding mice a chow diet supplemented with unsaturated LPA mimics the inflammatory effects of Western diets [48]. LPA that is generated during atherosclerosis may have pro-atherosclerotic, pro-inflammatory, and pro-thrombotic effects [4].

Cardiovascular Disease Burden[2]

Coronary artery disease (CAD) is due to a narrowing of the heart's blood vessels (stenosis) on account of the buildup of atherosclerotic plaques. Based on data from the National Health and Nutrition Examination Survey (NHANES), in 2013, CAD accounted for 1 out of every 7 deaths. Each year roughly 660,000 Americans suffer from a new myocardial infarction (MI), better known as a heart attack, and 305,000 have a recurrent attack. It is estimated that 15.5 million Americans over the age of 20 suffer from this disease with a prevalence of 7.6% and 5.0% of adult men and women respectively. The high prevalence of this disease is coupled with a high mortality rate that makes this

[2] Data presented in this section are from the AHA's annual publication on Heart Disease and Stroke Statistics [2].

disease such an impactful epidemic throughout the world. In fact, 34% of individuals who experience a coronary event -- defined as a MI, ischemic heart failure, or unstable angina -- will die of it. Data from large trials including the Framingham Heart Study, Atherosclerosis Risk in Communities Study, and several others indicate that within 1 year following a first MI 18% of men and 23% of women over the age of 45 will die. Within 5 years those numbers increase to 36% in men and 47% in women. These high rates of prevalence and subsequent consequences in mortality associated with CAD make it imperative that efforts in medical research are dedicated to understanding, predicting and treating not just CAD but CVD as a whole.

Risk Factors of Cardiovascular Disease

Framingham Heart Study Defines Classic Risk Factors

Classical risk factors for the development of CVD were first discovered through the Framingham Heart Study in 1948. These classical risk factors include both modifiable lifestyle behaviors and non-modifiable risk factors. Modifiable risk factors include dyslipidemia, hypertension, physical inactivity, type 2 diabetes, alcohol consumption and smoking [49, 50] whereas some of the non-modifiable risk factors include a family history of disease as well as aging itself. It is worth mentioning that in the United States there has been a significant decline in the incidence of modifiable risk factors such as smoking in adults which is currently at 16.9% (down from 24.1% in 1998) as well as certain aspects of nutritional quality, specifically the prevalence of ideal levels of diet which increased from 0.7% to 1.5% in adults from 2004 to 2012 [3]. This is good news, but smoking is still attributed to at least one third of all CAD related deaths and poor nutrition was the leading risk factor in 2010 for death and disability with 678,000 annual deaths attributable to all

causes [3]. Unfortunately, the prevalence of other modifiable risk factors has increased such as the death rate attributable to hypertension which increased 8.2% from 2003 to 2013 and the prevalence of type 2 diabetes in children and adolescents has increased 30.5% from 2001 to 2009 [3]. Lastly, based on data from 2009 and 2012, greater than 100 million adults in the United States over 20 years of age have total cholesterol over 200 mg/dL; and roughly 31 million have total cholesterol levels over 240 mg/dL [3].

Cardiovascular Disease Pathogenesis

Classifying the Progression of CAD

CVD is representative of several subcategories of disease such as CAD or ischemic heart disease, stroke, peripheral artery disease, heart failure and others. This section will focus on the pathogenesis of CAD which is the more deadly and the more costly subcategory of CVD. In 1994 and 1995, Herbert Stary led the AHA's Committee on Vascular Lesion along with the Council on Ateriosclerosis and created a histology based scoring system to define atherosclerotic plaque progression which has become known as the Stary scoring system [51, 52].

Naïve healthy arteries consist of a tunica intima layer composed of a single endothelial cell layer separating the lumen of the blood vessel from an underlying subendothelial matrix and a layer of internal elastic lamina. The tunica media surrounds the tunica intima and consists of layers of vascular smooth muscle cells and internal elastic lamina that act in consortium to both resist the stretch from the blood pressure as well as regulate vessel diameter. The outermost layer is the tunica adventitia which is primarily connective tissue and supportive structures such as blood vessels, known as the vasa vasorum, and nerves.

Type I plaques begin to develop during the first decade of life and are characterized by the deposition of low density lipoprotein cholesterol (LDL-C), which becomes oxidized over time, and an accumulation of foam cells in the subintimal space of coronary arteries [52]. Foam cells are lipid laden macrophage-like cells that develop as circulating monocytes, infiltrate the intimal layer through activated vascular endothelial cells (vECs), differentiate into macrophages and endocytose oxidized LDL-C (oxLDL) particles. A key step in type I plaque progression is the activation of vECs which tends to occur primarily in areas of turbulent or disturbed blood flow, typically around a curvature or bifurcation in the artery [53, 54]. The mechanical stress induced by the turbulent flow on vECs results in the recruitment of leukocyte adhesion molecules such as ICAM-1 and VCAM-1 on their luminal surface [54, 55]. It is through these adhesion molecules that circulating monocytes are able to “stick” to the vEC layer and infiltrate the subintimal space via diapedesis, a process that will be expanded upon later in this chapter. This process of vEC activation, monocyte infiltration and uptake of oxLDL via macrophages will continue to occur throughout the development of CAD and plays a primary role in the continued development of atherosclerotic plaques.

The appearance of yellow fatty streaks on a vessel wall signifies the next state in the development of CAD [51, 52]. These fatty streaks are representative of a large accumulation of foam cells that are swollen with endocytosed oxLDL. Only one feature distinguishes Type II from Type III plaques and that is the generation of an extracellular lipid pool in addition to the fatty streaks [51, 52].

Type II and III plaques are prone to give rise to Type IV plaques or atheromas. Atheromas are known for their well-defined lipid core [51] that develops as outward remodeling of the vessel progresses. In coronary vessels, a distance of ~200μm from the lumen is far enough to generate an ischemic environment subsequently leading to apoptosis and the

beginnings of a necrotic core [56]. Along with creating an ischemic environment, this extracellular pool of lipids accumulates insoluble crystals of cholesterol, which are toxic, and trigger nearby cells to undergo apoptosis [56, 57]. In a healthy physiological state, macrophages participate in efferocytosis, which is classified as a process in which apoptotic cells are “cleaned up” or cleared away in the tissue. However, the foam cells present in atherosclerotic tissue are not classical macrophages and are unable to carry out efferocytosis properly [58]; consequently, dead cell fragments and the artifacts of apoptotic cells remain in the tissue contributing to increased inflammation and a prothrombotic “stew” [56, 59]. High concentrations of the highly thrombotic protein tissue factor (TF) contribute significantly to the ability of the necrotic core to induce thrombosis if exposed to the circulation [60]. At this stage in CAD, there is still little stenosis of the coronary artery but there is still risk of artery occlusion due to thrombosis should the contents of the plaque leak into the bloodstream via rupture.

True stenosis occurs in Type V atherosclerotic plaques. A Type V plaque is characterized by the neointimal accumulation of migrated dedifferentiated vascular smooth muscle cells (vSMCs) which generate a tough fibrous cap between the fatty necrotic core and the lumen of the blood vessel [51]. The continued proliferation of vSMCs in the neointima in concert with increased deposition of extracellular matrix leads to the growth of the plaque into the lumen of the blood vessel which can, over time, lead to reduced blood flow or even occlusion of the artery [56, 59]. Interestingly, the generation of a fibrous cap over the atherosclerotic plaques makes the diseased tissue less likely to rupture. Type V plaques are susceptible to a plethora of developmental changes that lead to the most clinically relevant classification of plaques, Type VI plaques.

Type VI plaques experience intraplaque hemorrhage, fission, intimal denudation and expansive calcium deposition all of which leave the atheroma susceptible to rupture and

subsequent thrombogenesis and MI [51, 52]. Intraplaque hemorrhage occurs through rupture of leaky neovessels that have grown into the plaque from the vasa vasorum and sharply increase inflammation through the lysis of red blood cells, which contributes plasma membrane cholesterol to the necrotic core, and exposure of hemoglobin (Hb) to the local environment [56, 61]. Hb is a highly inflammatory protein outside of the red blood cell and contributes significantly to oxidative damage and reactive oxygen species (ROS) [61]. Fissures are essentially tears or breaks in the endothelial or fibrous lining of the plaque that potentially exposes the contents of the plaque to the circulation [62]. Typically these fissures reseal as vECs proliferate and cover the exposed underlying tissue [56], but it is particularly compromising to the integrity of the plaque as repeated fissures increases susceptibility to rupture [63, 64]. Intimal or endothelial denudation is a process describing the erosion of the vEC layer or fibrous cap overlying the highly pathogenic extracellular matrix and necrotic core of the atheroma [65]. Lastly, calcium deposits occur in the ECM, the necrotic core, and in the remnants of cells that have undergone apoptosis [56, 59]. The pathology of calcified atheroma is unclear; however the extent of calcification in the plaque can be used as a biomarker for advanced progression of disease [66, 67]. Many of these processes occur throughout plaque progression and are not restricted to Type VI plaques alone; they do however occur continuously and contribute to the development and subsequent erosion and rupture of the atheroma.

Murine Models of Atherosclerosis

Wild-type mice are resistant to the spontaneous development of atherosclerosis likely due to their drastically different lipoprotein profile compared to humans. In humans, most of the circulating cholesterol is found in the LDL-C whereas in mice it is in the HDL-C. Wild-type mice are also resistant to diet-induced hypercholesterolemia because, unlike humans, they do not absorb dietary cholesterol efficiently; specifically, humans absorb

between 53.5 and 57.2% of cholesterol when fed a high cholesterol diet [68] compared to C57BL/6 mice that exhibit 30% absorption of cholesterol when fed a high fat/high cholesterol diet [69]. Investigating the role of cholesterol and lipoproteins in mice began in 1992 when both Nobuya Maeda and Jan Breslow's groups independently reported their findings that *Apoe*$^{-/-}$ mice spontaneously develop hypercholesterolemia and atherosclerosis [70, 71]. One year later Ishibashi et al. reported the generation of the *Ldlr*$^{-/-}$ mouse and the observation that a high cholesterol diet induces severe hypercholesterolemia in these mice [72]. On regular chow diet *Apoe*$^{-/-}$ and *Ldlr*$^{-/-}$ mice display a ≈4- to 5-fold and ≈2-fold increase in total plasma cholesterol compared to wild-type mice [72, 73]. ApoE is required for the clearance of cholesterol-rich chylomicrons and VLDL-C particles from the plasma and mice deficient in this protein show marked increases in plasma chylomicrons and VLDL while showing no increase in LDL-C. The Ldlr$^{-/-}$ mouse is a better model for human familial hypercholesterolemia as they both exhibit significant increases in their LDL-C; however, unlike the Apoe$^{-/-}$ mouse, mice deficient in LDLr do not spontaneously develop atherosclerosis on chow diet. When placed on a high cholesterol diet, Ldlr$^{-/-}$ mouse plasma cholesterol increases up to 1,500mg/dL.

These mouse models are not without their limitations. For example, the lipoprotein profile of Apoe$^{-/-}$ mice is very different from the LDL-C heavy profile of humans. Additionally, while both strains are capable of producing extensive atherosclerotic lesions, plaque rupture is a rare occurrence and typically requires additional insults such as surgical manipulations [74], overexpression of human proapoptotic p53 [75], or using aged mice (60+ weeks old) [76].

Limitations aside, the *Apoe*$^{-/-}$ and *Ldlr*$^{-/-}$ mice provide a useful model of atherosclerosis in mice and their lesions are comparable to human disease. Both Apoe$^{-/-}$ and Ldlr$^{-/-}$ mice on

Western diet develop lesions that can be scored using the Stary System previously described (see Table 1.1, taken from Whitman, S 2004 [77]).

Endothelial Cell Dysfunction Contributes to CAD Development

vECs compose a monolayer of cells that separates the circulating blood from the rest of the blood vessel. They play a pivotal role in the vasculature through inhibiting platelet activation and thus thrombogenesis through the production of both adenosine monophosphate [78] and nitric oxide (NO) [56, 59, 79, 80]. NO and prostacyclin production in vECs are important vasodilators that triggers SMC relaxation in response to increased forces on the vessel wall due to high blood pressure [80-82]. Morphologically, vECs comprise a highly organized monolayer typically aligned elongated in parallel with the unidirectional high shear stress from laminar blood flow [59, 83, 84]. This parallel alignment permits tight cell-cell contact maintaining both adaptive signaling [59, 85], to inhibit proinflammatory gene expression of NF-κB through Rac-dependent ROS production and p21 activated kinase signaling [86], and a highly regulated selective barrier between the circulation and underlying ECM [56]. During cases of peripheral tissue inflammation, complex leukocyte-vEC interactions permit the capture and adherence of circulating leukocytes to the endothelium and facilitate transmigration across the vEC monolayer [55]. These aforementioned processes are tightly regulated and maintained in the healthy vasculature but undergo dynamic phenotypic alterations in atherosusceptible regions experiencing disturbed blood flow and low shear stress.

Regions of the proximal aorta and the coronary arteries where inner curvature or bifurcations of the vessel occur are known to be susceptible to atherosclerosis [53, 83]. The unidirectional high shear stress typical of laminar blood flow in atheroprotected regions turns into turbulent blood flow with drastic changes to flow direction. Changes in flow dynamics and direction lead to vEC activation and alter their morphology from the

parallel elongated arrangement into a pathological “cobblestone” appearance [87]. This altered vEC morphology coincides with dysfunction in many of the vEC processes mentioned above. Activated vECs display enhanced inflammation and a reduction in NO production [82], a hallmark of endothelial dysfunction, resulting in a diminished ability to regulate vessel lumen diameter in response to increases in blood pressure as well as NO-dependent inhibition of platelet activation. Both laminar and disturbed blood flow is detected in vECs by the Rho family GTPases RhoA, Rac, and cdc42 which permits cytoskeletal remodeling but the lack of directional flow in the atherosusceptible regions hinders the vECs from forming tight cell-cell contact and maintaining the adaptive signaling [88-90] mentioned previously. Compromised “cobblestone” vECs experience endothelial barrier dysfunction, heightened proinflammatory signaling and ROS production. Enhanced proinflammatory signaling leads to expression of the leukocyte adhesion molecules VCAM-1 and ICAM-1 and subsequent invasion of inflammatory cells into the vessel [55], as mentioned before, as well as increased deposition of LDL-C into the subintimal space. Accumulated LDL-C is modified to oxLDL which then binds to CD36 and lectin-like oxLDL receptor 1 (LOX-1) on vECs [91] leading to increased activation of ICAM-1 [92] perpetuating the progression of monocyte invasion and plaque development. Endothelial expression of adhesion molecules contributing to atherosclerosis is supported in murine models of atherosclerosis in which *Apoe*$^{-/-}$ *Icam1*$^{-/-}$ double knockout mice show decreased lesion sizes compared to *Apoe*$^{-/-}$ controls [93]. Another vEC-expressed cytokine with links to monocyte recruitment in the context of CAD is CXCL1 by binding to its ligand CXCR2 on circulating monocytes prompting cell arrest [94].

A Role for Leukocytes and Inflammation in CAD

This section will focus on the subpopulation of leukocytes known as monocytes as they are the predominant cell type found in atherosclerotic lesions. Monocytes make up roughly

5 to 10% of the total leukocytes in the circulation and are comprised of two main subtypes, $GR1^{+}/Lys6C^{high}$ and $GR1^{-}/Lys6C^{low}$ [95]. $GR1^{+}/Lys6C^{high}$ monocytes express CCR2, a cell surface receptor capable of binding monocyte chemoattractant protein 1 (MCP-1) on activated vECs, and are the primary subtype responsible for extravasation into peripheral tissue at sites of inflammation [96]. Upon infiltration into inflamed peripheral tissue, monocytes will differentiate into one of four known macrophage subsets. M1 macrophages differentiate from monocytes exposed to LPS and/or IFNγ and are the subset responsible for attacking and eliminating pathogens [97, 98]. M2 macrophages come from monocytes treated with IL-4 or IL-13 and are implicated in tissue repair probably following the initial M1 response in inflammation [97, 98]. A unique macrophage subset has emerged from exposure of oxidized phospholipids, such as oxPAPC, to monocytes and bears what is called a Mox phenotype which appears to be a blend of both M1 and M2 phenotypes [99]. Lastly, there is a subset of macrophages known as the M(Hb) macrophage which will be discussed later in this section. Classically monocyte/macrophages are known for their role in the innate immune response; however, there are significant maladaptive behaviors that contribute to the development and progression of CAD.

As mentioned before, $GR1^{+}/Lys6C^{high}$ monocytes harbor CCR2 on their plasma membrane and are capable of binding MCP-1 expressed on activated vECs. During the early stages of plaque development, increased expression of MCP-1, ICAM-1, VCAM-1 and macrophage colony stimulating factor (M-CSF) [56] on the cell surface of activated vECs is a crucial step in the recruitment of monocytes and their transmigration into the subintimal space of blood vessels. Monocytes that differentiate into macrophages with the M1 phenotype express high levels of the scavenger receptors CD36, LOX-1, and macrophage scavenger receptor class A (SR-A) all of which aggressively facilitate the uptake of oxLDL into the macrophage [100, 101]. Typically free LDL-C binds LDL-C receptor (LDLR) where

it is endocytosed in a clathrin coated pit and acidification of the vesicle liberates the LDL-C from its receptor where it can act to inhibit HMGCoA reductase-dependent cholesterol synthesis [56]. In the developing plaque however, LDL-C modified to oxLDL is endocytosed via the aforementioned scavenger receptors and leads to unregulated cholesterol uptake, heightened proinflammatory cytokine production, and foam cell formation [56, 91, 102, 103]. OxLDL internalization provides specific ligands for the nuclear hormone receptor PPARγ [104] whose activity leads to increased expression of CD36 creating a positive feedback loop for oxLDL uptake and the exacerbation of the foam cell phenotype [105-107]. *Cd36*$^{-/-}$ mice on an atherogenic *Apoe*$^{-/-}$ background fed Western diet show pronounced reductions in aortic tree lesion formation (76.5%) compared to control mice [108].

It was mentioned previously that ischemia in the atheroma leads to hypoxia-induced apoptosis and formation of the necrotic core. Profound oxLDL uptake in foam cells can also contribute to growth of the necrotic core as the formation of cholesterol crystals triggers foam cell death leaving behind the toxic cholesterol crystals, oxidized lipids, and cell remnants [58, 109]. M1 macrophage phenotypic switching to a foam cell diminishes its ability to carry out efferocytosis, the process of cleaning up apoptotic cell fragments, contributing to the continuous growth of the necrotic core

Lastly, as mentioned before, intraplaque hemorrhage results in the accumulation of cholesterol and Hb in the plaque providing a source of ROS and oxidative damage. The tissues endogenous protection against Hb-induced oxidative damage is through its binding to haptoglobin (Hp) forming a Hb:Hp complex which can be cleared by resident macrophages through the CD136 receptor [110]. Macrophages that uptake Hb:Hp develop a phenotype known as M(Hb) and are unique in that they are very resistant to the uptake of oxLDL *in vitro [111]*. M(Hb) macrophages are therefore considered to be

protective in the context of atherosclerosis in that they do not develop into foam cells and are capable of eliminating proinflammatory Hb from the atheroma.

Phenotypic Switching of Smooth Muscle Cells in Atherosclerosis

Vascular SMCs reside in the tunica media of blood vessels from arterioles up to the largest of the arteries, the aorta, while being absent in the capillaries; structurally, SMCs are arranged in an elongated fashion parallel to one another but perpendicular to the direction of blood flow. The primary role of SMCs in the tunica media is to regulate the vessel lumen diameter in response to changes in blood pressure (the myogenic mechanism), or external stimuli from the vECs or the sympathetic nervous system, through coordinated contraction and relaxation. Vascular SMCs are not terminally differentiated and therefore harbor significant plasticity [56, 59]. In healthy blood vessels, SMCs maintain a “contractile” phenotype that is characterized by low levels of proliferation and diminished capacity to secrete ECM proteins [54]. Contractile SMC markers are smooth muscle alpha-actin (ACTA2), smooth muscle 22α (SM22) and smooth muscle myosin heavy chain (SM-MHC) [112]. Prostaglandin2 (PGI_2) [113] and NO [114] secreted from vECs act as potent vasodilators by acting on signaling pathways in SMCs, but these molecules also play a significant role in maintaining the previously mentioned contractile phenotype. PGI_2 stimulates adenylyl cyclase-dependent cAMP generation capable of inhibiting myosin light chain kinase [115, 116], a kinase whose phosphorylation of the myosin light chain stimulates SMC contraction through myosin-actin crossbridge formation, hence leading to SMC relaxation. Aside from inhibiting crossbridge formation, PGI_2 signaling decreases intracellular Ca^{2+}, adding to its role as a vasodilator, but also inhibits SMC proliferation and growth [115, 116]. NO signaling leads to guanylyl cyclase-dependent cGMP production [117], a second messenger that stimulates myosin light chain phosphatase activity [117]. Myosin light chain phosphatase hydrolyzes the phosphate from myosin light

chain and breaks myosin-actin crossbridges resulting in SMC relaxation. Similar to PGI_2, NO-dependent cGMP production leads to decreased intracellular Ca^{2+} and inhibits proliferation and growth in SMCs [118] .

SMCs in CAD and other vascular injury models exhibit a vastly different phenotype than the contractile SMCs described above. During atherosclerotic plaque development SMCs dedifferentiate and migrate to the subintimal space, usually above the extracellular lipid pool/necrotic core, and both vigorously proliferate and secrete ECM proteins such as collagen and elastin to form a tough fibrous cap [119]. Pronounced SMC proliferation in the subintimal region creates a condition known as neointimal hyperplasia and is characterized best by significant increases in the intima size. vEC dysfunction increases susceptibility to atherosclerosis and may contribute to SMC phenotypic switching from a contractile state to a proliferative one due to loss of the NO-dependent inhibition of proliferation in SMCs. These “proliferative” SMCs downregulate expression of their contractile markers, ACTA2, SM22 and SM-MHC, and express macrophage markers such as CD68 [112]. Data suggest a role for the DNA-binding protein Krüppel-like factor-4 in binding the G/C repressor element on the promoter of SMC marker genes, leading to their downregulation [112]. Phenotypic switching may also push SMCs towards a macrophage-like state capable of internalizing oxLDL in atherosclerotic plaques; in fact, evidence suggests that up to 50% of oil red-O stained cells in plaques display ACTA2-positive staining and thus may significantly contribute to the foam cell population [120]. *In vitro,* vascular SMCs treated with oxidized phospholipids, such as oxPAPC, oxLDL, and unsaturated LPA for 72 hours display phenotypic switching characterized by decreased expression of SMC markers, upregulation of CD68 and even positive oil red-O staining suggesting foam cell formation [121, 122].

LPA and Atherosclerosis

LPA-mediated effects on vEC barrier function and SMC phenotypes have been reported. Not surprisingly, LPA has also been implicated in CAD by eliciting effects through both vEC and macrophages. *Ex vivo* perfusion of murine carotid artery with mildly oxidized LDL-C (moxLDL) leads to an LPA-dependent increase in monocyte rolling and adhesion that can be completely inhibited by the addition of the LPA1/3 antagonist Ki16425 [14]. It appears that LPA is generated from LPC on moxLDL by ATX and blocking the enzyme with inhibitor S32826 diminishes the rolling and adhesion of monocytes to the vessel wall [14]. Intravenous injection (i.v.) of unsaturated 20:4 LPA, but not saturated 18:0 LPA, increases atherosclerotic lesion formation in *Apoe*$^{-/-}$ mice fed high-fat diet for 4 weeks displaying significantly increased macrophage Mac-2+ staining [14]. *Ldlr*$^{-/-}$ mice fed chow diet supplemented with unsaturated LPA resulted in lesion formation similar to Western diet fed mice, which was ameliorated by the addition of the ATX inhibitor PF8380 [123].

Evidence also supports a role for LPA in foam cell formation as the treatment of primary human monocytes with 5μM oleoyl LPA for 16 hours increases oxLDL uptake measured by oil red-O, and increases CD36 expression on the cell surface [124]. Additionally, it appears as though the LPA-dependent upregulation CD36 only occurs when the human CD36 promoter contains the PPAR responsive element suggesting LPA is a ligand for PPARγ [124].

Identification of Novel Risk of CAD through Genome Wide Association Studies (GWAS)

Once the human genome was sequenced a whole new avenue of identifying heritable risk of disease opened up. Technology quickly permitted the sequencing of thousands of individual genomes both faster and cheaper until present day GWAS are capable of

generating massive quantities of genomic data on a population scale. More specifically, genomes from populations of patients diagnosed with cardiovascular disease were sequenced by SNP genotyping and compared to a healthy control population in order to identify single nucleotide polymorphisms (SNPs) that could predict one's increased risk of disease. SNPs are the most common form of DNA variation that occur in individuals and are single nucleotide differences. A SNP occurs, on average, once every 300 base pairs which translates to roughly 10 million SNPs in the human genome [125]. By comparing SNP frequency in patients with CAD versus healthy populations, scientists are able to identify "risk alleles" or SNPs that associate with disease. A meta-analysis was published in Nature Genetics in 2011 that compared the results of several GWAS studies looking at CAD and identified 13 novel risk loci as well as reaffirming 10 previously identified SNPs. One of these novel risk loci termed rs17114036 is located in the final intron of the gene *PPAP2B* that encodes the lipid phosphate phosphatase 3 enzyme [4].

Polymorphisms in PPAP2B Associate with CAD

The novel risk locus in *PPAP2B* is found at 1p32.2. The risk allele is an adenine (A) with a frequency of 0.91 while the other protective allele is a guanine (G) at a frequency of 0.09. rs17114036 bears a composite p-value of 3.81×10^{-19} suggesting a significant correlation with disease and an odds ratio of 1.17[4]. Another important consideration is that while three novel loci from this meta-analysis were found in genes that are associated with traditional risk factors of CAD, the majority of SNPs, including rs17114036, are found in gene regions that have no previous implication in the development of atherosclerosis.

GWAS are capable of identifying risk alleles pertaining to a particular disease; however, the SNP reported may not be the particular locus causing the functional insult. Commonly, SNPs or alleles exhibit non-Mendelian genetic patterns and tend to associate together in nonrandom fashion with other SNPs in close proximity. This particular genetic

phenomenon is known as linkage disequilibrium and a grouping of SNPs in linkage disequilibrium is termed a haplotype. Rs17114036 is in linkage disequilibrium with roughly 20 proxy SNPs with an r^2 of 0.81 or higher, any one of which could be the functional disease-causing locus. This tendency to travel as a haplotype is important because of subsequent investigations led by Jake Lusis at UCLA and Chris O'Callaghan at Oxford looking into SNPs that are in linkage disequilibrium with rs17114036. Erbilgin et al. identified a proxy SNP, rs6588635, which associates with the earlier identified SNP rs17114036 at an $r^2 = 0.831$. Utilizing this proxy SNP as a biomarker that is found to be in linkage disequilibrium with the original rs17114036, the group from UCLA reported marked changes in *PPAP2B* expression in human aortic endothelial cells (HAECs) relative to an individual's SNP genotype. In fact, individuals homozygous for the proxy SNP risk allele, in this case a thymine (T), show marked decreases in expression relative to those who are heterozygous (CT) suggesting that possessing the homozygous risk allele genotype (TT) renders the HAEC unable to express *PPAP2B* to the same degree as heterozygotes.

Reschen et al. sought to identify regions of the genome that are subject to transcriptional regulation following exposure to atherogenic stimuli such as oxLDL. In their study published in PLOS Genetics in 2015, Reschen et al. demonstrated using FAIRE-seq and ChIP-seq that the conversion of naïve human monocytes to foam cells via exposure to oxLDL results in dramatic remodeling of open chromatin regions. One site in particular harbors the SNP rs72664324 that lies within the gene *PPAP2B.* Sequencing the regions of newly exposed open chromatin revealed that the aforementioned locus falls within a C/EBPβ binding motif (CC**A**AT) and that the risk allele disrupts this motif (CC**G**AT) rendering the transcription factor unable to bind. In collaboration with the group we looked at *PPAP2B* expression of LPP3 in monocytes before and after oxLDL exposure. While naïve monocytes show very modest levels of LPP3 protein, observed via immunoblot, and

LPP3-dependent phosphatase activity, oxLDL treatment significantly increases both LPP3 levels and LPP3-dependent phosphatase activity roughly 3-fold. Similar to the HAECs investigated by Lusis et al. [126], monocytes from individuals homozygous for the risk allele exhibited a reduced ability to upregulate *PPAP2B* expression relative to heterozygote monocytes following oxLDL treatment.

Large-scale GWAS analysis combined with independent research investigations into genotype specific SNP activity in *PPAP2B* suggests that the risk alleles responsible for an increase in an individual's risk of CAD appear to be acting, at least in part, in a *cis* manner by reducing the gene's expression in various human vascular cells.

PPAP2B encodes Lipid Phosphate Phosphatase 3

PPAP2B encodes the protein LPP3 that belongs to a family of proteins known as lipid phosphate phosphatases or LPPs. LPPs are transmembrane enzymes capable of degrading various phospholipids such as lysophosphatidic acid (LPA), sphingosine-1-phosphate (S1P), ceramide-1-phosphate (C1P), phosphatidic acid (PA), and a few others.

Structure and Function of the LPPs[3]

Structurally, the LPPs contain six transmembrane domains with 5 extramembrane loops [127]. Their catalytic domains are found on the third and fifth loop facing the extracellular/luminal surface and the LPPs' enzymatic activity are dependent upon a

[3] *Portions of this section were taken from Mueller et al. [15]. Some additions and modifications to the text and figures have been made for clarity of information.*

variably glycosylated site on the third loop. Additionally, both the N- and C- termini are located on the cytosolic surface (Figure 1.2). The LPP family consists of three proteins LPP1, LPP2 and LPP3 encoded by the genes *PPAP2A, PPAP2C* and *PPAP2B* respectively. Spatially speaking, the LPPs' localization varies depending on the cell type and degree of glycosylation, but can range from the endoplasmic reticulum, the Golgi, and the plasma membrane. These proteins are capable of forming both hetero- and homo oligomers in the plasma membrane while retaining enzymatic activity that is independent of the other LPPs in the complex [128].

Although the three LPP enzymes demonstrate similar catalytic activities and substrate preferences *in vitro*, the phenotypes of mice with targeted inactivation of the *Ppap2* genes establishes that their functions are non-redundant. Primary cells isolated from mice harboring an exon trap inactivated allele of *Ppap2a* gene display a reduced ability to dephosphorylate exogenously provided LPA, indicating a role for LPP1 as a cell surface "ecto" LPA phosphatase [129]. Mice homozygous for an inactivated allele of the *Ppap2c* gene, encoding murine LPP2, are phenotypically indistinguishable [130]. By contrast, inactivation of *Ppap2b* results in embryonic lethality in part to due to failure of extra-embryonic vasculature [131]. Media from cultured embryonic fibroblasts isolated from *Ppap2b*-null mice contains 2.6-fold higher levels of LPA suggesting that the other LPPs cannot compensate for the regulation of extracellular accumulation of LPA.

Mukherjee et al. published a study in 2013 demonstrating a role for the LPP3 homologs in *Drosophila*, Wunen and Wunen2, in generating and regulating phospholipid gradients *in vivo [132]*. Normally germ cells in the developing *Drosophila* embryo begin as a cluster of cells at Stage 9, separate and migrate in an organized fashion into the mesoderm by Stage 12 where they partition bilaterally to interact with somatic gonadal precursor cells. As the germ cells migrate they tend to avoid somatic tissues expressing *wun* and *wun2*

suggesting that the phosphatases play a role in directing migration. In fact, when Wunen and Wunen2 are knocked out in somatic tissues the germ cells' migration pattern is dramatically disrupted. Mukherjee et al. defined the maximum range of influence of Wunen-expressing cells on germ cells as approximately 33µm.

LPP3 Modulates LPA-dependent Vascular Endothelial Cell (vEC) Function

LPP3 is clearly important in the development of multiple species, but its role in the mature vasculature is less understood. As it turns out, endothelial cell-specific deletion of *Ppap2b* is embryonically lethal due to vascular defects similar to what was observed in the *Ppap2b*-null mice [22]. To study the effects of endothelial deletion of LPP3 in a murine vascular injury model, a tamoxifen-inducible model of endothelial cell-specific deletion was achieved by breeding *Ppap2b*$^{fl/fl}$ mice to transgenic mice expressing a recombinant estrogen receptor-Cre fusion protein under the control of the tyrosine kinase *Tek* promoter (ERT2-Cre). Following LPS injections, mice targeted for endothelial cell deletion of LPP3 (ERT2-Δ) displayed enhanced systemic inflammation detected by a 3.3-fold increase in IL-6 and a 1.9-fold increase in KC compared to the control mice (fl/fl) suggesting that LPP3 in the endothelium is anti-inflammatory. ERT2-Δ mice also displayed marked differences in endothelial barrier function compared to the fl/fl counterparts. Deletion of LPP3 in the endothelial cells results in ~2.2-fold increase in vascular leakage as measured by Evans blue dye (EBD) leakage into the lungs which is exacerbated when mice are injected with LPS. This effect on endothelial barrier function is specific to endothelial cells and not the hematopoietic deletion of LPP3 as ERT2-Δ bone marrow transplantation into fl/fl mice showed no changes in EBD leakage whereas EBD leakage into the lungs of ERT2-Δ mice harboring fl/fl bone marrow was pronounced. Finally, and potentially most importantly, compromised endothelial barrier function in mice lacking endothelial LPP3 is ameliorated upon the administration of either ATX inhibitors or a pan-LPA receptor antagonist

suggesting that LPA signaling, at least in part, is responsible for this phenotype. Data from Panchatcharam et al. strongly implicates a role for LPP3 in protecting endothelial barrier function as well as systemic inflammation and that the former role is through the regulation of LPA signaling [22].

Endothelial cell-specific deletion of LPP3 leads to a decrease in endothelial barrier function in mice as quantified by EBD leakage into the lungs suggesting a physiological role for LPP3 in maintaining vascular endothelial barrier integrity. In human umbilical vein endothelial cells (HUVECs) LPP3 is localized in areas of cell-cell contact sites while it appears absent in areas of non-contact sites [84]. Yukiura et al. showed in 2015 that treatment of HUVECS with 1μM LPA induced stress fiber formation, increased the incidence of intracellular gaps and increased endothelial cell permeability as measured by leakage of FITC-labelled dextran across a monolayer of cells. LPP3 plays a critical role regulating this LPA-induced stress fiber formation which appears to be signaling through LPA6. Reducing LPP3 expression using *PPAP2B*-siRNAs results in HUVEC stress fiber formation at a dose of 0.1μM LPA that is otherwise absent in cells treated with control-siRNA. Additionally, silencing LPA6 using siRNA abolishes LPA-induced stress fiber formation providing a mechanistic role for LPP3 in regulating LPA-induced endothelial cell remodeling and vascular permeability.

Wu et al. demonstrated another potential role for LPP3 in maintaining vascular health in 2015 [83]. In atherosusceptible areas of the vasculature harboring disturbed blood flow and low shear stress, *PPAP2B* appears to be downregulated in vECs by miRNA-92a. As mentioned previously, disturbed flow and low shear stress alters the morphology and alignment of vECs from a parallel alignment to the classic cobblestone arrangement leading to increased vascular permeability, inflammation and expression of adhesion molecules. By reducing *PPAP2B* expression using siRNA in HAECs under

atheroprotective (laminar) flow; HAECs take on the cobblestone morphology similar to those in an atherosusceptible flow that is accompanied by increased expression of inflammatory cytokines and adhesion molecules *MCP1* and *VCAM1* respectively. Interestingly, use of the LPA receptor 1 and 2 antagonist ki16425 ameliorated *MCP1* and *VCAM1* upregulation. These data allude to another mechanistic role for LPP3 in regulating LPA-dependent remodeling of HAECs in the context of atherosusceptible blood flow.

LPP3 Limits Neointimal Hyperplasia and Inflammation in mice

Our lab has also identified a role for LPP3 in limiting the development of neointimal hyperplasia following carotid artery ligation [133]. In wild-type mice, *Ppap2b* expression significantly increases 7 and 28 days post-ligation and LPP3 levels are significantly increased at 28 days post ligation while there is apparent elevation at 14 days. SMC-specific LPP3 deletion in mice (SM-$Ppap2b^{\Delta}$) resulted in ≈3- to 4-fold increases in the intimal area compared to $Ppap2b^{fl/fl}$ mice 4 weeks after carotid artery ligation suggesting that LPP3 limits the development of neointimal hyperplasia. Uninjured vessels from SM-$Ppap2b^{\Delta}$ mice have marked downregulation of SMC markers *Acta2, Tagln, Myh11,* and *Cnn* (≈1.8-, 2.3-, 3.9-, and 3.0-fold respectively) relative to the control mice. SMCs isolated from the thoracic aorta of SM-$Ppap2b^{\Delta}$ also demonstrate increased proliferation and migration compared to controls.

Overview

There is little question that CAD is the leading cause of death in both men and women worldwide and a major socio-economic burden in the United States. The multi-factoral disease arises from both environmental and heritable insults that incorporate the dysfunction of nearly all vascular-cell types and many other tissues as well. Significant

evidence points to a role for the ATX-LPA-LPP3 axis in the development and progression of atherosclerotic plaques in part because of their influence on so many of the vascular tissues contributing to disease, but even more so is the considerable genomic data implicating a risk loci in *PPAP2B* that confers an increase in CAD risk. The work presented in this dissertation is to demonstrate 1) that *Ppap2b* expression limits atherosclerotic lesion formation in a murine model of atherosclerosis (Chapter 2) 2) CAD associated risk-alleles decrease expression of *PPAP2B* in a *cis*-dependent manner (Chapter 2 and 3) and 3) LPA content increases in plasma fractions containing atherogenic LDL-C in murine models of hyperlipidemia and atherosclerosis.

Table 1.1

Mouse Model (Diet)	Atherosclerotic Lesion Stage Obtained in the Ascending Aorta					
	I	II	III	IV	V	VI
[a]*apoe-/-* ([c]standard diet)	1-2 months	4-5 months	7-9 months	8-11 months	10> months	N/A
[b]*apoe-/-* ([d]Western diet)	4-6 weeks	8-10 weeks	12-14 weeks	14-16 weeks	18-20 weeks	N/A
[a]*ldlr-/-* ([c]standard diet)	6-7 months	9-10 months	12> months	N/A	N/A	N/A
[b]*ldlr-/-* ([d]Western diet)	4-6 weeks	6-12 weeks	16-20 weeks	[e]24> weeks	N/A	N/A

[a]Time refers to the age of the mouse in months.
[b]Time refers to the length of time the mice have been fed the Western diet, with the mice being started on the diet when they are between 4-8 weeks of age.
[c]Standard chow diet generally consists of 20% (wt/wt) protein from plant and animal sources, 4.5%(wt/wt) fat (generally a non-specific source is given), 0.02% (wt/wt) cholesterol, no casein, no sodium cholate.
[d]Two common sources of Western Diet are from Harlan Teklad (#88137; Madison, Wisconsin, USA) and Dyets Inc. (#112286; Bethlehem, Pennsylvania, USA). Both of these diets consist of 21% (wt/wt) fat (butterfat) and 0.15% (wt/wt) cholesterol, 19.5% (wt/wt) casein and no sodium cholate.
[e]Western diet that was augmented so that the final concentration of cholesterol was 1% (wt/wt).
N/A = not applicable.
Use this table as a guideline only noting that mice predicted to have lesions of stage IV or greater will also have lesions that would also be classified in the early stages (I-III) of development.

Lesion Stage and Timeframe for Development in both Apoe$^{-/-}$ and Ldlr$^{-/-}$ Mice [77]

Figure 1.1

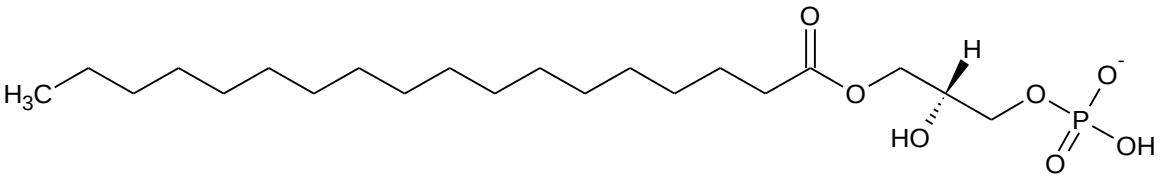

Lysophosphatidic acid. A potent lysophospholipid signaling molecule consisting of a phosphate group bound to a glycerol backbone and a variable fatty acid chain that signals through one of six known GPCRs (LPA1-6).

Figure 1.2

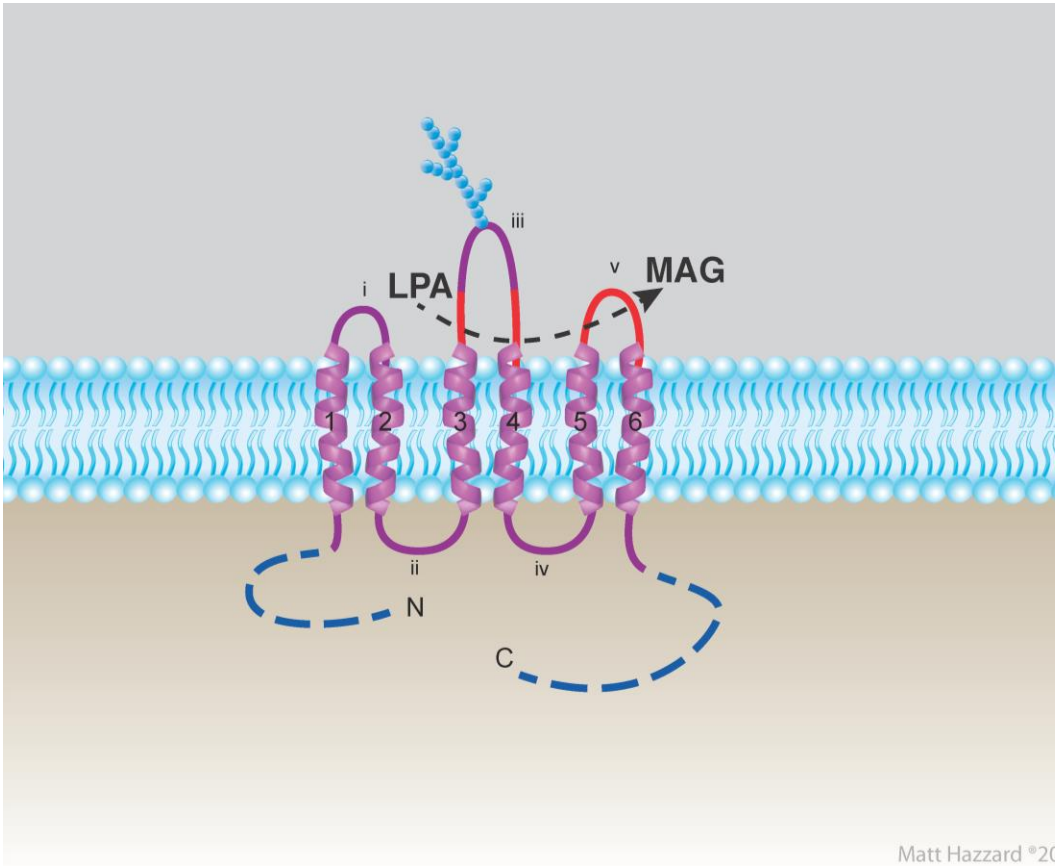

Structure of lipid phosphate phosphatases. The LPPs contain six transmembrane domains with 5 extramembrane loops [127]. Their catalytic domains are found on the third and fifth loop facing the extracellular/luminal surface and the LPPs' enzymatic activity are dependent upon a variably glycosylated site on the third loop. Additionally, both the N- and C- termini are located on the cytosolic surface. Illustration by Matt Hazzard, University of Kentucky, Information Technology.

Chapter 2: Ppap2b Expression Regulates CAD in a Tissue-specific Manner

Introduction

CAD is the leading cause of death in both men and women worldwide and is defined as a narrowing of the coronary arteries as a result of the growth and accumulation of atherosclerotic plaques. The development of atherosclerotic lesions is a complex process initiated by the deposition of LDL-C in coronary artery vessel wall and involves the dysfunction of multiple vascular tissues as well as unchecked inflammation. Advanced lesions harbor a highly prothrombotic necrotic core that, upon plaque rupture, is exposed to the circulation, stimulating thrombosis and potentially MI. Risk of CAD has a strong heritable component and advances in genome sequencing have identified upwards of 46 disease-associated loci many of which are independent of the traditional risk factors [134]. A meta-analysis of GWAS studies looking into CAD-associated SNPs identified a noncoding polymorphism termed rs17114036 that confers an increase in risk of disease [4]. Rs17114036 lies within the final intron of *PPAP2B* at chromosomal band 1p32.2, which is on the same chromosome of the LDL-C regulator *PCSK9* and could thus be acting in *trans* affecting PCSK9 and cholesterol levels. Searching publically available databases revealed a SNP in linkage disequilibrium with rs17114036 that shows allele-dependent variations in the expression of *PPAP2B,* but not *PCSK9,* in peripheral blood cells suggesting that the SNP is capable of acting in a *cis*-manner and is not changing *PCSK9* expression (unpublished data; see Chapter 3). Supporting this data, the CAD-associated risk allele correlates with decreased expression of *PPAP2B* in HAECs [126]; additionally, it has been shown to inhibit C/EBPβ-dependent upregulation of *PPAP2B* in primary human macrophages exposed to oxLDL by interrupting a CCAAT binding motif [135].

PPAP2B encodes the protein LPP3, a member of the integral membrane protein LPP family whose primary enzymatic function is the degradation of phospholipids such as LPA, S1P, C1P, PA and others [136]. Germline deletion of LPP3 is embryonically lethal due to vascular defects [137]; whereas the other LPPs show unremarkable phenotypes suggesting a nonredundant role for LPP3 in development [138]. LPP3 homologs, Wunen and Wunen2, play a large role in generating phospholipid gradients, up to a distance of 33μm, that is critical in directing the migration of germ cells [132]. Our lab has previously identified a role for SMC-specific LPP3 in limiting neoinitimal hyperplasia and inflammation in murine models of vascular injury [133]; as well as a role for endothelial cell-specific LPP3 in maintaining vEC barrier function in murine models of systemic inflammation [22]. Furthermore, endothelial cell *Ppap2b* expression is downregulated in atherosusceptible regions of murine aorta where turbulent blood flow drives phenotypic alterations and vEC dysfunction [83]. Considering CAD-associated risk allele-dependent effects on *PPAP2B* as well as LPP3's role in murine vascular models of injury, systemic inflammation and turbulent nonlinear flow, we hypothesize that LPP3 is protective in murine models of CAD.

Materials and Methods

Animals

All procedures conformed to the recommendations of *Guide for the Care and Use of Laboratory Animals* (Department of Health, Education and Welfare publication number NIH 78-23, 1996), and were approved by the Institutional Animal Care and Use Committee. The production, initial characterization, and backcrossing of *Ppap2b*$^{fl/fl}$ mice to a C57BL/6 background for >10 generations has previously been described [137, 139]. In order to generate mice susceptible to atherosclerosis, *Ppap2b*$^{fl/fl}$ were crossed to *LDLr*$^{-/-}$ mice obtained from The Jackson Laboratory (Bar Harbor, ME) to yield *Ppap2b*$^{fl/fl}$ *LDLr*$^{-/-}$ mice. Generation of an atherosusceptible inducible global LPP3 KO mouse: To generate

mice with an inducible global reduction in *Ppap2b,* female *Ppap2b*$^{fl/fl}$ *LDLr*$^{-/-}$ mice were crossed to male *Ppap2b*$^{fl/fl}$*LDLr*$^{-/-}$mice expressing Cre recombinase under the control of the inducible MX-1 promoter to generate *mx1-ppap2b*$^{\Delta}$ *Ldlr*$^{-/-}$ (referred to as *MX*-1Δ) mice following polyinosinic-polycytidylic acid (pI:pC) treatment. pI:pC (Sigma Cat#P1530-100mg) was dissolved in sterile 0.9% saline (concentration of 10mg/mL) and 50µL was administered via i.p. injection between post-natal days 3 to 5. Littermates not harboring Cre recombinase were used as controls. Generation of an atherosusceptible SMC-specific LPP3 KO mouse: To generate mice with SMC-specific *Ppap2b* deletion*,* female *Ppap2b*$^{fl/fl}$ *LDLr*$^{-/-}$ mice were crossed to male *Ppap2b*$^{fl/fl}$*LDLr*$^{-/-}$mice expressing Cre recombinase under the control of the SM22 promoter to generate *sm22-ppap2b*$^{\Delta}$ (referred to as SM22-Δ) mice. Littermates not harboring Cre recombinase were used as controls. Generation of Leukocyte-specific LPP3 KO Mice: To generate mice with leukocyte-specific *Ppap2b* deletion*,* female *Ppap2b*$^{fl/fl}$ mice were crossed to male *Ppap2b*$^{fl/fl}$ mice expressing Cre recombinase under the control of the LysM promoter to generate *lysm-ppap2b*$^{\Delta}$ (referred to as LysM-Δ) mice. Littermates not harboring Cre recombinase were used as controls. Mice were housed in cages with HEPA-filtered air in rooms on 12-hour light cycles, and fed RD Western Diet (Research Diets Cat#D12079B) ad libitum for 12 weeks.

Immunoprecipitation of LPP3

10µL/sample of protein G Sepharose beads (GE Healthcare Cat# 17-0618-01) was washed three times with cold 1x PBS, and then resuspended in 20µL/sample of 1x PBS. Antibody (1mg/mL) was incubated with the protein G Sepharose beads for 1 hour at 4°C with periodic mixing. The beads-antibody mixture were washed again three times with cold 1x PBS, and then resuspended in 20µL/sample of 1x PBS. 100µg of whole protein was added to the beads-antibody solution and incubated for 1 hour at 4°C with periodic mixing. The beads-antibody-protein mixture was once again washed three times with cold 1x PBS.

Phosphatase activity assay

Protein G Sepharose beads bound to LPP3 protein were resuspended in 30µL of ddH_2O, 20µL of 5x Assay buffer containing 50mM tris base and 5mM EDTA pH 7.4, and 50µL of 0.2mM C17-sphingosine-1-phosphate in 6.4mM Triton X-100. Samples were incubated at 37°C in an Eppendorf thermomixer at 1,400rpm for 10 minutes. The reaction was stopped by adding 400µL of 0.1M HCl to each sample and placed on ice. Samples were then processed for lipid extraction.

Lipid extraction for analysis via mass spectroscopy

500µL of sample in 0.1M HCl were added to a 12mL glass lipid extraction tube containing 1mL of chloroform, 2mL of methanol, and 50µL of 1µM D7-sphingosine-1-phosphate as an internal standard. Samples in the lipid extraction tubes were vortexed for 5 minutes, and then placed on ice/kept at 4°C for at least 1 hour. 1mL of chloroform and 1.3mL of 0.1M HCl was added to the lipid extraction tubes and vortexed again for 5 minutes. The samples were centrifuged at 3,000×g for 10 minutes at room temperature, and the lower aqueous was transferred to 4mL screw cap glass tube using a Pasteur pipette being careful not to include the protein interphase. Samples were evaporated to dryness using nitrogen in an N-evap under a fume hood. Once the samples were completely dried, 100µL of methanol was added and the tubes were vortexed. Samples sat at room temperature for 10 to 15 minutes and then transferred to an autosampler insert vial for analysis via Agilent Zorbax C8 column and quantified by tandem mass spectrometry using an ABI 4000 QTrap hybrid linear ion trap triple quadrupole mass spectrometer. The mass spectrometer was operated in selective reaction monitoring mode to measure lipid species specific precursor product ion pairs with quantification accomplished by reference to calibration curves generated using synthetic standards obtained from Avanti Polar Lipids that were independently quantitated by phosphorous analysis as described previously.

Quantification of Atherosclerosis

Aortas were cleaned of the adventitia and dissected from the aortic root to the iliac bifurcation and stored in 10% formalin for 24 to 48 hours. After treatment with paraformaldehyde, the aortas were transferred to a 0.9% Saline solution and stored at 4°C for at least one day. Aortas were cut open longitudinally, exposing the intimal surface, and secured with pins to be photographed. Atherosclerosis was quantified on the intimal surface of the aorta by an *en face* technique described previously [140].

Quantification of LPA and cholesterol from mouse aorta

Aortas were cleaned of the adipose tissue and dissected from the aortic root to the iliac bifurcation. The aorta was cut 3mm below the left subclavian artery (this section of the aorta is defined as the proximal aorta) and the tissue was weighed. Aortic roots were homogenized in 0.5mL of 0.1M HCl and underwent lipid extraction as described previously. Internal standards used for this experiment were C17-LPA, C17-LPC, and D7-cholesterol. Levels of LPA and cholesterol were normalized the tissue weight. *Note: S1P was undetectable in the proximal aortic tissue.*

Gene Expression Analysis of Proximal Aortas

Murine proximal aorta was collected as described above in the Quantification of LPA, and cholesterol. Tissue was weighed and stored in RNA*later*® Solution (Ambion AM7020) at -80°C. Proximal aortas were homogenized and treated with the Qiagen RNeasy Fibrous Tissue Mini Kit (Qiagen Cat# 74704) for the extraction of RNA. 1.0μg of RNA was used for the generation of a cDNA library using MultiScribe™ Reverse Transcriptase (Life Technologies Cat#4311235). cDNA was diluted 1:10 and used in a reaction with the

TaqMan® Fast Universal PCR Master Mix (2X) (Life Technologies Cat#4364103) with VIC/FAM primers from Life Technologies designed for specific gene targets.

Immunoblotting of Proximal Aortic Tissue

Murine proximal aorta was collected as described above in the Quantification of LPA, and cholesterol. Tissue was homogenized in lysis buffer containing: 50mM Tris Base; 500mM NaCl; 4mM $MgCl_2$; 1% Triton X-100; 1mM PMSF protease inhibitor. Protein concentrations were determined with the Pierce™ BCA Protein Assay Kit (Cat# 23225) and 40µg of total protein was added to a 10% polyacrylamide gel which was then transferred to a nitrocellulose membrane. Antibody dilutions were as follows: LPP3 (1:200) and beta-actin (1:5,000). Membranes were scanned using a Li-Cor Odyssey scanner.

Isolating Plasma from Peripheral Blood in Mice

Peripheral whole blood was collected from mice via the retro-orbital vein while mice were anesthetized with isoflurane. Whole blood was collected in a 1.5 mL Eppendorf tube containing 10 µL of 0.5 M EDTA and 50 µL CTAD (BD Vacutainer Ref# 367947). Blood samples were centrifuged at 12,000 rpm for 4 minutes and the plasma fraction collected. Samples were placed on dry ice and subsequently stored at -80°C.

Measuring Total Cholesterol and Lipoprotein Cholesterol Distributions in Murine Plasma

Total plasma cholesterol was measured using the Wako Diagnostics Cholesterol E Assay (Wako Diagnostics Cat#439-175001) according to the manufacturer's protocol. Plasma lipoprotein cholesterol distributions were determined via fast-performance liquid chromatography (FPLC). In short, 40µL of plasma from mice, diluted to a concentration of

1mg/mL of total plasma cholesterol, was injected on to a Superose 6 FPLC column. Cholesterol concentrations are determined by enzymatic colorimetric assay (Wako Diagnostics) reading at 600nm as the elute flows off of the column.

Measuring Total Triglyceride Content in Murine Plasma

Total plasma triglycerides was measured using the Wako Diagnostics L-type TG M Assay and the Multi-Calibrator Lipid Standard to generate a standard curve (Wako Diagnostics Cat# 461-08992, 461-09092, 464-01601) according to the manufacturer's protocol.

Measuring Phospholipid Content in Murine Plasma

50 μL of plasma was added to 450 μL of 0.1 M HCl and underwent lipid extraction as previously described in "Lipid extraction for analysis via mass spectroscopy"

Isolation and Culture of Bone Marrow Derived Macrophages

Femur and tibia isolated from mice were cut at both ends and flushed with 5mL pre-warmed (37 degree C) DMEM Glutamax media using a 25 gauge needle. Red blood cells were lysed with 0.8% ammonium chloride in 1x PBS for 5 minutes. Media-cell suspension was pressed through a 70μm nylon mesh filter and centrifuged at 1000×g for 5 minutes. The cell pellet was resuspended in DMEM Glutamax containing 10% FBS, 1% PenStrep and 10% L929 media then transferred to a 6 well plate at a concentration of 1 million cells per well. After 72 hours the wells were washed with sterile 1x PBS and cultured in DMEM Glutamax containing 10% FBS, 1%PenStrep and 10% L929 media. Cells were cultured for 7 to 10 days while refreshing media every 2 to 3 days. Culture conditions were 37°C at 5% CO_2.

Isolation and Culture of SMCs

Mice were anesthetized terminally with isoflurane, then doused in 70% ethanol and cut open from the abdomen through the thorax. A 20mL syringe attached to a butterfly needle (21 G3/4 X12" Vacutainer BD Cat# 367281) was used to inject 20mL of 1x PBS (kept at 37ºC) into the left ventricle and the vascular systems was perfused with a minimum speed, after cutting open the femoral artery or the artery near the kidney. The perfusion was performed twice, with a total of 40mL sterile 1x PBS at 37°C perfusion. The aorta was separated from surrounding tissue starting from the aorta arch until the kidney vessel. Enough care was taken to isolate the aorta without any fat bodies and any other surrounding tissue. After isolation, the aorta was placed in isolation buffer (60mm plate having 4ml of pre-warmth to 37°C isolation buffer) and flushed with isolation buffer to remove all the RBCs. The aorta was transferred into a new 60mm plate containing isolation buffer. The dish was incubated at 37°C while the rest of the animals were dissected. Once two aortas per 60mm dish were collected, they were subjected to 2.5mL of collagenase digestion buffer (3.1mg – 3.9mg collagenase type II dissolved in 5ml of isolation buffer kept at 37°C) to remove the adventitia. The digestion was done for 20 minutes at 37°C incubator on the rocker. After digestion, aortas were transferred to a new 60mm dish with fresh isolation medium. The adventitia was gently removed by pulling over the other end or tearing it. Aortas were washed once again and kept in the fresh isolation medium until all of them were done. Finally, two aortas were placed in a 60mm dish, covered with 2.5ml DMEM media (25mM glucose with 10% FBS and 1% PenStrep) and incubated at 37°C for 12 to 18 hours till next day. Culture conditions should be at 5% CO_2.

On the next day the aortas were subjected to elastase and collagenase digestion using 2.5ml of digestion medium (containing elastase and collagenase) at 37ºC in a rotating

rocker and after 22 minutes the aorta were gently sucked in a glass Pasteur pipette 15-20 times and once again placed in 37ºC. The whole digestion procedure was for 45min including all the manipulation. 8ml of DMEM (25mM glucose, 10% FBS and 1% PenStrep) was added to the digested aorta and centrifuged at 800rpm for 10min at 22ºC. The pellet was plated in a 60mm dish containing 2.5ml of DMEM (25mM) with 10% FBS and 2.5ml of proliferation media. Cells were gently aspirated and separated with a 10ml pipette and left for 24hr. After 24hr (on the next day) the plate was washed 4 to 5 times with sterile PBS and 2.5ml of DMEM (25mM) with 10% FBS and 2.5ml of proliferation media was added again. Wait till confluence (takes three to four days). For RNA isolation use the culture at about 70% confluence.

Aortic Root Sectioning and Immunofluorescent Imaging of Aortic Arches

Aortic roots were sectioned as described previously [141]. Hearts were excised, the aorta was cut at its base as close to the heart as possible, and stored in OCT compound at -80°C. The hearts were cut horizontally ≈3mm from the base of the aortic root. The remaining heart-aortic root was placed in a tissue mold with the root perpendicular to the bottom surface of the mold and covered in OCT compound. The refrozen tissue block was mounted to the cryostat chuck with the ventricular tissue facing outward. The ventricular tissue was sectioned away until the aortic sinus is reached. Serial sections were collected at 10μm/section, and 8 to 10 slides per aorta until the aortic wall was no longer visible. Slides were stored at -20°C until used.

Microscope slides containing frozen tissue sections were submerged in chilled acetone for 10 minutes and then incubated in Redusol 0.05% Cr_3O_3 for 2 minutes at 40°C. Slides were washed 5 to 6 times in automation buffer (GeneTex Cat# GTX 30931) and then

submerged in methanol containing hydrogen peroxide (3.2%) at 40°C for 2 minutes. Slides were washed 5 times in automation buffer and incubated with Triton X-100 0 (0.5%) for 10 minutes at 40°C. Again, slides were washed 5 times with automation buffer and incubated with the blocking agent (goat serum 15µL/mL) for 5 minutes at 40°C. Slides were washed 5 times with automation buffer and incubated with the primary antibody for 20 minutes at 40°C. Primary antibodies used were LPP3 (Biosensis Cat# M-1560; 1:100), Smooth muscle alpha-actin (Abcam Cat# ab5694; 1:100), CD68 (Abcam Cat# ab53444; 1:100), PECAM (BD Biosciences Cat# 553370; 1:100) and podocalyxin (R&D Systems Cat# AF1556; 1:100). Slides were washed again 5 times in automation buffer and covered in the immunofluorescent antibody (R&D Systems; 1:500) and incubated for 1 hour in the dark at room temperature. Slides were washed 5 times in automation buffer and submerged in Sudan Black (1% Sudan black in 70% EtOH) for 1 hour at room temperature before a final wash with automation buffer and imaging. Imaging was performed using a Nikon A1R confocal microscope with a spectral detector.

Statistical Analysis

All data are expressed as mean ± SEM unless otherwise noted. Statistical analysis was performed using an unpaired, two-tailed Student t-test unless otherwise noted. P-value < 0.05 is regarded as significant. Two-way ANOVA was used when multiple comparisons were made. Statistical analysis was performed using GraphPad Prism 7.

Results

Noncoding SNPs Decrease oxLDL-induced PPAP2B Upregulation and Impair C/EBPβ Binding

A meta-analysis of several GWAS investigations has implicated the gene *PPAP2B* in the development of CAD in humans conferring an increase in risk of disease for those harboring the risk allele. Rs17114036, the original risk loci implicated in the meta-analysis, lies in a noncoding region of *PPAP2B*, specifically in the final intron. We provided additional evidence by searching publically available microarray data and found that a proxySNP (rs9970807) is associated with decreased expression of *PPAP2B* in peripheral blood cell [142] – This is discussed in further detail in Chapter 3. Subsequent investigations into SNPs in linkage disequilibrium with rs17114036 reveal HAECs homozygous for the risk allele exhibit a diminished capacity to upregulate *PPAP2B* at baseline as well as following treatment with oxPAPC relative to heterozygote cells; therefore, the risk loci may act in a *cis*-manner on the gene in which it resides. A study exploring changes in transcriptional regulation during the lipid-induced transition of macrophages to foam cells identified rs72664324, in a noncoding region of PPAP2B, which is subject to dramatic chromatin remodeling. This SNP is in linkage disequilibrium with the CAD risk locus rs17114036 with an $r^2 > 0.8$ and falls within a C/EBPβ binding motif. As mentioned in the introduction, the risk allele G disrupts the CCAAT binding motif, diminishing C/EBPβ binding, and correlates with lower *PPAP2B* expression relative to the protective G allele.

In collaboration with Chris O'Callaghan's group at Oxford, we demonstrated with Western blotting that primary human macrophages display marked increases in LPP3 protein following exposure to oxLDL compared to vehicle treatment (Figure 2.1a) LPP3-specific phosphatase activity was significantly increased in oxLDL treated macrophages versus

vehicle controls determined by incubating immunoprecipitated LPP3 with LPA (Figure 2.1b) or S1P (Figure 2.1c) and measuring their respective product formation over time. These data support O'Callaghan's groups' work demonstrating a functional role for oxLDL-dependent C/EBPβ binding to the rs72664324 loci to potentially drive increased expression of *PPAP2B.*

Risk loci in *PPAP2B*'s locus at 1p32.2 are also on the same chromosome as the master LDL-C regulator *PCSK9* at 1p32.3; therein, it is feasible that these risk loci are acting in on *PCSK9* expression because PCSK9 levels can dramatically impact circulating LDL-C, and thus the development of atherosclerotic lesions. Looking at the previously mentioned proxySNP, rs9970807, we found no association with the risk allele and PCSK9 expression suggesting that SNPs in linkage disequilibrium with rs17114036 does not act on *PCSK9* [142]. Evidence provided by our group, Jake Lusis' and Chris O'Callaghan's groups demonstrate risk allele-dependent *cis* effects on *PPAP2B* expression. Considering LPP3's role regulating levels of LPA in addition to the ATX-LPA-LPP3 axis' extensive impact on vascular development, maintenance and pathogenesis it is conceivable that CAD-risk loci in *PPAP2B* are acting in *cis* to confer increased risk of CAD through diminished levels of LPP3.

LPP3 Expression is Upregulated in Mammalian Models of Atherosclerosis

Mounting genome-sequencing data has implicated PPAP2B in the risk of developing CAD through the presence of risk allele associations. Indeed, SNPs in linkage disequilibrium with rs17114036 display allelic-dependent variations in PPAP2B expression observed through independent studies investigating different vascular tissues. LPP3 expression is apparent in foam cells of human atheroma; however, little is known about its regulation in the progression of CAD. C57BL/6 mice are resistant to hypercholesterolemia and thus the development of atherosclerosis even on a high cholesterol diet and indeed display no

signs of plaque formation in the aortic roots of mice after 12 weeks of Western diet (Figure 2.2 left panel). *Apoe*$^{-/-}$ mice are very susceptible to hypercholesterolemia and lesion formation and following Western diet treatment show obvious upregulation of positive LPP3 staining in the vessel lesions that is not observed in the IgG control (Figure 2.2 middle and right panels). To delineate cell-specific LPP3 localization we analyzed the aortic roots of C57BL/6 mice and *Ldlr*$^{-/-}$ mice, another model of murine atherosclerosis, after 12 weeks of Western diet. Immunofluorescent confocal imaging shows colocalization of LPP3 with endothelial marker CD31 in C57BL/6 roots (Figure 2.3 top panel) consistent with vEC expression of LPP3; however, no LPP3 staining was observed in the remaining intima or media. *Ldlr*$^{-/-}$ aortic root lesions display pronounced positive LPP3 staining in both the endothelial cells as well as throughout the vessel/lesion wall (Figure 2.3 bottom panel). LPP3 also shows colocalization with SMC marker SMA (Figure 2.4 top panel) and macrophage maker CD68 (Figure 2.4 bottom panel) in the subintima indicating upregulation of LPP3 in these cells within atherosclerotic lesions. Colocalization of LPP3 and podocalyxin in *Ldlr*$^{-/-}$ roots (Figure 2.5) suggests, in endothelial cells, that LPP3 is localized to the apical membrane. To determine if CAD-dependent LPP3 upregulation is unique to mice, we examined LPP3 expression in porcine coronary arteries with pronounced lesion formation. LPP3 expression is substantial and colocalizes with SMA throughout porcine vessel lesions (Figure 2.6) suggesting that LPP3 is upregulated in multiple mammalian species with CAD. Finally, to delineate that the upregulation of LPP3 is specific to atherosclerotic lesions and not just the vasculature of hypercholesterolemic mice, we analyzed LPP3 protein in atherosusceptible (proximal aorta) and atheroprotected (thoracic aorta) regions of murine aorta with Western blotting. Indeed, LPP3 was upregulated only in the proximal aorta of *Apoe*$^{-/-}$ and *LDLr*$^{-/-}$ compared to the thoracic aorta (Figure 2.7). Consistent with our observations in the C57BL/6 aortic roots, LPP3 levels

were lower in the proximal aorta of wildtype mice, compared to its hypercholesterolemic counterparts, and was comparable to the levels observed in the thoracic aorta.

We found that the rs17114036 and rs72664324 SNP regions in *PPAP2B* are conserved in the mouse monocyte cell line RAW264.7 and that the rs17114036 locus serves as a binding site for the transcription factor c-Fos. The monocyte cell line contains the risk allele for rs72664324 (G/C) but the protective allele for rs17114036 (G/C). We designed major (Hrs4324G/C, Mrs4324G/C, Hrs4036A/T) and minor (Hrs4324A/T, Hrs4036G/C) allele-containing oligos with human and mouse DNA sequences containing the SNP regions and performed DNA affinity precipitation assays. Western blotting of RAW264.7 nuclear extracts that were immunoprecipitated with Hrs4324G/C (risk allele) did not display binding to C/EBPβ; however nuclear extracts immunoprecipitated with Hrs4324A/T (protective allele) did (Figure 2.8a), thus supporting the observations of Reschen et al. [135]. Similarly, Hrs4036A/T (risk allele) did not exhibit c-Fos binding whereas Western blots run with nuclear extracts immunoprecipitated with Hrs4036G/C (protective allele) and Mrs4036G/C display c-Fos binding (Figure 2.8b). Development of CAD coincides with increased expression of LPP3 in the SMCs and macrophages within lesions; additionally, the CAD-associated risk loci are conserved in a mouse-derived cell line and murine C/EBPβ and c-Fos transcription factors exhibit allele-specific binding to human and mouse oligos containing the SNP alleles suggesting that the phosphatase may play a role in the development and/or progression of disease.

Inducible Global Reduction of Ppap2b Increases Lesion Formation in Murine Models of Atherosclerosis

Our lab has previously identified a role for endothelial-derived LPP3 in the maintenance of vEC barrier function, in a LPA-dependent manner, and reducing inflammation in a model of LPS-induced systemic inflammation *in vivo;* as well as a role for SMC-specific

LPP3 decreasing neointimal hyperplasia and IL-6 expression following carotid artery ligation *in vivo.* Seeing that LPP3 reduces vEC barrier dysfunction, limits neointimal hyperplasia following injury and limits proinflammatory cytokine expression, all of which are hallmarks of CAD, its upregulation in atherosclerotic lesions could be a vascular mechanism to combat CAD. To test this hypothesis we examined the development of atherosclerotic lesions in a murine model of CAD.

Both germline deletion and endothelial cell-specific deletion of *Ppap2b* are embryonically lethal as described previously. In order to study the effects of a global reduction in LPP3 in the context of atherosclerosis we generated an inducible global knockdown of *Ppap2b* by crossing *Ppap2b*$^{fl/fl}$ *Ldlr*$^{-/-}$ (referred to as fl/fl henceforth) mice with mice expressing Cre recombinase under the control of the inducible MX-1 promoter to generate *mx1-ppap2b*$^{\Delta}$ *Ldlr*$^{-/-}$ (referred to as *MX*-1Δ) mice following pI:pC treatment at postnatal days 3 to 5. MX-1-mediated knockdown of *Ppap2b* was confirmed through relative gene expression analysis using qRT-PCR on bone marrow cells (Figure 2.9a). Upon weaning, mice were placed on a Western diet for 12 weeks to induce hyperlipidemia and atherosclerotic lesion formation. We used Western blotting to measure proximal aortic LPP3 and observed diminished levels of the phosphatase in MX-1Δ mice compared to fl/fl controls (Figure 2.9b). Confocal immunofluorescent imaging of aortic root lesions shows colocalization of LPP3 and vEC marker PECAM in fl/fl mice, which is absent in MX-1Δ mice (Figure 3.8c). *Ppap2b* deficiency did not alter body weight in either male or female mice (Table 2.1) nor was there a difference in blood pressure among fl/fl and MX-1Δ mice (Table 2.2) determined by tail-cuff measurement. We next analyzed circulating plasma lipids using enzymatic colorimetric assays provided by Wako Diagnostics and FPLC. There were no differences in total plasma cholesterol or the cholesterol distribution (Figure 2.10a and b) between MX-1 Δ and fl/fl controls; similarly, total plasma triglycerides remained

unchanged (Figure 2.10c). LPP3 enzymatically inactivates a variety of bioactive phospholipids such as LPA and S1P that are found in abundance in the plasma and are known to alter vEC barrier function. We looked at levels of LPP3 substrates in the plasma using HPLC MS/MS and found that MX-1Δ mice display significant increases in total LPA (≈2.2-fold, $p<0.001$) and S1P (≈1.5-fold, $p<0.01$) but not LPC compared to controls (Figure 2.10d) indicating that global reductions in LPP3 alter its phospholipid substrates in the circulation. MX-1Δ mice have 30% ($p<0.01$) increase in lesion formation in the proximal aorta compared to the fl/fl control mice reported as percent of total area using *en face* analysis (Figure 2.11a). Coinciding with the increase in atherosclerosis development, lipid analysis of the proximal aortas revealed ≈2-fold increase in total LPA content ($p<0.05$) compared to fl/fl mice (Figure 2.11b). Relative gene expression analyses in the proximal aortas using qRT-PCR reveal ≈1.9-fold increases in expression of macrophage marker *Cd68* ($p<0.05$) in MX-1Δ mice and a trend towards increased proinflammatory *Il-6* relative to fl/fl control mice (Figure 2.11c). Confocal immunofluorescent imaging of aortic root lesions from the MX-1Δ and fl/fl mice, in accordance to the *Cd68* expression, appears to show increased positive CD68 staining in the *Ppap2b* deficient mice (Figure 2.11d). Leukocyte-adhesion molecule ICAM-1 expression is markedly upregulated in the lesions of MX-1Δ mice compared to fl/fl as well (Figure 2.12).

Leukocyte-derived LPP3 Fails to Protect Against CAD

MX-1Δ lesions showed increased levels of ICAM-1 which is consistent with a preponderance of macrophage infiltration into the vessel wall [55] and consistent with our observations of increased CD68 staining in lesions and *Cd68* expression in proximal aorta of MX-1Δ compared to fl/fl mice. The inducible MX-1 promoter is expressed in epithelial and endothelial cells throughout the body including aorta, liver, lung, spleen, etc. [citation]; it also shows pronounced expression in hematopoietic cells including monocytes.

Because LPP3 expression is upregulated during the conversion of primary human macrophages to foam cells *in vitro [135]* and global *Ppap2b* deficiency increases macrophage markers in lesions we investigated whether leukocyte-specific expression of LPP3 conveys protection against lesion formation in mice.

We generated a murine model of myeloid-specific deficiency in *Ppap2b* by crossing *Ppap2b*$^{fl/fl}$ mice with mice harboring Cre recombinase under the control of the LysM promoter to yield *Lysm-ppap2b*$^{\Delta}$ offspring. We transplanted *Lysm-ppap2b*$^{\Delta}$ (LysM-Δ) and *Ppap2b*$^{fl/fl}$ bone marrow cells into lethally irradiated *Ldlr*$^{-/-}$ host mice (referred to as LysM-Δ-LDLr and fl/fl-LDLr respectively for this study). LysM-mediated deletion of Ppap2b was confirmed using relative gene expression analysis of bone marrow-derived macrophages (BMDMs) (Figure 2.13a). As before, mice were fed Western diet for 12 weeks to induce hyperlipidemia and lesion formation. LysM-Δ-LDLr mice show no change in plasma total cholesterol compared to fl/fl-LDLr mice (Figure 2.13b). In contrast to observations in mice with global reductions in *Ppap2b*, leukocyte-specific deficiency of *Ppap2b* did not alter circulating levels of LPA; however, we did see an increase in total circulating S1P ($p<0.05$, Figure 2.13c). Similar to our observations in human macrophages, BMDMs from *Ppap2b*$^{fl/fl}$ mice treated with oxLDL (50μg/mL) for 48 hours show significant upregulation of *Ppap2b* expression following treatment with oxLDL (Figure 2.13a). *Ppap2b* deficient foam cells exhibit significantly increased levels of proinflammatory *Il-1β* and *Il-12b* (≈2.7-fold, $p<0.01$ and ≈6.4-fold, $p<0.01$ respectively) relative to BMDMs from *Ppap2b*$^{fl/fl}$ mice (Figure 2.13b). *En face* analysis of the proximal aortas revealed no differences in atherosclerotic lesion formation between LysM-Δ-LDLr mice and their fl/fl-LDLr controls (Figure 2.14) suggesting that leukocyte-derived LPP3 is not sufficient to confer the same protection to atherosclerosis as was observed in the MX-1 model. These data suggest that while leukocyte-derived LPP3 alone is not sufficient to protect against the formation of

atherosclerotic lesions, it does play a role in regulating foam cell LPA accumulation and proinflammatory cytokine expression.

SMC-specific Ppap2b Expression is Athero-protective in Mice

We next investigated whether LPP3 expressed by SMCs alters the development of CAD in mice. Utilizing Cre recombinase under the control of the SM22 promoter, we generated SMC-specific knockout of LPP3 in mice on an *Ldlr*$^{-/-}$ background (SM22-Δ). SMCs were isolated from the aorta of SM22-Δ and fl/fl mice and knockdown of *Ppap2b* was confirmed with relative gene expression analysis using qRT-PCR (Figure 2.15a). Similar to the two previously described mouse models, SM22-Δ and fl/fl mice show no differences in cholesterol or total circulating LPA following 12 weeks on Western diet (Figure 2.15b and c). A ≈2.7-fold increase ($P<0.001$) in lesion formation was observed in the proximal aorta of SM22-Δ mice compared to fl/fl (Figure 2.16a). Analysis of the proximal aortas of these mice reveal a ≈1.9-fold increase ($p<0.05$) in SM22-Δ total LPA content compared to fl/fl controls (Figure 2.16b); as well as, ≈5.2-fold upregulation ($p<0.05$) of *Il-6* expression in SM22-Δ proximal aorta (Figure 2.16c). Confocal immunofluorescent imaging of aortic root lesions display a pattern of increased CD68 staining in SM22-Δ lesions compared to fl/fl controls (Figure 2.16d). These data implicate SMC-derived LPP3 in conferring protection against atherosclerotic lesion formation in mice and reduced LPP3 in SMCs results in an increase in proinflammatory *Il-6* expression as well an increase in the area of CD68 positive cells.

Phenotypic Switching of Contractile SMCs to Foam Cells Increases C/EBPβ binding in PPAP2B

SMC-derived LPP3 is known to limit the development of intimal hyperplasia and reduce expression of inflammatory cytokine *Il-6* in mice which very well may be the mechanism of protection we see in our murine model of CAD presented in this study. Recent evidence

indicates that SMCs contribute to foam cell populations in atherosclerotic lesions and up to 50% of oil red-O stained cells in plaques may be of SMC origin [112, 120, 122]. Cholesterol loading of murine vascular SMCs *in vitro* causes a phenotypic switch of contractile SMC to a foam cell-like state characterized by downregulation of contractile SMC markers such as *Acta2* and upregulation of macrophage marker *Cd68 [112]. O*ur lab has previously reported downregulation of *Acta2* and *Tagln* in uninjured vessels from *Sm22-ppap2bΔ* compared to *Ppap2b*$^{fl/fl}$ controls suggesting an absence of LPP3 contributes to dedifferentiation of SMCs [133]. We investigated whether *PPAP2B* expression is altered in the phenotypic switching of a SMC to a foam cell *in vitro*.

Loading human coronary artery SMCs (caSMCs) with cyclodextran-cholesterol (10μg/mL) for 72-hours (referred to as SMC foam cells) results in significant decreases in *TAGLN and ACTA2* ($p<0.0001$) as well as significant increases in *CD68* expression ($p<0.01$) that was not observed in vehicle treated SMCs (referred to as SMCs) (Figure 2.17a). SMC foam cells exhibited a ≈2.4-fold increase ($p<0.05$) in *PPAP2B* expression compared to SMCs (Figure 2.16b). SMC foam cells also display ≈3.0-fold upregulation ($p<0.05$) of *IL-6* expression compared to vehicle treated controls (Figure 2.17b) suggesting heightened inflammation from these cells.

SMC conversion to SMC foam cells results in a 2.3-fold increase ($p<0.05$) in *CEBPB* expression whereas other transcription factors show no change (Figure 2.17c). Interestingly, Western blotting with SMC foam cell nuclear extracts immunoprecipitated with Hrs4324A/T (protective allele) and not Hrs4324G/C (risk allele, show C/EBPβ binding that is not observed in the vehicle treated SMCs (Figure 2.18) indicating that cholesterol loading induces C/EBPβ localization to the nucleus.

Discussion

PPAP2B has been implicated in development of CAD due to the presence of noncoding SNPs in the final intron of the gene that confers an increase in risk of disease [4]. A proxySNP in linkage disequilibrium with rs17114036 is associated with decreased *PPAP2B* expression in human peripheral blood cells [142]. HAECs homozygous for the risk allele have a diminished ability to upregulate *PPAP2B* expression associated with exposure to oxPAPC compared to heterozygote cells [126]. In this study we present data obtained in collaboration with Chris O'Callaghan's group at Oxford that demonstrates human macrophages display an oxLDL-induced upregulation of LPP3 protein and LPP3-associated phosphatase activity compared to vehicle treated macrophages (Figure 2.1). LPP3 expression is also upregulated in models of vascular injury [22, 133] and limits development of neointimal hyperplasia. We compared murine models of atherosclerosis, *Ldlr*$^{-/-}$ and *Apoe*$^{-/-}$ mice, to C57BL/6 wildtype mice, which are known to be resistant to hyperlipidemia and lesion formation. LPP3 expression appears absent in the vessel subintima and media of C57BL/6 mice but is dramatically upregulated in *Apoe*$^{-/-}$ and *Ldr*$^{-/-}$ lesions as well as atherosusceptible regions of the proximal aorta compared to atheroprotected thoracic aorta (Figure 2.2, 2.3 and 2.7). We also demonstrated murine C/EBPβ binding to the protective allele of rs72664324 and an additional transcription factor, c-Fos, which binds to the protective allele of rs17114036 (Figure 2.8). We hypothesized that LPP3 is protective in murine models of atherosclerosis. Using a model of global reduction of *Ppap2b* expression driven by Cre Recombinase under the control of the MX-1 promoter we generated adult animals with reduced LPP3 expression on the *Ldlr*$^{-/-}$ background. MX-1Δ mice developed larger lesion formation (Figure 2.11a) despite no differences in circulating cholesterol levels (Figure 2.10a). To test whether there is a cell-specific effect we generated mice with leukocyte-specific and SMC-specific deletion of *Ppap2b*. LysM-Δ-LDLr mice show no differences in development of atherosclerosis after

12-weeks on Western diet (Figure 2.14). Contrary to LysM-Δ-LDLr mice, SM22-Δ mice displayed greater atherosclerotic lesion formation compared to controls (Figure 2.16a) implicating SMC-derived LPP3 as a protective agent in the context of CAD. Finally, we examined the expression of *PPAP2B* in the phenotypic switching of primary human SMCs to SMC foam cells. Similar to observations in primary human macrophages, caSMCs upregulate *PPAP2B* expression 2.4-fold compared to controls (Figure 2.17b). *CEBPB* expression is increased 2.3-fold in SMC foam cells compared to SMCs (Figure 2.17c) and treatment of caSMCs with cyclodextran-cholesterol, to drive the phenotypic switch, stimulates C/EBP-β binding to the rs72664324 protective allele (Figure 2.18) suggesting similar epigenetic changes in chromatin structure may be affecting C/EBPβ-dependent *PPAP2B* expression in SMCs that were observed in primary human macrophages.

Disease-associated noncoding SNPs identified in GWAS analyses carry out their mechanism of action in either a *cis*- or *trans*-manner. *Cis*-acting SNPs typically alter the expression of the gene in which they reside, are at least 1Mb proximal to the start of the gene or are at least 1Mb distal to the end of the gene; whereas *trans*-acting SNPs are capable of changing the expression of genes up to anywhere else in the genome and have been shown to act on genes upwards of 50Mb away [143]. Rs17114036 in *PPAP2B* is at locus 1p32.2, which happens to be on the same chromosome as the master LDL-C regulator *PCSK9* at locus 1p32.3. PCSK9 binds LDLr driving internalization and subsequent lysosomal degradation of the LDLr-PCKS9 complex [144]. Decreased LDLr in the liver leads to increases in plasma LDL-C; in fact, individuals with gain-of-function mutations in *PCSK9* are classified as having familial hypercholesterolemia, have profound levels of circulating LDL-C and experience premature development of CAD between ages 30-40 [145]. Despite evidence from microarray databases demonstrating no altered rs-9970807-dependent *PCSK9* expression it is still conceivable that rs17114036 could act

as a *trans*-regulator of *PCKS9* and increase risk of disease by altering LDL-C. In this study we demonstrate a protective role for LPP3 in the development of atherosclerotic lesion formations in mice on an *Ldlr*$^{-/-}$ background. By using mice deficient in the LDLr we can eliminate any PCSK9-dependent effects that is confirmed in our models by observing LPP3-dependent protection in CAD, which despite no differences in circulating cholesterol levels (Figures 2.10a and 2.15b). Taking into consideration that CAD-associated risk alleles are associated with diminished expression of *PPAP2B* and that reductions in *Ppap2b* in mice result in exacerbated lesion formation independent of PCSK9-mediated alterations in cholesterol we posit that CAD-associated rs17114036 confers its increased risk of disease through a *cis*-regulatory effect on *PPAP2B.*

In a study published in PLOS Genetics in 2015, Reschen et al. [135] investigated changes in transcriptional regulation induced during the oxLDL-induced conversion of macrophages to foam cells, a critical process in the progression of CAD [135]. Formaldehyde-assisted inducible regulatory element sequencing (FAIRE-seq) analysis reveals dynamic remodeling of open chromatin regions throughout the genome including in a region of *PPAP2B,* which harbors rs72664324. Rs72664324 is in linkage disequilibrium with CAD risk-associated allele rs17114036 with an $r^2 > 0.8$ and happens to be in a CCAAT binding domain for the transcriptional regulator C/EBP-β. The risk allele interrupts the binding motif and inhibits oxLDL-induced C/EBP-β binding; subsequently, upregulation of *PPAP2B* expression in the conversion of human macrophages to foam cells was diminished in cells homozygous for the CAD-risk allele (GG) compared to cells that were heterozygotes (AG). SMC-specific LPP3 expression limits the development of atherosclerotic lesions in our model implicating the phosphatase as being protective in CAD. *PPAP2B* upregulation in foam cells may be an intrinsic means of protection although the mechanism remains to be described. In the present study we show that primary human

caSMCs show similar upregulation of *PPAP2B* expression and cholesterol-dependent C/EBP-β binding to rs72664324 (2.17b and 2.18) that was observed by Reschen et al. in primary human macrophages, albeit an allelic-dependent variation in *PPAP2B* expression should still be confirmed. Because SMC-derived LPP3 is sufficient to confer protection against lesion formation in mice, and that C/EBPβ binding to rs72664324 is inhibited in macrophages homozygous for the CAD-associated risk allele, it is feasible that individuals homozygous for the rs17114036 risk allele are at greater risk of developing CAD due inhibited C/EBPβ-dependent upregulation of *PPAP2B* in vascular SMCs.

In this study we demonstrate a protective role for LPP3 in the development of lesion formations in a murine model of atherosclerosis. Global reductions in LPP3 resulted in increased lesion formation (Figure 2.11a) independent of changes in cholesterol (Figure 2.10a). The MX-1 promoter is inducible in a wide range of epithelial cells throughout the body including liver, lungs, spleen, aorta, and hematopoietic cells [146]. Confocal immunofluorescent staining showed MX-1-mediated deletion of *Ppap2b* in the vEC of aortic root lesions (Figure 2.9c). MX-1Δ mice also showed significant increases in total LPA in their circulation and their proximal aortas compared to fl/fl controls. Our lab has previously identified a role for endothelial cell-specific LPP3 in maintaining vEC barrier function [22]. vEC-specific deletion of *Ppap2b* increased vascular permeability which could be ameliorated with a pan-receptor antagonist BrP-LPA and the ATX inhibitor PF8380 suggesting that LPA signaling is mediating the LPP3-dependent barrier dysfunction. Similar reports on LPA1 and LPA6 suggest that LPA induces vEC barrier dysfunction and that siRNAs targeting LPP3 exacerbate the LPA6-dependent cytoskeletal changes in HUVEC cells [84]. Considering the role of vEC dysfunction in the development and progression of CAD, it is feasible that MX-1Δ mice develop increased lesion formation through an LPP3-LPA dependent increase in vEC barrier permeability. Similarly,

increased lesion formation in SM22-Δ mice coincided with increased total LPA content in the proximal aorta compared to fl/fl controls (Figure 2.16b). Our lab has previously identified a role for LPP3 in regulating LPA-dependent SMC migration and proliferation. Presumably, the decreases in SMC-LPP3 could confer LPA-dependent migration and proliferation of vascular SMCs driving an increase the lesion development in these mice.

We propose a model of LPP3-dependent protection against the development and progression of CAD in mice that is independent of cholesterol and LDLr effects and that individuals harboring CAD-associated risk alleles in *PPAP2B* are at greater risk of disease due to a diminished ability to upregulate LPP3 expression (Figure 2.17).

Acknowledgements

The data presented in this chapter would not be possible without the help and collaborative efforts of many members of Dr. Smyth and Dr. Morris' lab. Immunofluorescent staining was performed by Julia Vandra and confocal images were taken by Dr. Ja Anthony Brandon. LC/MS/MS to determine phospholipid content was carried out by the expertise of Manjula Sunkara and Dr. Sony Soman and interpreted by either myself or Dr. Andrew Morris. BMDM isolation, culture, and experiments from our leukocyte-specific knockout mice was performed with the integral help of Margo Ubele. Dr. Guogen Mao designed and performed the DNAP assays to determine transcription factor binding to SNP regions in *PPAP2B*. Dr. Alan Daugherty's lab was integral in these experiments as well as they trained me in performing and analyzing the *en face* technique. Finally, Liping Yang was critical for this project as she performed most of the experiments involving the SMC-specific knockout mice.

Table 2.1

	fl/fl			MX-1Δ		
	n	Body Weight (g)	SEM	*n*	Body Weight (g)	SEM
Males	11	31.49	0.88	18	30.75	1.14
Females	13	23.15	0.92	27	23.59	0.53

Global deletion of LPP3 does not affect body weight. Mice were placed on Western diet for 12 weeks in order to induce hyperlipidemia and development of atherosclerosis. Prior to take down, mouse weights were recorded with respect to sex.

Table 2.2

		Systolic		Diastolic	
	n	Blood Pressure (mmHg)	SEM	Blood Pressure (mmHg)	SEM
fl/fl	6	108.37	1.34	80.90	1.82
MX-1Δ	7	103.34	1.34	71.85	1.15

Global deletion of LPP3 does not alter blood pressure. Blood pressure was recorded using the non-invasive CODA® tail-cuff blood pressure system. 25 blood pressure readings were taken from each mouse every day for 5 days and averaged. Daily averages were then used to determine the average blood pressure reading for each mouse.

Figure 2.1

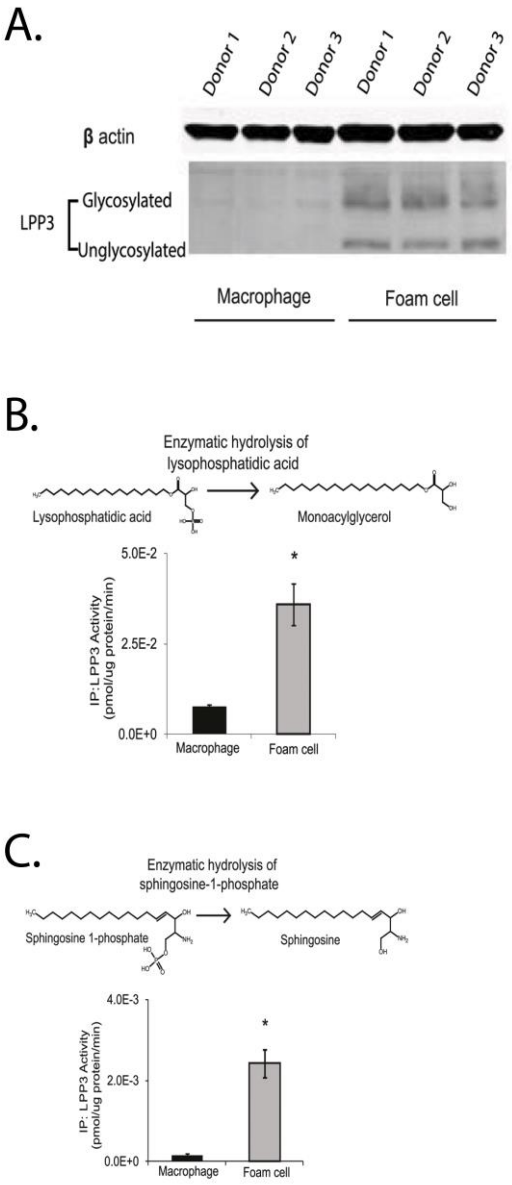

oxLDL increases LPP3 expression and LPP3-specific phosphatase activity. **(A)** Primary human macrophages were treated with oxLDL (50µg/mL) for 48 hours and LPP3 protein was determined by Western blotting and normalized to beta-actin. **(B and C)** LPP3 was immunoprecipitated from vehicle or oxLDL treated macrophage lysates (n=3 donors per condition) and phosphatase activity was determined by LC MS/MS from samples incubated with **(B)** LPA and measuring the generation of MAG or **(C)** incubating with S1P and measuring sphingosine generation. Data shown are mean ± SEM. *P<0.05 by unpaired Student's t-test.

Figure 2.2

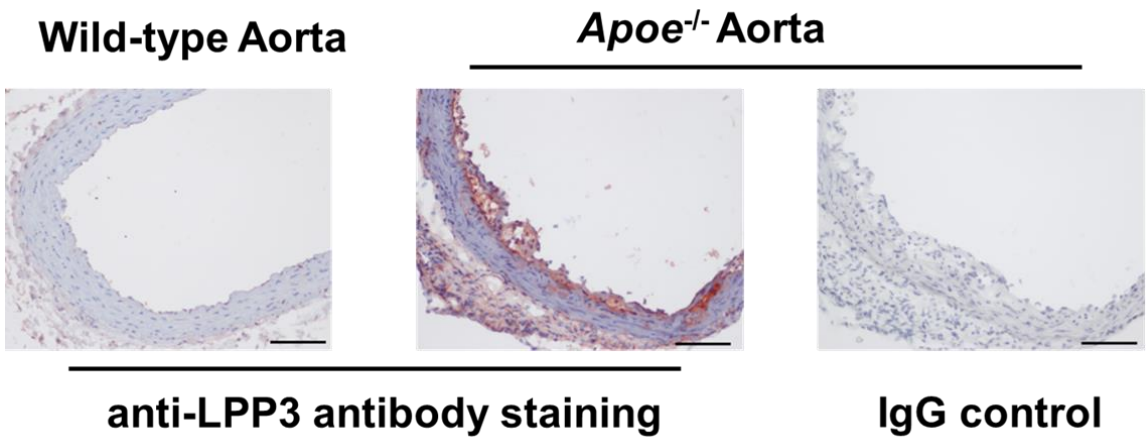

LPP3-positive staining is upregulated in *Apoe*$^{-/-}$ atherosclerotic lesions. C57BL/6 wildtype mice and atherosusceptible *Apoe*$^{-/-}$ mice were fed Western diet for 12 weeks. Immunohistochemical staining of aortic roots of type mice and *Apoe*$^{-/-}$ mice was performed with rabbit anti-LPP3 (Left and Middle) or rabbit anti-IgG (Right) as an immunoglobulin control. Scale bar = 300µm.

Figure 2.3

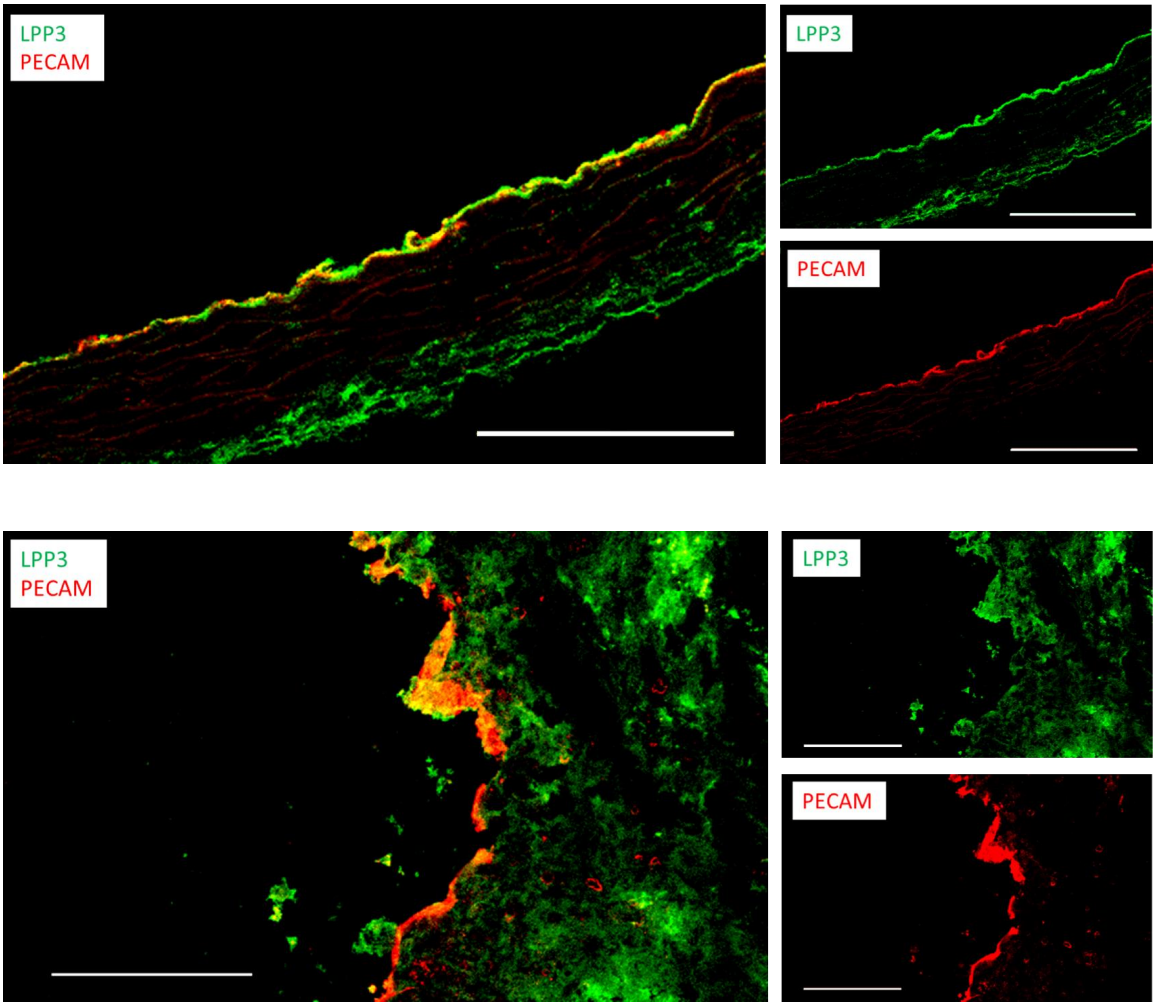

LPP3 expression in LDLr$^{-/-}$ mouse atherosclerotic lesions compared to C57BL/6 mice. (Top) C57BL/6 wild-type mice and **(Bottom)** Ldlr$^{-/-}$ mice were fed Western diet for 12 weeks. Aortic root sections were stained for LPP3 (Green) and endothelial marker PECAM (Red) as described in Materials and Methods. Scale bar = 100µm.

Figure 2.4

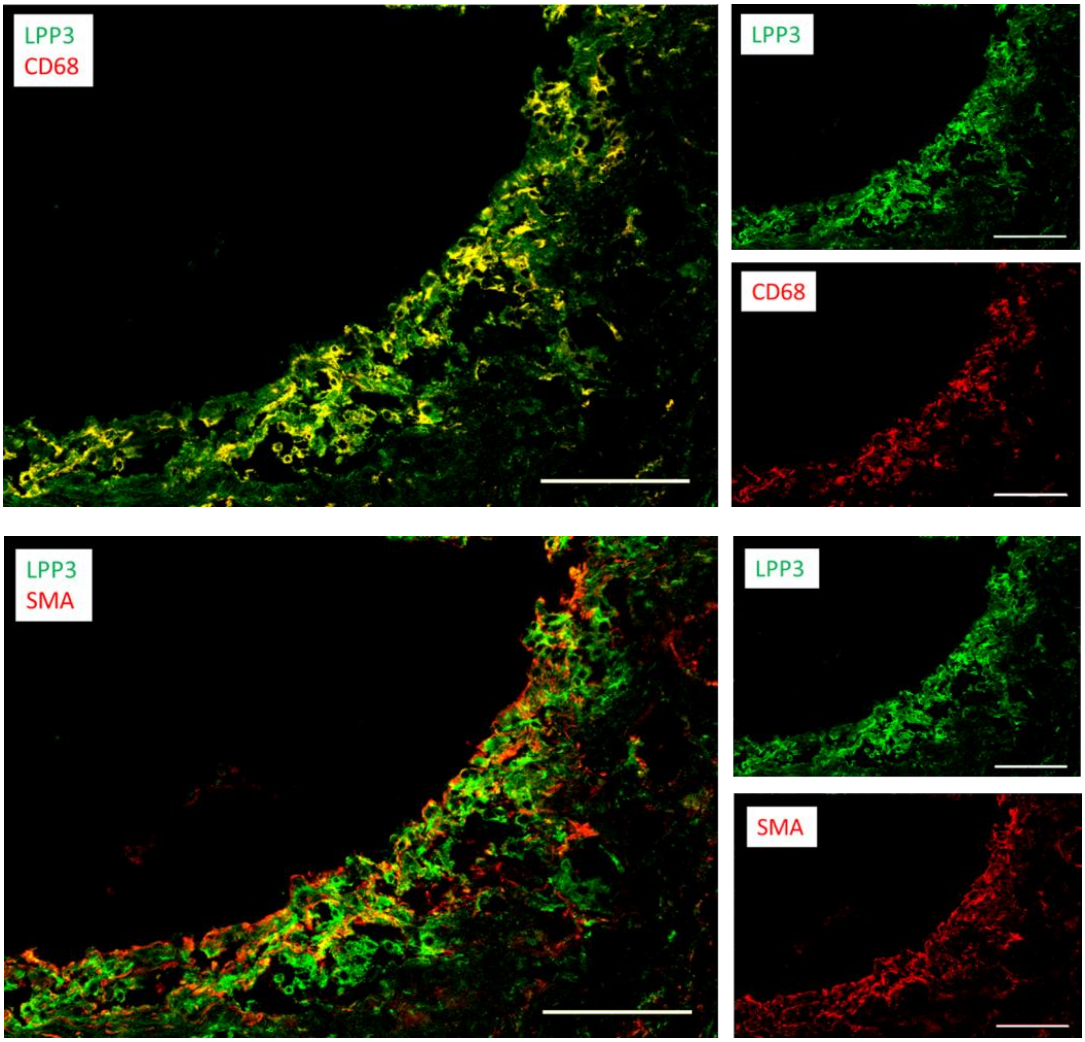

LPP3 colocalizes with SMCs, and macrophages, in LDLr$^{-/-}$ mouse atherosclerotic lesions. Aortic root sections from Ldlr$^{-/-}$ mice fed Western diet for 12 weeks were stained with LPP3 (Green) and macrophage marker CD68 (red; top) or SMC marker smooth muscle alpha-actin (Red; bottom) as described in Materials and Methods. Scale bar = 100µm

Figure 2.5

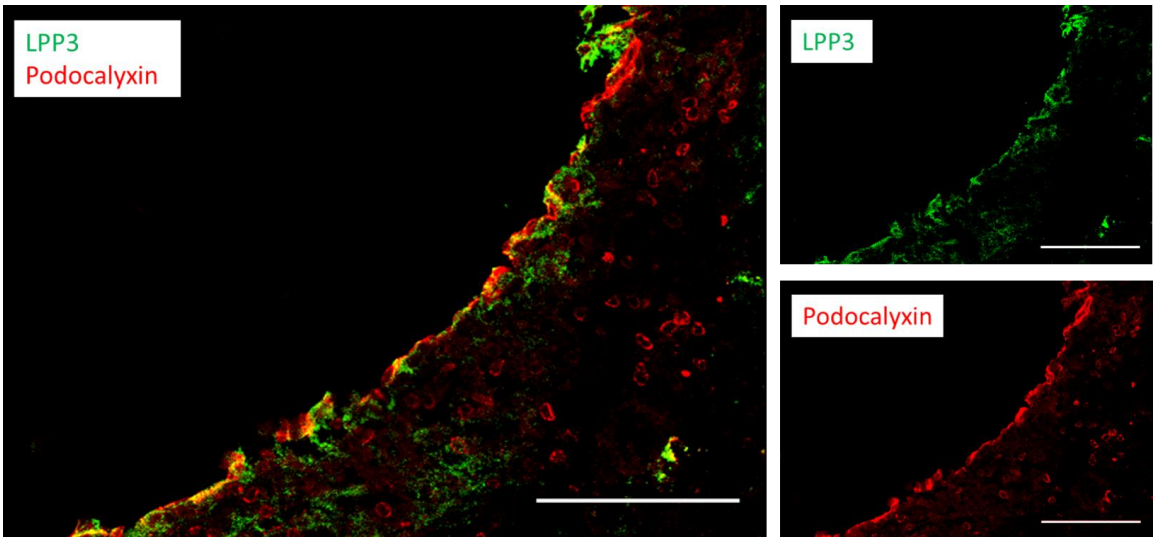

LPP3 localizes to the apical membrane of aortic endothelial cells. Aortic root sections from Ldlr$^{-/-}$ mice fed Western diet for 12 weeks were immunofluorescently stained with antibodies to LPP3 (Green) and apical membrane marker podocalyxin (Red) as described in Materials and Methods. Scale bar = 100µm

Figure 2.6

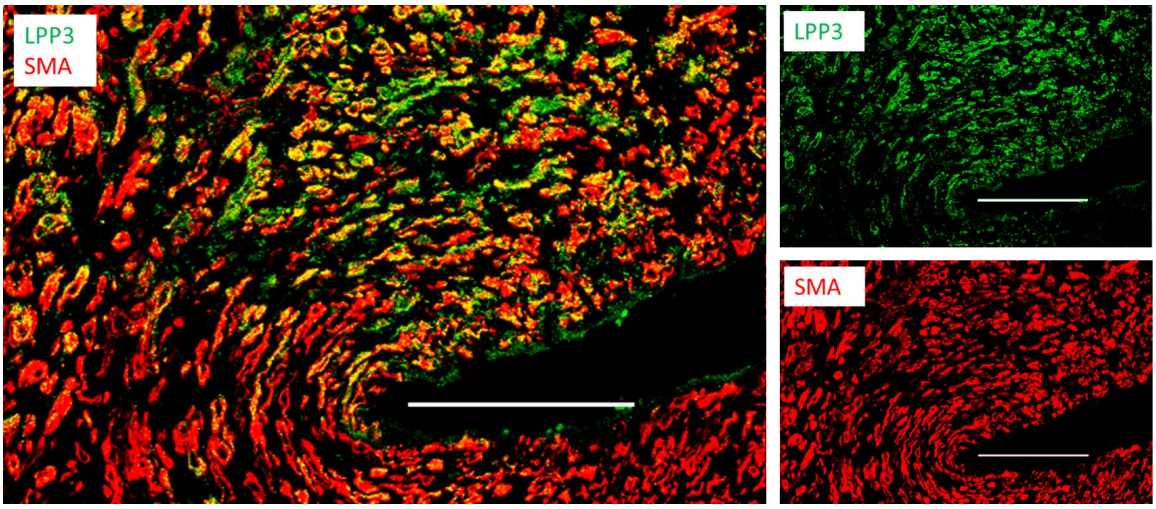

LPP3 is abundantly expresesed in porcine atherosclerotic lesions. Aortic root sections from Ldlr$^{-/-}$ mice fed Western diet for 12 weeks were immunofluorescently stained with antibodies to LPP3 (Green) and SMC marker smooth muscle alpha-actin (Red) as described in Materials and Methods. Scale bar = 100μm

Figure 2.7

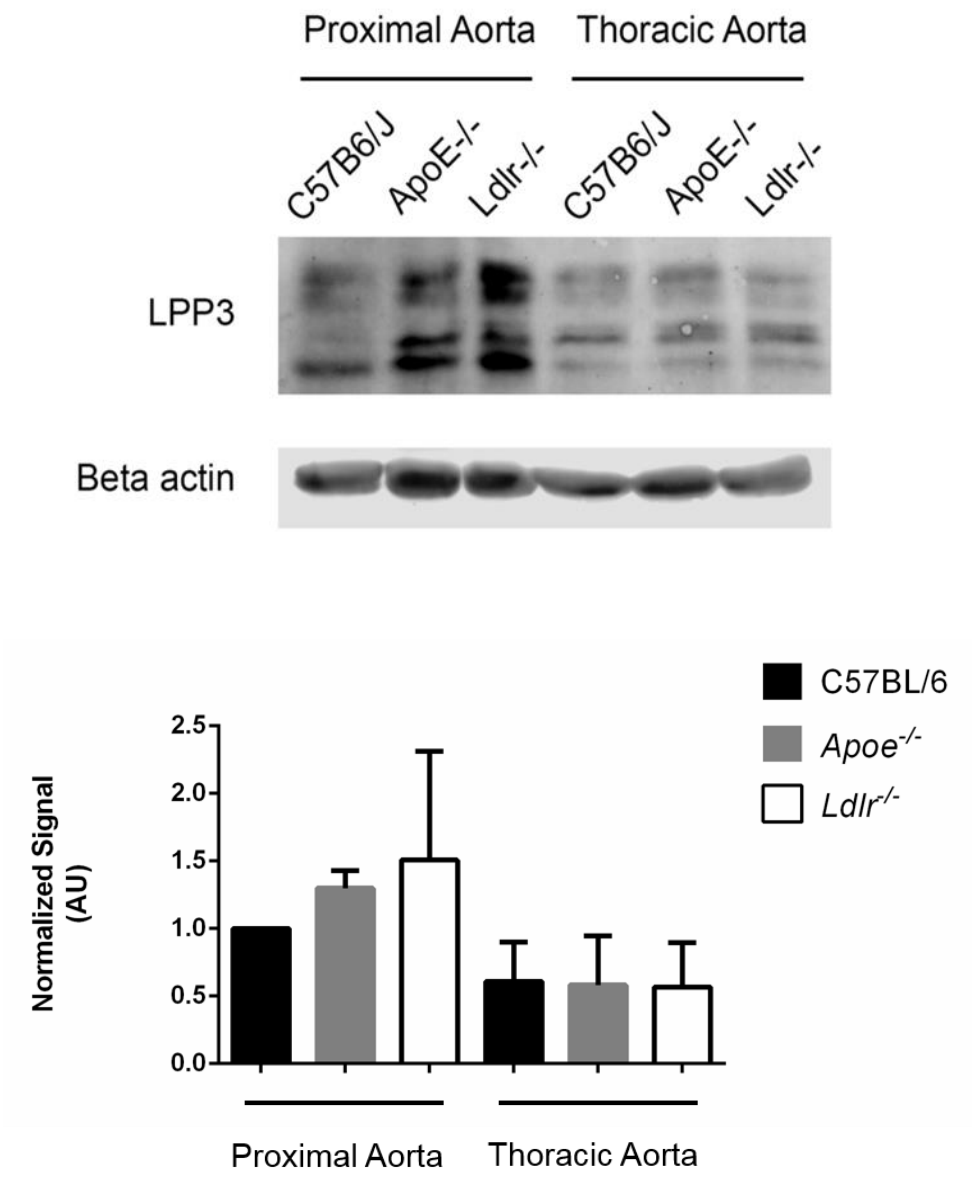

LPP3 expression in atherosusceptible regions of murine aorta. LPP3 in atherosusceptible proximal aorta and atheroprotected thoracic aorta of C57BL/6 wild-type, Ldlr$^{-/-}$ and Apoe$^{-/-}$ mice (n=3 tissue from each genotype was pooled) was measured by immunoblot analysis (Top). LPP3 at ≈37kD was normalized to beta-actin at ≈42kD as described in the Methods and Materials. (Bottom) Western blot quantification normalized to beta-actin. Data presented as mean ± SEM.

Figure 2.8

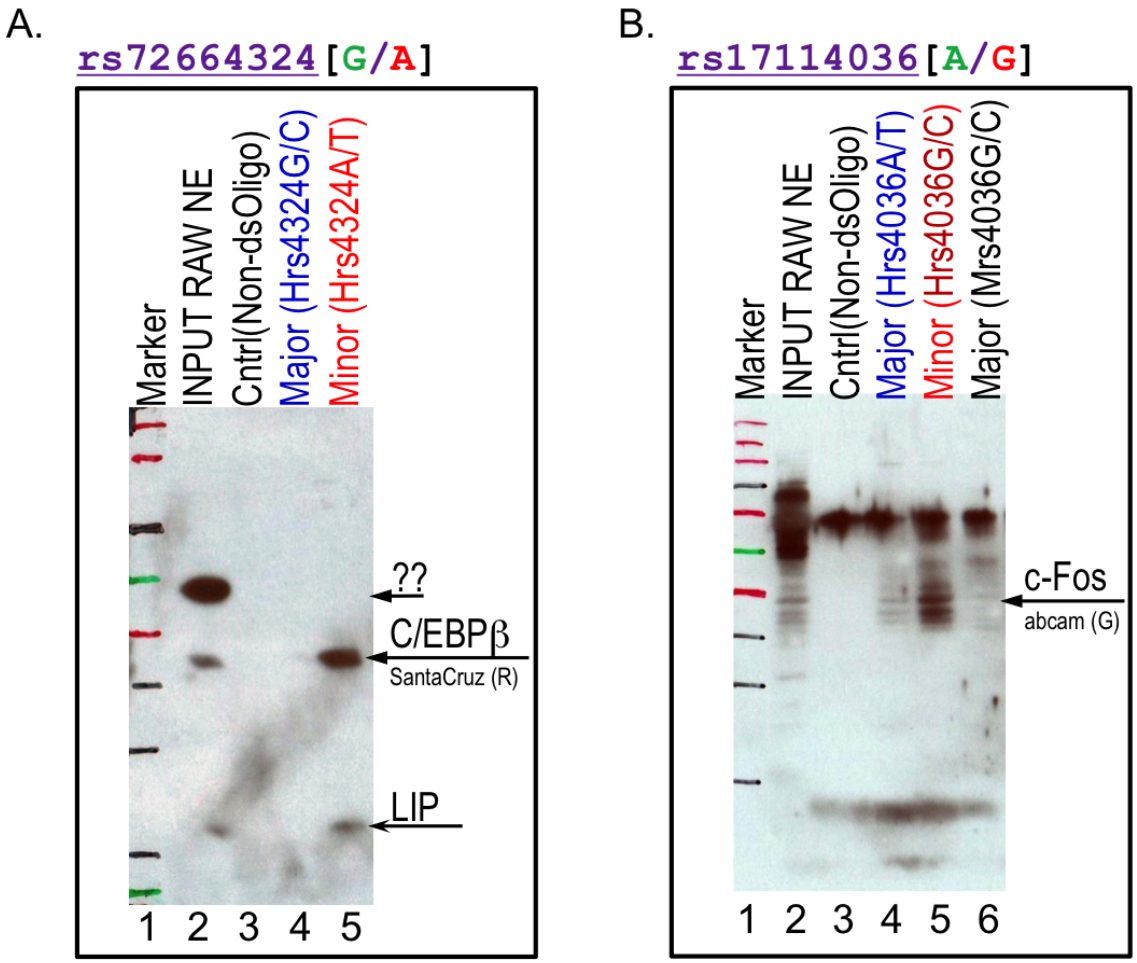

C/EBPβ binding in mouse monocyte cell line RAW264.7 RAW264.7 cells were treated with oxLDL (50μg/mL) for 24 hours. Transcription factor binding determined by DNA affinity precipitation assay (DNAP) using biotin-labeled oligos for rs72664324 risk and protective alleles and rs17114036 risk and protective alleles with nuclear extracts as described in Materials and Methods. After DNAP, C/EBPβ (Left) and c-Fos (Right) binding was determined with Western blotting.

Figure 2.9

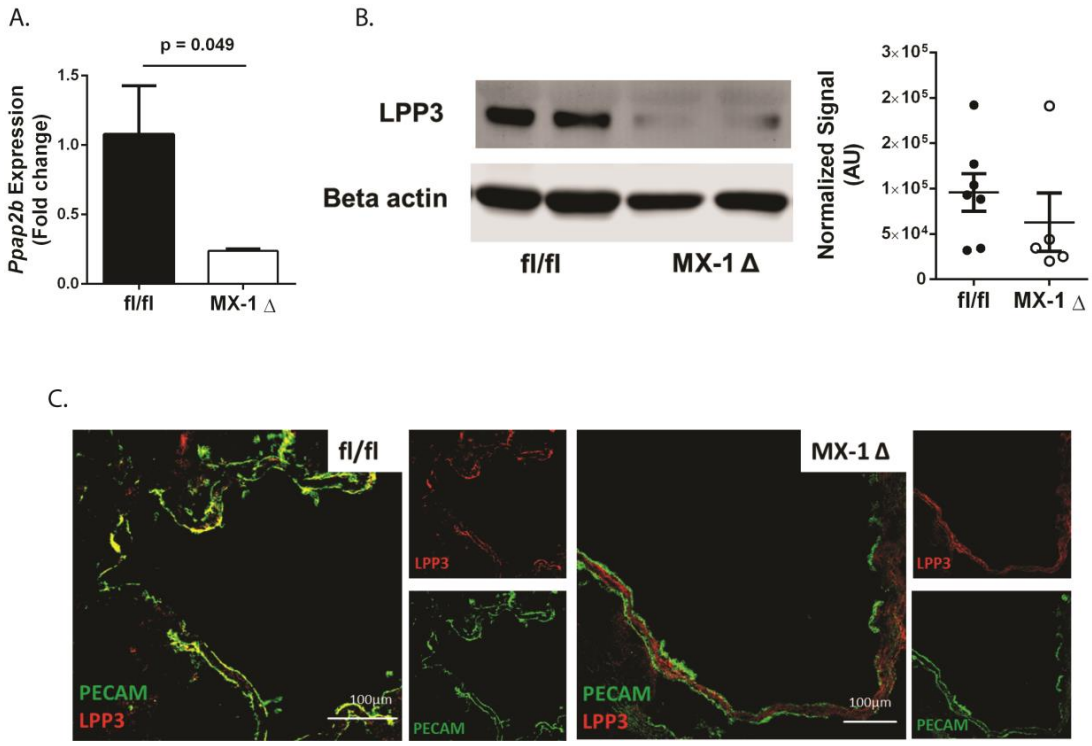

Reduced *Ppap2b* expression in bone marrow and proximal aorta from MX-1Δ mice. *Ppap2b*$^{fl/fl}$ mice without (fl/fl) or with Mx1-Cre transgene (MX-1Δ) on *Ldlr*$^{-/-}$ background were injected with pI:pC (50μL of 10mg/mL) between postnatal days 3 and 5. **(A)** Bone marrow cells were isolated from the femurs of MX-1Δ and fl/fl mice (n=3 of each genotype) and qRT-PCR analysis was performed as described in Methods and Materials. Data are presented as mean ± SEM. *P<0.05 determined by Students t-test. **(B)** Following 12 weeks on Western diet, protein lysates from the proximal aortas of MX-1Δ and fl/fl mice were analyzed by Western blotting. LPP3 levels were quantified by normalizing to beta-actin as described previously. Data are presented as mean ± SEM. P<0.05 determined by Students t-test. **(C)** Aortic root sections fl/fl and MX-1Δ were stained with immunofluorescent antibodies to LPP3 (Red) and PECAM (Green) as described in Materials and Methods.

Figure 2.10

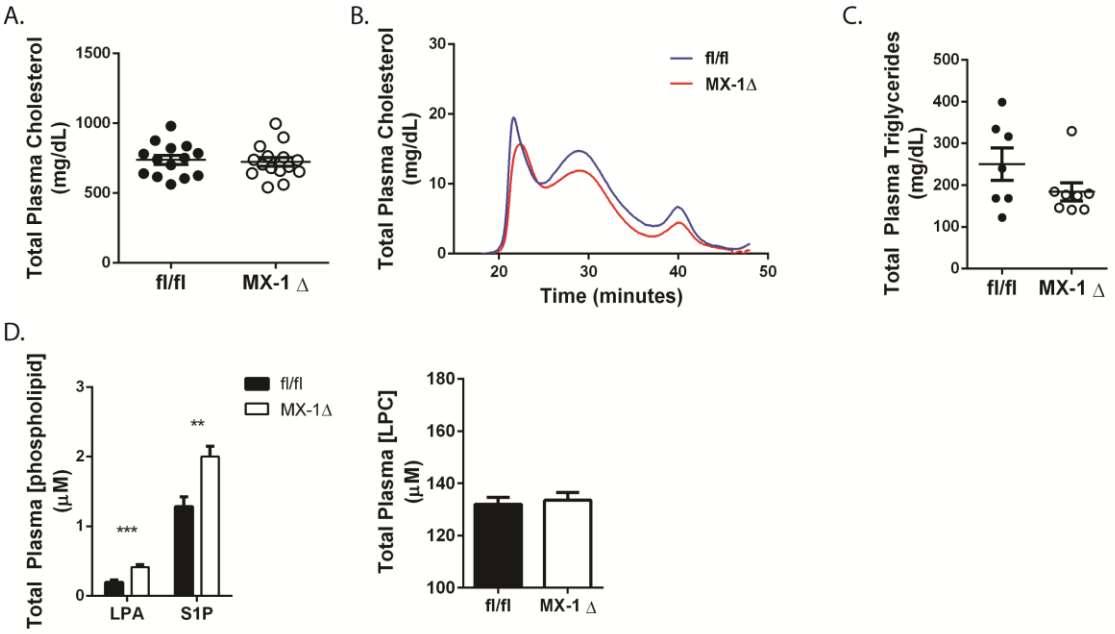

Global reductions in *Ppap2b* alter LPP3-specific plasma phospholipid substrates but not cholesterol or triglycerides. Peripheral blood was collected from mice via retro-orbital vein. **(A)** Total circulating cholesterol was measured using enzymatic colorimetric assays from Wako Diagnostics (n=14 fl/fl; n=15 MX-1Δ). **(B)** Plasma cholesterol (20μg) was separated by size exclusion chromatograph as described in Methods and Materials. Cholesterol detected at 600nm is reported (mg/dL) over time (seconds) **(C)** Total plasma triglycerides were measured using enzymatic colorimetric assays from Wako Diagnostics (n=7 fl/fl; n=9 MX-1Δ). **(D)** Plasma lipid content (from 50μL plasma) was determined using LC MS/MS as previously described (n=15 mice per genotype). Data are represented as mean ± SEM. **P<0.01; ***P<0.001 determined with Students t-test.

Figure 2.11

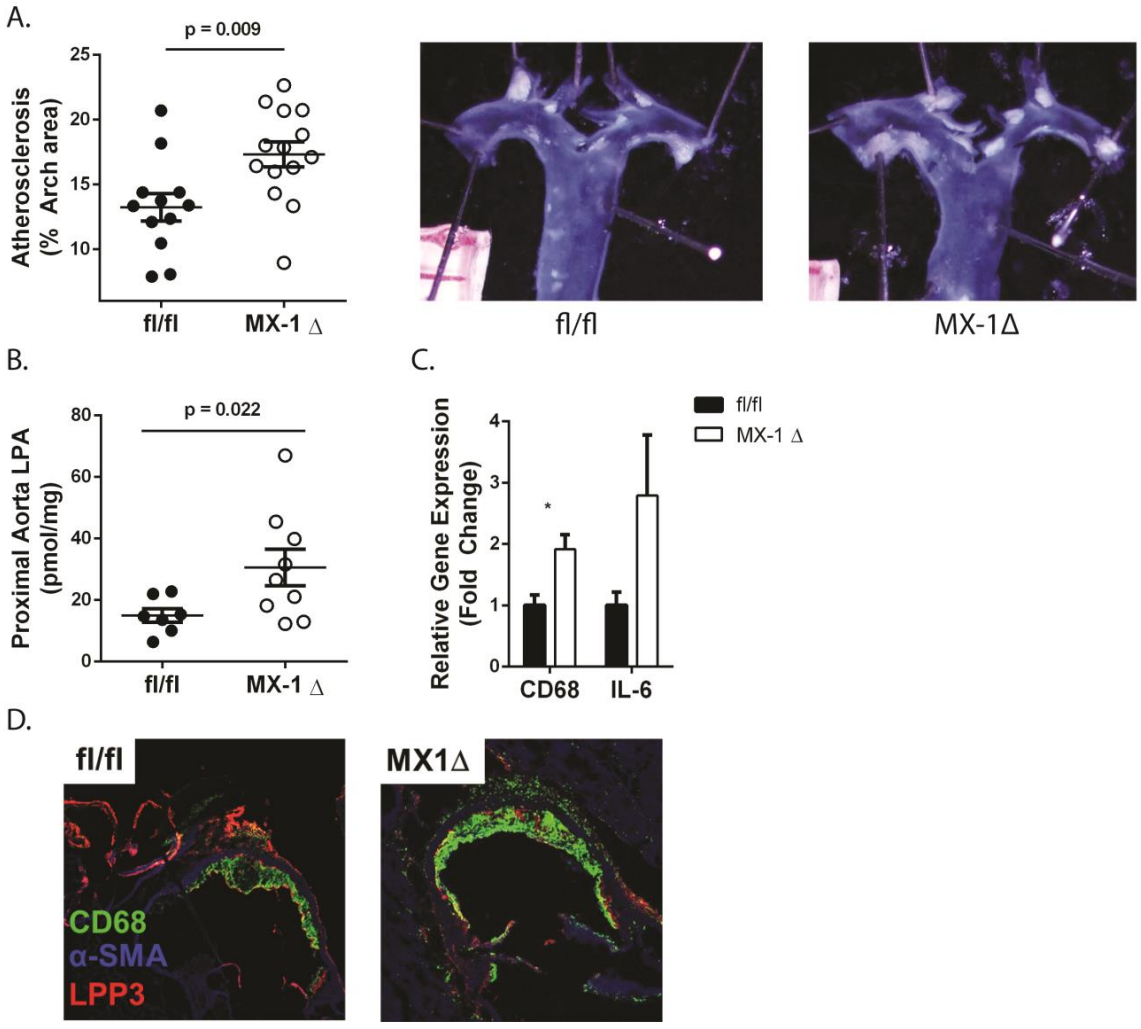

Global reduction of LPP3 increases atherosclerotic lesion formation and CD68 expression in murine aorta. Mice were fed Western diet for 12 weeks **(A)** Atherosclerosis was quantified using the *en face* technique in proximal aorta (n=12 fl/fl; n=14 MX-1Δ). Values are reported as lesion percent of the proximal aorta area (% Arch Area). Individual percent and mean ± SEM are presented. **(B)** Proximal aortas were homogenized and subjected to lipid extraction and LC MS/MS as described in materials and methods. **(C)** Gene expression analysis by qRT-PCR from proximal aorta. **(D)** Aortic root sections from MX-1Δ and fl/fl were immunofluorescently stained with antibodies to LPP3 (Red), SMA (Blue) and CD68 (Green) as described in Materials and Methods. Data are presented as mean ± SEM. *P<0.05 determined by Student's t-test.

Figure 2.12

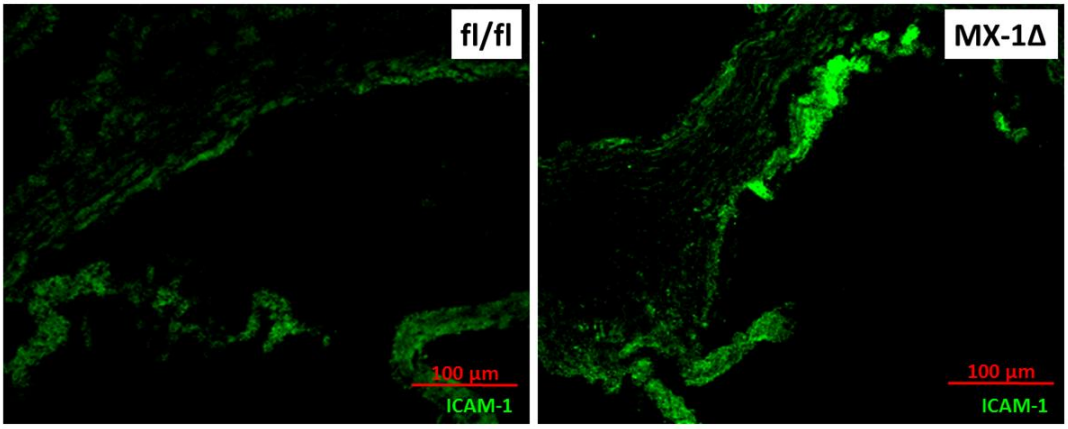

LPP3 limits ICAM-1 expression in murine models of atherosclerosis. Mice were fed Western diet for 12 weeks. Aortic root sections from MX-1Δ and fl/fl were stained with antibodies to ICAM-1 (Green).

Figure 2.13

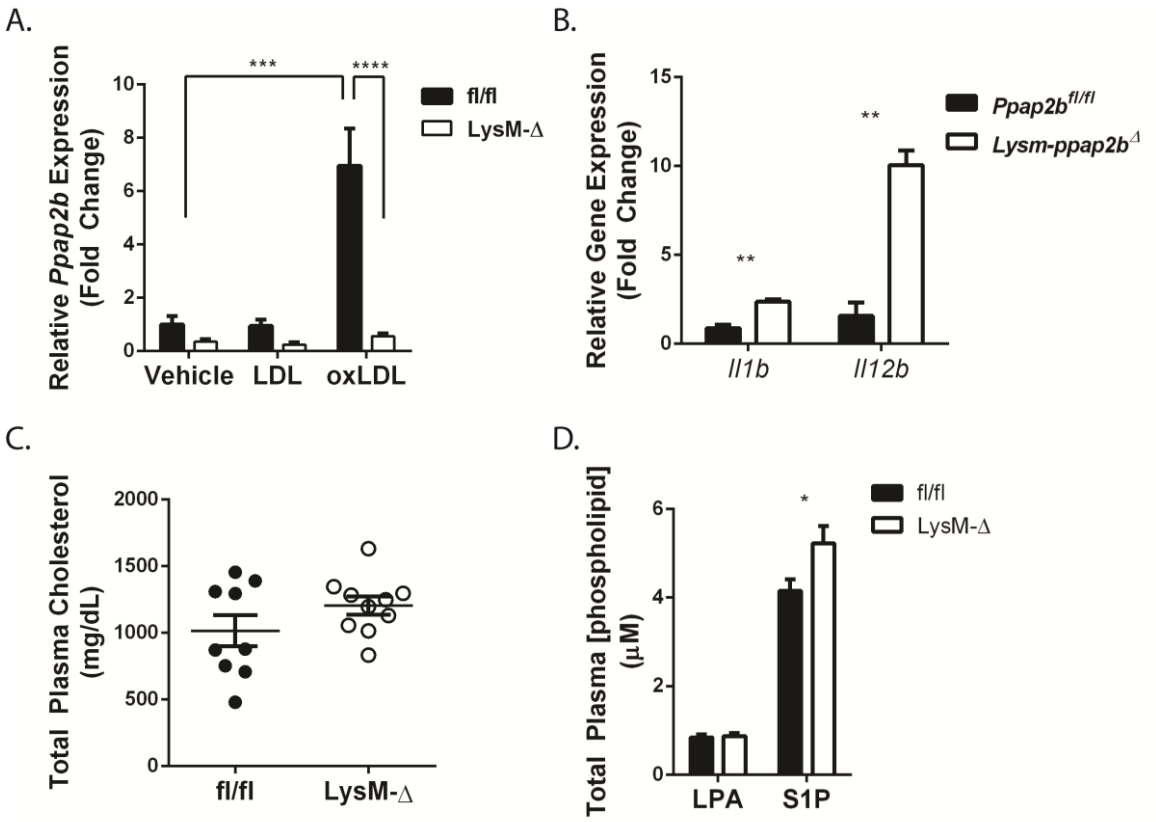

OxLDL-induces upregulation of *Ppap2b* in murine macrophages and deletion of leukocyte-specific LPP3 does not alter plasma cholesterol. (A) Bone marrow-derived macrophages were isolated from fl/fl and LysM-Δ mice femurs and cultured as described in methods and materials. Macrophages were treated with vehicle, LDL (50μg/mL) or oxLDL (50μg/mL) for 48 hours. Expression was analyzed by qRT-PCR for **(A)** *Ppap2b.* ***P<0.001; ****P<0.0001 determined by two-way ANOVA. **(B)** *Il1b* and *Il12b* expression. **P<0.01 determined by Student's t-test. **(C)** Total circulating cholesterol was measured using enzymatic colorimetric assays from Wako Diagnostics (n=9 fl/fl; n=10 LysM-Δ). Data are presented as mean ± SEM. *P<0.05 determined by Student's t-test. **(D)** Lipids were extracted from 50μL of plasma (n=10 mice per genotype) and lipid content was determined using LC MS/MS as previously described. Data are presented as mean ± SEM. *P<0.05 determined by Student's t-test.

Figure 2.14

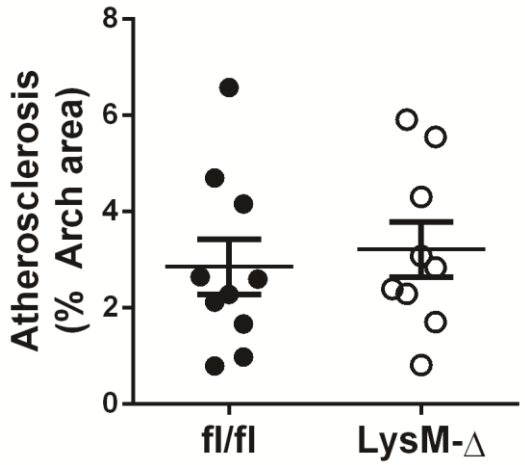

Leukocyte-specific LPP3 does not limit lesion formation in mice but does upregulate proinflammatory cytokines in foam cells. Mice were fed Western diet for 12 weeks**.** Atherosclerosis was quantified using the *en face* technique in proximal aorta (n=10 fl/fl; n=10 LysM-Δ). Values are reported as lesion percent of the proximal aorta area (% Arch Area). Individual percent and mean ± SEM are presented.

Figure 2.15

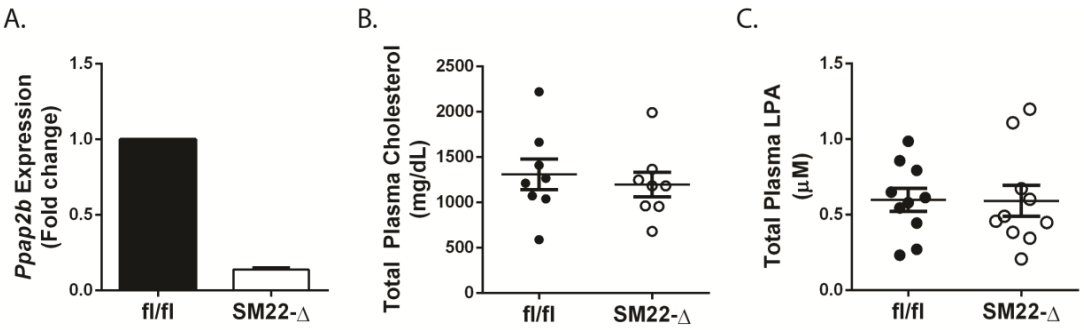

SMC-specific deletion of *Ppap2b* does not alter circulating lipids. (A) SMCs were isolated from fl/fl and SM22-Δ mice aortas and cultured as described in methods and materials. *Ppap2b* expression was determined by qRT-PCR. **(B)** Total circulating cholesterol was measured using enzymatic colorimetric assays from Wako Diagnostics (n=8 fl/fl; n=7 SM22-Δ). **(C)** Lipid content from 50μL of plasma was determined using LC MS/MS as previously described (n=10 fl/fl; n=10 SM22-Δ). Data are presented as mean ± SEM.

Figure 2.16

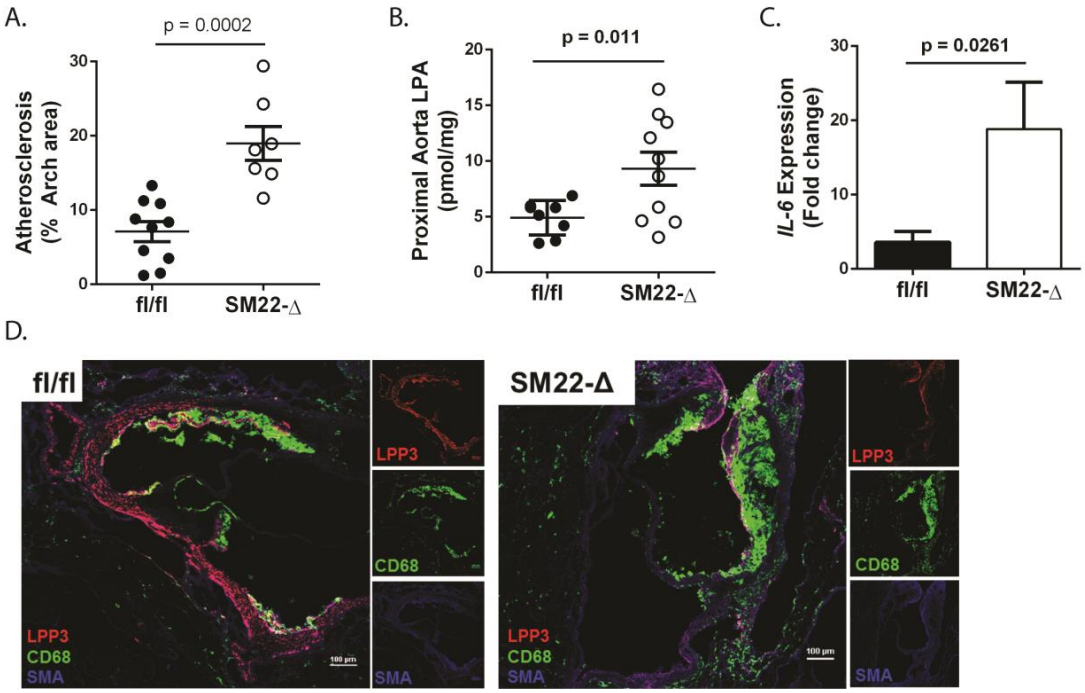

SMC-specific LPP3 limits the development of atherosclerotic lesions in mice. Mice were fed Western diet for 12 weeks **(A)** Atherosclerosis is quantified using the *en face* technique in proximal aorta (n=10 fl/fl; n=7 SM22-Δ). Values are reported as lesion percent of the proximal aorta area (% Arch Area). Individual percent and mean ± SEM are presented. **B)** Lipid content from proximal aorta determined by LC MS/MS as described in Materials and Methods. **(C)** Proximal aorta gene expression determined by qRT-PCR analysis. **(D)** Aortic root sections from MX-1Δ and fl/fl were stained with antibodies to LPP3 (red), SMA (blue) and CD68 (green) as described in Materials and Methods. Data are presented as mean ± SEM. P<0.05 determined by Student's t-test.

Figure 2.17

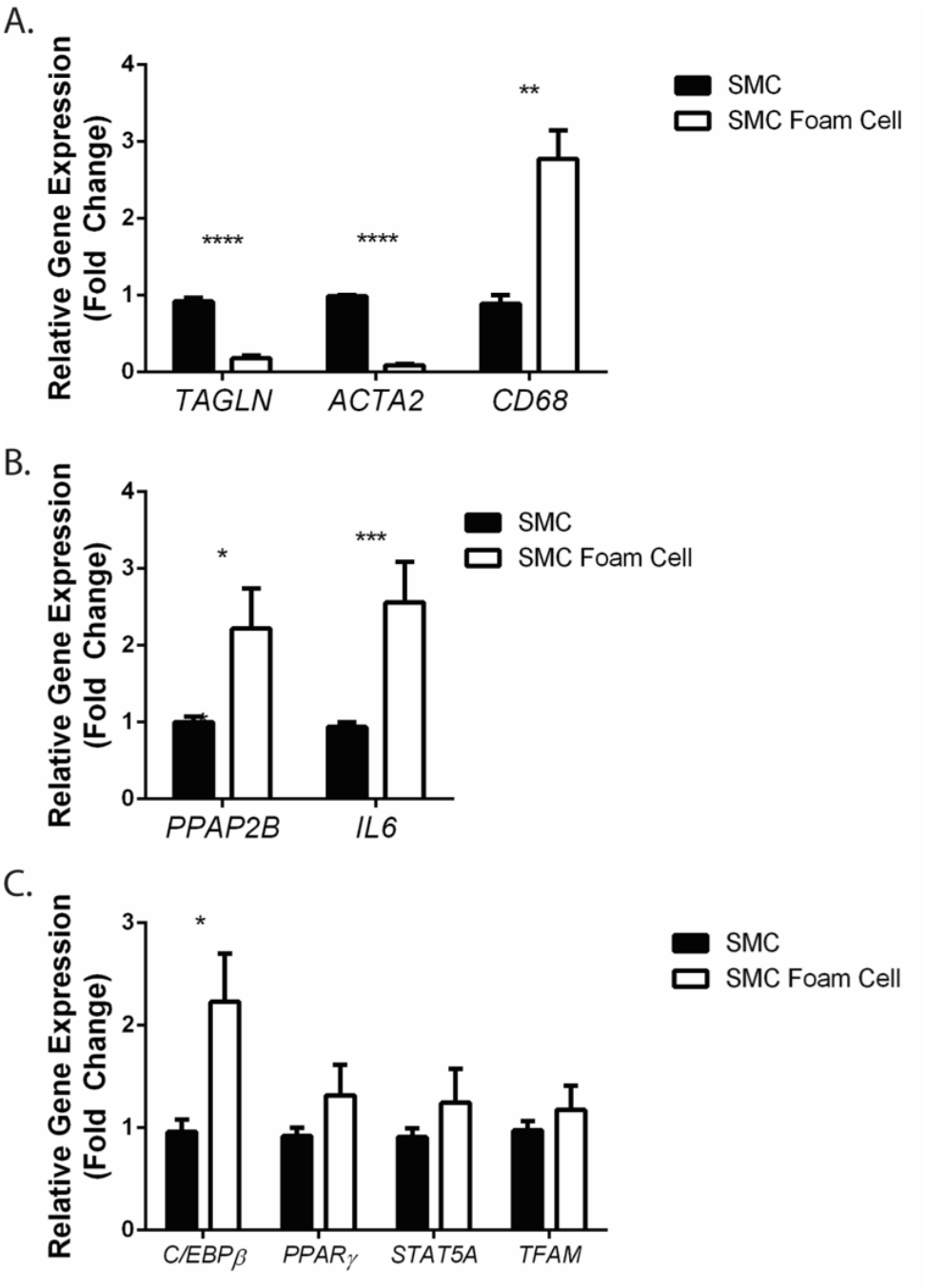

SMC to foam cell phenotypic switching increases *PPAP2B* expression in human caSMCs. Human caSMCs are treated with vehicle or cyclodextran-cholesterol (10μg/mL) for 72 hours. **(A, B and C)** Gene expression determined by qRT-PCR analysis as described in Materials and Methods. Data are presented as mean ± SEM. *P<0.05; **P<0.01; ***P<0.001; ****P<0.0001 determined by Student's t-test.

Figure 2.18

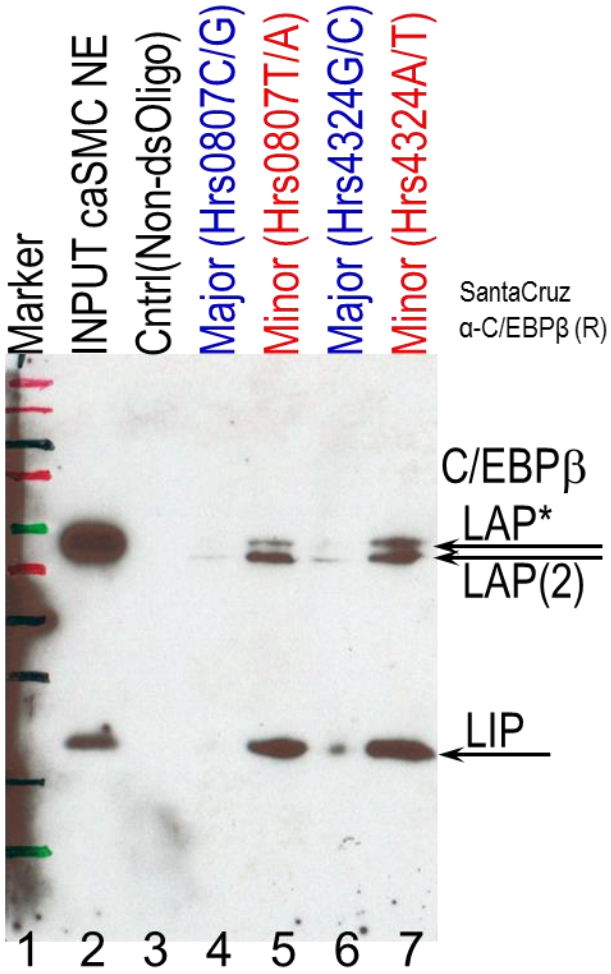

Primary human caSMCs exhibit cholesterol-induced C/EBPβ binding to the CAD-associated protective allele. Human caSMCs were treated with cyclodextran-cholesterol (10μg/mL) for 72 hours. DNA affinity precipitation assay (DNAP) was performed by incubating biotin-labeled oligos for rs9970807 risk and protective alleles and rs72664324 risk and protective alleles with nuclear extracts as described in Materials and Methods. After DNAP, C/EBPβ binding was determined with Western blotting.

Figure 2.19

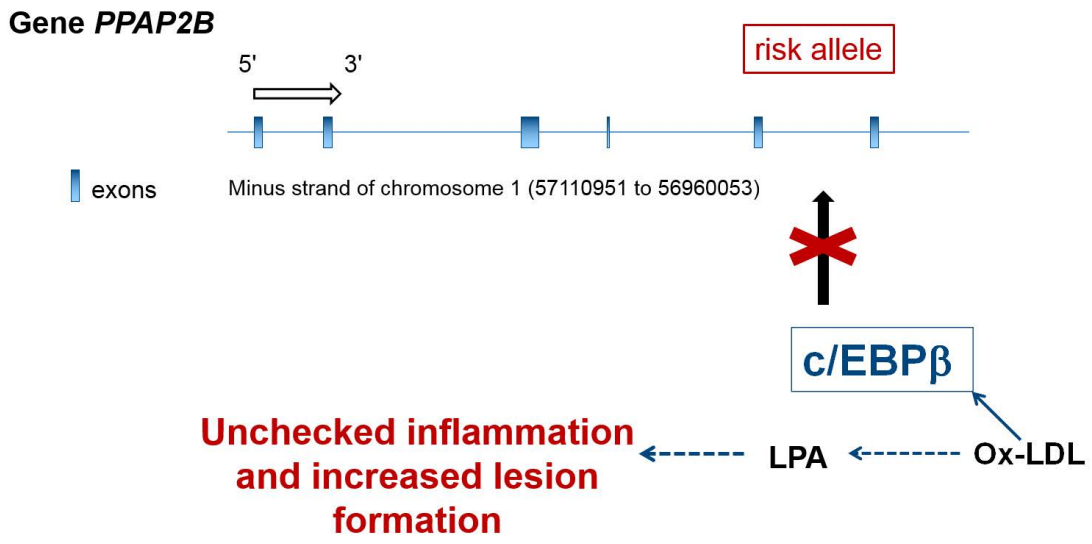

Accumulation of oxLDL in atherosusceptible vessel walls stimulates C/EBPβ binding to the SNP region of PPAP2B to drive expression of LPP3. However, presence of the CAD-associated risk allele impedes this upregulation by breaking C/ETPβ's binding motif leaving the vessels prone to unchecked inflammation and progression of atherosclerosis.

Chapter 3: Peripheral Blood does not Upregulate *PPAP2B* Expression Following Acute Myocardial Infarction

Introduction

Acute myocardial infarction (acute MI) is a leading cause of morbidity and mortality worldwide. Acute MI is said to occur when myocardial ischemia, a lack of blood supply to the heart tissue, overwhelms myocardial repair mechanisms that maintain normal myocardial cell function and homeostasis ultimately resulting in irreparable ischemia-induced damage and death of the myocardium most distal to the infarct site. Atherosclerotic plaque rupture resulting in the generation of an intracoronary thrombus is the most common cause of acute MI [147]. CAD is defined as a narrowing of the coronary blood vessels as a result of the accumulation of atherosclerotic plaques. These lipid-laden plaques develop throughout life and as early as the first decade in atherosusceptible blood vessels and are initiated by the deposition of LDL-C within the tunica intima [52, 53]. LDL-C is modified to a proinflammatory oxLDL microparticle that triggers vEC activation and subsequent recruitment of leukocytes such as monocytes and neutrophils [55, 56]. While the role of neutrophils in CAD is uncertain, monocyte/macrophage conversion to foam cells is a well-understood phenomenon that generously contributes to the progression of disease. As individuals' age, CAD progresses, and early lesions marked by fatty streaks develop into complex atheroma with a highly thrombotic necrotic core laden with oxidized lipids underlying a tough fibrous cap that grows into the vessel lumen [51-53]. If rupture occurs there is potential for generation of an intracoronary thrombus, with platelet deposition, white blood cell accumulation with our without fibrin formation that can ultimately result in acute MI.

CAD is the leading cause of death in both men and women worldwide and carries with it a wide range of risk factors. Modifiable risk factors for CAD include poor nutrition (development of type II diabetes), sedentary lifestyle, tobacco use, hypertension and high LDL-C [49, 50]. The latter two can be modifiable with appropriate medication. Non-modifiable risk factors include the male sex, age, and inherited genetic risk. Analyses of GWAS have revealed up to 47 distinct genetic risk loci that associate with an increased risk of CAD [134]. A meta-analysis published in 2011 identified a genetic risk locus; a noncoding SNP termed rs17114036, in the gene *PPAP2B* conferring an increase in risk of CAD [4]. SNPs identified from GWAS are not necessarily the disease-causing locus but may merely be in linkage disequilibrium with the culprit polymorphism; therefore polymorphisms in close proximity to the GWAS-identified SNP (proxySNPs) in high linkage disequilibrium (r^2>0.8) should also be considered. Additionally, noncoding SNPs implicated in disease may confer their risk through *cis*-mediated effects on the gene they reside or are nearest to, or through *trans*-mediated effects on genes anywhere else on the chromosome.

PPAP2B encodes LPP3, a member of the LPP family responsible for dephosphorylating bioactive phospholipids such as LPA, S1P, C1P, and PA. Our lab has previously identified tissue-specific roles for LPP3 in maintaining vEC barrier function [22] as well as limiting neointimal hyperplasia following vascular injury [133].

In the current chapter we examined expression of *PPAP2B* in blood cells in healthy volunteers and in patients suffering from acute MI. First, we examined LPP3 expression in human blood cells. Then, we identified, using publically available microarray data [142, 148], a proxySNP in linkage disequilibrium with rs17114036 (r^2>0.901) that is associated with decreased expression of *PPAP2B* in peripheral blood cells [142]. We failed to observe allele-dependent variation in LPP3 expression in neutrophils from volunteers either

homozygous or heterozygous for the rs17114036 risk allele. Finally, investigating *PPAP2B* expression in the peripheral blood from patients with acute MI, stable ischemic heart disease (SIHD) or healthy volunteers reveals no significant changes in expression among the three cohorts.

Materials and Methods

Patients and study design

This study was approved by the University of Kentucky Institutional Review Board (Protocol #: 11-0367). Subjects were asked to donate blood for research purposes. 30 – 50 cc of venous blood was collected by phlebotomy. Normal volunteers were at least 18 years old were recruited from laboratory and staff personnel by word-of-mouth. Women and minorities were included. Children were excluded because they are not routinely employed as laboratory or staff personnel and because they are not a patient population that normally develops CAD. Individuals with acute MI were recruited from the cardiac catheterization laboratory at UK Chandler Medical Center, from the cardiology outpatient clinics at the Gill Heart Institute and the UK Good Samaritan Professional Building. Patients with SIHD were referred by their treating physician.

Genotyping of LPP3 rs17114036 polymorphism

DNA isolated from peripheral whole blood is collected from healthy donors as well as patients that have consented to participate in the IRB approved study protocol. DNA was isolated from whole blood (300µL) using the Maxwell® 16 Blood DNA Purification Kit protocol (Promega Cat# AS1010). Genotyping was performed according to the TaqMan

SNP Genotyping Assay for rs17114036 (Life Technologies Cat# 4351379) with an Applied Biosystems 7500 Fast Real-Time PCR System, 11.25µL of DNA along with 12.50µL of TaqMan Universal Mix (2x) and 1.25µL of 20x SNP assay primers were added to a MicroAmp® Fast Optical 96-well reaction plate (Life Technologies Cat#4346906). The plate was run using the "SNP Genotyping Assay" configuration on the RT-PCR software. Donors were classified as being homozygous for the risk allele (A/A), heterozygous (A/G), or homozygous for the protective allele (G/G).

RNA quantification of PPAP2B from human whole blood

RNA isolated from peripheral whole blood was collected from healthy donors as well as patients. RNA was isolated from whole blood (300 – 500µL) using RiboPure™ RNA Purification Blood Kit (Life Technologies Cat# AM1928) protocol. RNA was treated with DNase for the removal of DNA contaminates (provided in the RiboPure™ blood kit). 1.0µg of RNA was used to generate a cDNA library using the SuperScript® VILO cDNA Synthesis Kit (Life Technologies Cat# 11754-050). RNA samples in the SuperScript® reaction mix were incubated at 25°C for 10 minutes, 42°C for 60 minutes, and the reaction terminated at 85°C for 5 minutes. 1.0µg of cDNA was used for qRT-PCR using primers designed for generated a 65bp amplicon in *PPAP2B* spanning exons 1 and 2 (Life Technologies Cat# 4331182 Hs00170359_m1). qRT-PCR was performed on the Applied Biosystems 7500 Fast Real-Time PCR System. Transcript copy number of *PPAP2B* was determined using a copy number calibration curve generated using serial dilutions of a copy number control designed for the region of *PPAP2B* for which the aforementioned Life Technologies' primers span as described below. Relative gene expression is quantified using the $\Delta\Delta C_T$ method using ribosomal *18s* as an endogenous control.

Generation of a copy number calibration control for qRT-PCR analysis of PPAP2B

In order to generate an amplicon that was detected by the qRT-PCR primers obtained from Life Technologies, oligo primers were designed to cover >70 base pairs in both directions starting from the border of exons 1 and 2 of *PPAP2B* (Operon Forward Primer: AACAACAACCCGAGGAGGAG; Reverse primer: GCAGTAAAACCCTCGGTGGT). PCR cycle set up: 94°C for 1:00 minute; [94°C for :30; 60° for :30; 72° for :30] x 35 cycles; 72° for 2:00 minutes. PCR amplicons generated from this PCR were run on a 1% agarose gel at 100mV until the bands were detectable at their expected size of 138bp. The DNA bands were cut from the gel and weighed. In a 1.5mL Eppendorf tube, the gel-DNA bands were treated with 3 volumes of Qiagen Buffer QG (Qiagen Cat#19063) for 1 volume of gel (300µL Qiagen buffer for every 100mg of gel). Samples were incubated at 55°C for 10:00 minutes with frequent vortexing. Once the gel was dissolved, 1 volume of 100% isopropanol was added for every 1 volume of gel and mixed well. The DNA-gel mixture was then run through Qiagen quick spin columns 700µL at a time, and finally washed with PE Buffer (provided in the QIAquick Gel Extraction Kit Cat#28704). The DNA was eluted from the column with 50µL of ddH_2O and was quantified via Thermo Scientific Nano Drop 2000. Calculation of the amplicon copy number in the eluted sample was performed assuming that double stranded DNA is 660g/mol/bp.

Isolation of neutrophils from whole blood

18 to 20cc of whole blood in ACD was added to a 50mL conical vial containing 12mL of 6% Dextran. The solution was gently mixed and redistributed into four 15mL conical tubes and allowed to sit at room temperature for 45 minutes. Once the red blood cells (RBCs) have settled out of solution, the top yellow layer was removed and combined in a 50mL conical tube. This fraction was centrifuged at 1,150rpm for 12 minutes using a low braking speed at 4°C. The supernatant was discarded, and the pellet resuspended in 12mL of ice

cold ddH_2O for no more than 30 seconds in order to lyse the RBCs. 4mL of 0.6M KCl was added to the solution in order to neutralize the osmotic shock. The volume was increased to 50mL using ice cold 1x PBS and centrifuged at 1,300rpm for 6 minutes using a high brake at 4°C. The RBC lysis step was repeated with ddH_2O and KCl until no more RBCs were visible in the pellet after centrifugation. The supernatant was discarded and the pellet resuspended in 2.5mL of 1x PBS and kept chilled. 3mL of Ficoll Histopaque 1119 (Sigma Aldrich Cat# 11191-100mL) was added to a separate sterile 15mL conical tube. The resuspended pellet was carefully layered on top of the Ficoll while tilting the conical tube 45°. The mixture was centrifuged at 1,500rpm using a low brake for 30 minutes at 4°C. The supernatant was discarded leaving the neutrophil pellet. The pellet was resuspended in 1mL of 1x PBS in order to perform a cell count. The neutrophil pellet was lysed at a concentration of 5.0×10^6 cells/mL in Buffer containing: 50mM Tris Base; 500mM NaCl; 4mM $MgCl_2$; 1% Triton X-100; 1mM PMSF protease inhibitor.

Immunoblotting of Neutrophil Protein Lysates

Protein lysates were treated with PNGase F (New England Biolabs Cat# P0705S) according to the manufacturer's protocol. Protein concentrations were determined with the Pierce™ BCA Protein Assay Kit (Cat# 23225) and 20µg of total protein was added to a 10% polyacrylamide gel and transferred to nitrocellulose membrane. Antibody dilutions were as follows: LPP3 (1:200) and beta-actin (1:5,000). As an alternative loading control, after the protein transfer, gels were placed in 0.1% coomassie stain overnight and destained for 2 hours in 10% acetic acid, 50% methanol and 405 ddH2O. Gels and membranes were imaged with a Li-Cor Odyssey Scanner.

Statistical Analysis

All data are expressed as mean ± SEM unless otherwise noted. Statistical analysis was performed using an unpaired, two-tailed Student t-test unless otherwise noted. P-value <

0.05 is regarded as significant. ANOVA was used when multiple comparisons were made. Statistical analysis was performed using GraphPad Prism 7.

Results

Neutrophils express detectable levels of LPP3

We evaluated LPP3 expression in separate blood fractions and observed that neutrophils (PMNs), but not other leukocytes, platelets or red blood cells, express detectable levels of LPP3 by Western blot (Figure 3.2a). We also determined LPP3-specific phosphatase activity is significantly higher in the PMN fractions compared to the other blood cells by immunoprecipating LPP3, incubating the lysates with LPA and measuring the production of monoacylglyercol via HPLC MS/MS (Figure 3.2b).

Similar observations are discussed in Chapter 2 when we looked at LPP3 expression in human macrophages treated with vehicle or oxLDL (50µg/mL). Naïve macrophages exposed to vehicle show nearly undetectable levels of LPP3 but treatment with oxLDL for 48 hours resulted in significant increases in expression (Figure 2.1a).

Rs17114036 proxySNP rs9970807 associates with lower PPAP2B expression in leukocytes

A meta-analysis was published in 2011 that associated a SNP in *PPAP2B*, rs17114036, with CAD. The CARDIoGRAM Consortium reported that the SNP rs17114036, located within the final intron of the gene PPAP2B, was highly predictive of CAD (odds ratio 1.17; P = 3.81 X 10-19). Based on those observations, we interrogated publically available data sets using information obtained with software tools and data available online at http://www.sanger.ac.uk/resources/software/genevar/ (details provided in 45 and http://compute1.lsrc.duke.edu/softwares/SNPExpress/1_database.php (details provided

in 46. Using rs9970807 as a proxy SNP (r^2=0.901), we found a significantly lower expression of most of the *PPAP2B* exons in mRNA isolated from peripheral blood monocytes from individuals with the risk-associated allele (Table 2.1). In contrast, the proxySNP did not associated with altered expression of *PRKAA2*, encoding the α2 catalytic sub-unit of AMP-activated protein kinase, which is the closest known structural gene to rs17114036 located ~66,000bp from *PPAP2B* on the opposite strand of the chromosome in either blood cells (which express *PRKAA2* at low levels), or in skin and adipose tissue where the gene is expressed more strongly. We also queried the SNPExpress database for an allele-associated change in *PCKS9* expression but no significant changes were observed in any of the probed exons (Table 2.2). These observations support our hypothesis that the major allele of rs9970807, (and therefore, the risk allele in rs17114036), is associated with decreased expression of LPP3.

Individuals homozygous for rs17114036 risk allele show no change in neutrophil-specific LPP3

Data from online microarray databases demonstrate a significantly lower level of *PPAP2B* expression in PBMCs associated with rs9970807, a proxySNP in linkage disequilibrium with rs17114036. Given the high expression of LPP3 in neutrophils we investigated whether individuals homozygous for the CAD-associated risk allele for rs17114036 express lower levels of LPP3 compared to heterozygote PMNs. 75 volunteers were enrolled in the study. The PMN fraction was isolated as described in materials and methods and LPP3 expression was determined with Western blot. We were unable to detect a difference in LPP3 expression between genotypes with Western blotting (Figure 2.3). We observed a risk allele frequency of 0.90 and a protective allele frequency of 0.10 in this cohort.

Peripheral blood from patients with acute myocardial infarction does not have upregulated PPAP2B expression

PMNs exhibit high levels of LPP3 expression, but no difference was observed in the tissue from volunteers homozygous for the rs17114036 risk allele and those who were heterozygous. The microarray database SNPExpress shows risk allele-associated decreases in *PPAP2B* in PBMCs, which include monocytes but not the poly-nucleated neutrophils suggesting that the SNP-effect may be cell-specific. As mentioned previously, in a collaborative study with Reschen et al., our lab observed an upregulation of *PPAP2B* during the conversion of primary human macrophages to foam cells (Figure 2.1) that coincides with a CAD-associated risk allele-dependent variation of *PPAP2B* expression, the details of which were described in greater detail in Chapter 2, further supporting the concept of a tissue-specific SNP-effect. Mounting genomic data supports a role for SNP-mediated *PPAP2B* expression in increasing an individual's risk of developing CAD and recent collaborative data suggests monocytes can upregulate LPP3 in response to a characteristic CAD process; therefore, we hypothesized that *PPAP2B* expression would be upregulated in the blood of patients with acute MI, another critical event in CAD.

To explore this possibility, we performed a pilot study that enrolled 29 subjects who either healthy (n=10), had SIHD (n=10) or presented with acute MI (n=9). Blood was collected within 24 hours of presented with MI. The demographics and clinical information on subjects are presented in Table 2.3. We were unable to detect LPP3 reliably by Western blotting and so we employed gene expression analysis. There was no observable difference in *PPAP2B* expression between the three cohorts determined by qRT-PCR using the $\Delta\Delta C_T$ method (Figure 2.5). To eliminate the possibility that comparative quantification overlooked any differences in expression we generated a copy number standard targeting *PPAP2B.* qRT-PCR using a standard curve revealed no differences in absolute *PPAP2B* copy number between the three cohorts (Figure 2.6). We observed a risk allele frequency of 0.86 and a protective allele frequency of 0.14 in our pilot study.

Discussion

There is a strong heritable component, aside from modifiable lifestyle behaviors, that contributes to varying degrees of risk of developing CAD [4, 49, 50, 126, 134]. In 2011 a meta-analysis confirmed 10 previously known risk-associated loci as well as identified 13 novel loci that contribute to an increased risk of disease [4]. Many of the aforementioned loci, including rs17114036 in the final intron of PPAP2B, are not found in genes identified as traditional risk factors. SNPs identified in GWAS analyses are not necessarily the disease-causing loci and may simply represent a haplotype of many SNPs in linkage disequilibrium; in fact, rs17114036 is in linkage disequilibrium with roughly 20 SNPs (Figure 2.1). We interrogated publically available microarray databases [142, 148] and identified rs9970807, a proxySNP to rs17114036 (r^2=0.901), as having an allele-dependent association with decreased *PPAP2B* expression in blood cells (Table 3.1) that was not observed in *PCSK9* (Table 3.2). We hypothesized that individuals homozygous for the major allele (the risk allele) will exhibit decreased *PPAP2B* expression and thus levels of its respective protein LPP3. We enrolled 75 volunteers in our study that were genotyped for the SNP rs17114036 and evaluated levels of LPP3 in their PMNs with Western blotting; however, we saw no differences in LPP3 based on the individuals' genotypes (Figure 3.3). Recent evidence leads us to believe that the SNP-effect on *PPAP2B* expression is tissue-dependent and could be observed in models evaluating CAD processes such as foam cell formation (Figure 2.1) [135]. A hallmark event in CAD is the rupture of the atherosclerotic plaque and subsequent MI; we therefore investigated whether *PPAP2B* expression increases in peripheral blood cells from patients suffering acute MI or SIHD relative to healthy controls. We enrolled 29 volunteers to our study and, using RNA isolated from their peripheral blood, determined *PPAP2B* expression levels.

We saw no differences in expression among the three cohorts enlisted in our study suggesting that *PPAP2B* is not increased in circulating blood cells of patients with acute MI or SIHD (Figure 3.4).

Data from SNPExpress are derived from peripheral blood mononuclear cells, which are mononuclear blood cells such as lymphocytes and monocytes. We looked at LPP3 expression in blood cells and observed detectable levels exclusively in the neutrophil (PMN) fraction and not other leukocytes, platelets or red blood cells (Figure 3.2). Because of this observation we investigated LPP3 expression relative to the rs17114036 SNP genotype in neutrophils. Lysates from neutrophils show marked variability in LPP3 bands on a Western blot likely due to the proteins variable glycosylation coupled with the interindividual variation in its expression. We treated lysates bound for a Western blot with PNGase F, an amidase that cleaves between the innermost GlcNAc and asparagine residues of high mannose, hybrid, and complex oligosaccharides from *N*-linked glycoproteins, effectively removing glycans from LPP3 in order to generate one solid quantifiable band at ≈31kDa. However, as mentioned previously, no detectable difference was observed between lysates from homozygotes and heterozygotes (Figure 3.3) suggesting that a SNP-mediated effect on LPP3 expression is not taking place in the PMN fraction. A sample size determination analysis reveals that a group sample size n=28 for both genotypes would be required to achieve 90% power to reject the null hypothesis of equal means when the population mean difference is $\mu 1 - \mu 2 = 0.6 - 0.7 = -0.1$ with a standard deviation for both groups of 0.2 and with a significance level (alpha) of 0.050 using a two-sided two-sample equal-variance t-test.

Acute MI is a defining moment in the progression of CAD as it is confers life threatening risks to patients both in its acute phase through arrhythmia and sudden cardiac death as

well as chronic sustained damage leading to left ventricular dysfunction and heart failure. Generation of a thrombus in a coronary artery creates an ischemic environment in the surrounding myocardium which immediately begins to necrose resulting in the release of several measurable proteins into the circulation such as cardiac troponins T and I, myoglobin and CK-MB [149]. Because the CAD-related process of foam cell formation evoked upregulation of PPAP2B in monocytes we hypothesized that the gene's expression is also altered in another critical CAD event, MI. We investigated whether peripheral blood from patients suffering from acute MI would demonstrate altered expression of *PPAP2B* compared to patients with SIHD or healthy volunteers. Amy Chen and I recruited volunteers for this study in accordance to the University of Kentucky IRB approved protocol 11-0367 and analyzed *PPAP2B* expression in the three cohorts. Neither comparative qRT-PCR nor absolute copy number qRT-PCR analysis revealed any difference in the expression of *PPAP2B* suggesting that the gene's expression is unaffected following acute MI or in patients with SIHD (Figure 3.4). A sample size determination analysis reveals that in a one-way ANOVA study, sample sizes of n=43 for each group whose means are to be compared. The total sample of 129 subjects achieves 90% power to detect differences among the means versus the alternative of equal means using an F test with a 0.0500 significance level. The size of the variation in the means is represented by their standard deviation which is 10.50. The common standard deviation within a group is assumed to be 32.94. Alternatively, the upregulation of LPP3 observed in our collaborative efforts with Reschen et al. may be dependent on cholesterol-specific effects within vascular tissue and not the blood cells in circulation. One potential drawback from this particular study is that we looked at RNA from all peripheral blood cells whereas monocyte-specific LPP3 expression was affected upon oxLDL treatment.

CAD is the leading cause of death for both men and women worldwide and is characterized by the narrowing of coronary arteries due to the accumulation of atherosclerotic plaques within the vessel wall. CAD is considered a multi-factoral disease involving uncontrolled inflammation, intravascular deposition of lipids, endothelial dysfunction and dynamic vessel remodeling; all of which may lead to plaque rupture, triggering thrombogenesis and MI. 660,000 Americans suffer from their first MI every year and statistics say that 36% of men and 47% of women will die within 5 years of their initial MI [150]. Predicting individuals' risk of developing CAD is imperative to initiating preventative care and lifestyle changes that may slow the progression of disease. The Framingham Heart Study in 1948 was pivotal in identifying many of the classical risk factors that are associated with CAD today. However, in spite of improvements in modifiable risk factors, CAD remains the primary cause of death in the United States. CAD has a strong heritable component and with the onset of genome-wide sequencing technology, our capacity to predict genetically-associated CAD risk has tremendously expanded. In 2016 the number of CAD-risk associated loci is up to 47, many of which are not found in genes identified as traditional risk factors. Rs17114036 was identified as a noncoding intronic SNP in *PPAP2B* that incurs an increase in CAD risk [4]. In the study presented here we identified, based on publically available microarray data, a decrease in *PPAP2B* expression in PBMCs associated with the risk allele of rs9970807, a proxySNP in linkage disequilibrium with rs17114036; additionally, we investigated whether a SNP-dependent variation in LPP3 expression was detectable in human PMNs; as well as, whether peripheral blood from patients with acute MI exhibit altered *PPAP2B* expression. Although no differences were observed in neutrophil-specific LPP3 levels or peripheral blood *PPAP2B* following acute MI, we can rule out the possibility that rs17114036 plays a major role in the basal expression of LPP3 in PMNs and that acute MI or SCD contribute to changes in *PPAP2B* expression.

Acknowledgements

This investigation was a collaborative effort from members in our lab including Amy Chen and Dr. Travis Sexton and myself and was integral in earning my Certificate in Clinical and Translational Research. Amy and I performed the volunteer enrollment: specifically, Amy enrolled all patients whose RNA was analyzed in Figure 2.3 and compiled the data used to generate Table 2.2. Dr. Travis Sexton's expertise in molecular biology and genetics designed the oligos used to generate a copy number standard for *PPAP2B* used to generate data for Figure 2.3.b Amy and I shared the task of enrolling and drawing blood from the volunteers whose samples were important in generating Figure 2.2. Under the guidance of my mentor Dr. Susan Smyth I performed the SNPExpress analysis of rs9970807 used to generate Table 2.1. I was able to generate Figure 2.1 using SNP Annotation and Proxy Search software provided by the Broad Institute and NCBI dbSNP Short Genetic Variations GeneView. All genotyping, PMN isolations, Western blots and qRT-PCR experiments were performed and interpreted by myself.

Table 3.1

rs9970807 Associates with Decreased Expression of *PPAP2B* Exons in PBMCs

Exon Probe ID	p-Value	Beta Coefficient
Transcript	0.5252	6.367
2414371	0.5693	5.414
2414373	**0.007934**	44.45
2414374	**0.001704**	60.11
2414380	**1.60E-04**	147.5
2414381	**0.1643**	-35.21
2414386	**2.44E-04**	81.23
2414387	**0.001353**	68.95
2414398	**0.009513**	188.4
2414418	**9.09E-05**	77.81
2414419	0.3132	37.46
2414420	0.2352	-78.01
2414421	**0.008217**	14.27

SNPExpress software is downloadable free of charge from Columbia University Medical Center's website and was developed by Dongliang Ge and David Goldstein [142]. I performed a real-time association test for *PPAP2B* and the rs17114036 proxySNP rs9970807. Output data displays genotype-specific expression of *PPAP2B* exon probes and their respective p-value and beta coefficient of regression. Exon probes showing significant ($P<0.05$) genotype-specific variation in expression are highlighted in yellow.

Table 3.2

No observable association between rs9970807 and changes in expression of *PCSK9* Exons in PBMCs

Exon Probe ID	p-Value	Beta Coefficient
Transcript	0.9126	0.6958
2337420	0.458	-4.3
2337421	0.6604	-4.861
2337422	0.1879	-105.7
2337423	0.09877	12.06
2337425	0.8072	-3.246
2337426	0.1993	-39.41
2337429	0.4829	-54.96
2337431	0.7079	2.321
2337432	0.4198	-16.39
2337433	0.1557	-23.16
2337434	0.4395	6.272
2337435	0.8142	2.69

SNPExpress software is downloadable free of charge from Columbia University Medical Center's website and was developed by Dongliang Ge and David Goldstein [142]. I performed a real-time association test for *PCSK9* and the rs17114036 proxySNP rs9970807. Output data displays genotype-specific expression of *PCSK9* exon probes and their respective p-value and beta coefficient of regression. None of the exon probes displayed significant differences.

Table 3.3

Volunteer Demographics and Clinical History

	Healthy	SIHD	Acute MI
Total Volunteers	10	10	9
Genotype			
A/A	9	9	5
A/G	1	1	0
G/G	0	0	1
Average Age	25.6	67.9	51.9
Demographics			
Male	6 (60.0%)	9 (90.0%)	5 (55.5%)
Female	4 (40.0%)	1 (10.0%)	4 (44.4%)
BMI	23.3 ± 3.8	29.6 ± 1.6	34.9 ± 8.2
Labs			
Sodium	-	140 ± 4.3	139 ± 4.5
Creatinine	-	1.3 ± 0.5	0.97 ± 0.3
Past Medical History			
Hypertension	0 (0.0%)	4 (40.0%)	8 (88.9%)
Obesity	1 (10.0%)	1 (10.0%)	3 (33.3%)
Tobacco	0 (0.0%)	0 (0.0%)	6 (66.7%)
Diabetes	0 (0.0%)	2 (20.0%)	4 (44.4%)

Figure 3.1

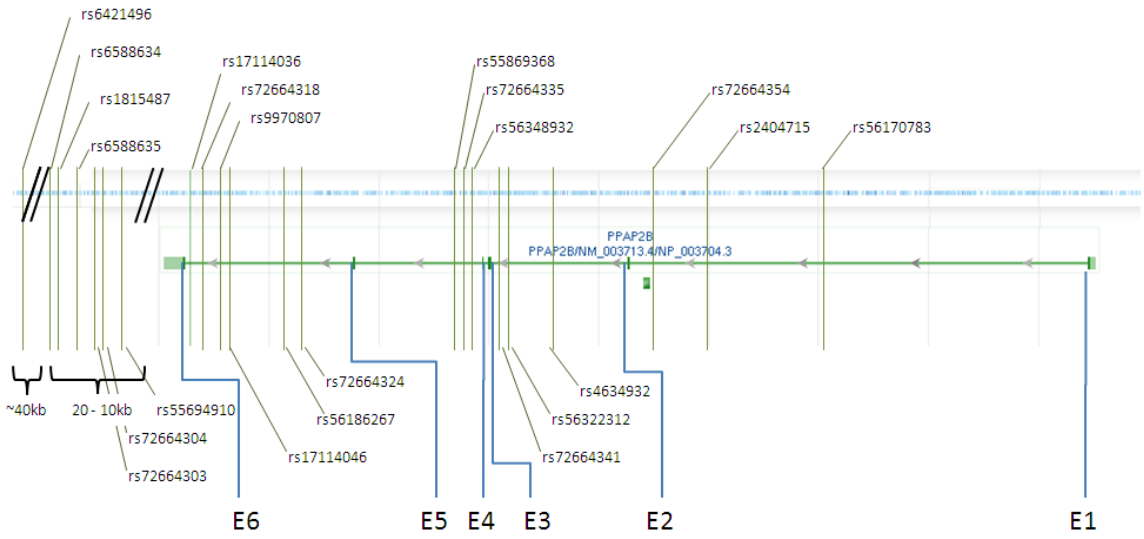

SNP Map of *PPAP2B:* ProxySNPs in linkage disequilibrium (r^2 threshold > 0.8) with rs17114036 were identified using SNP Annotation and Proxy Search software provided by the Broad Institute. Relative SNP locations were determined using NCBI dbSNP Short Genetic Variations GeneView.

Figure 3.2

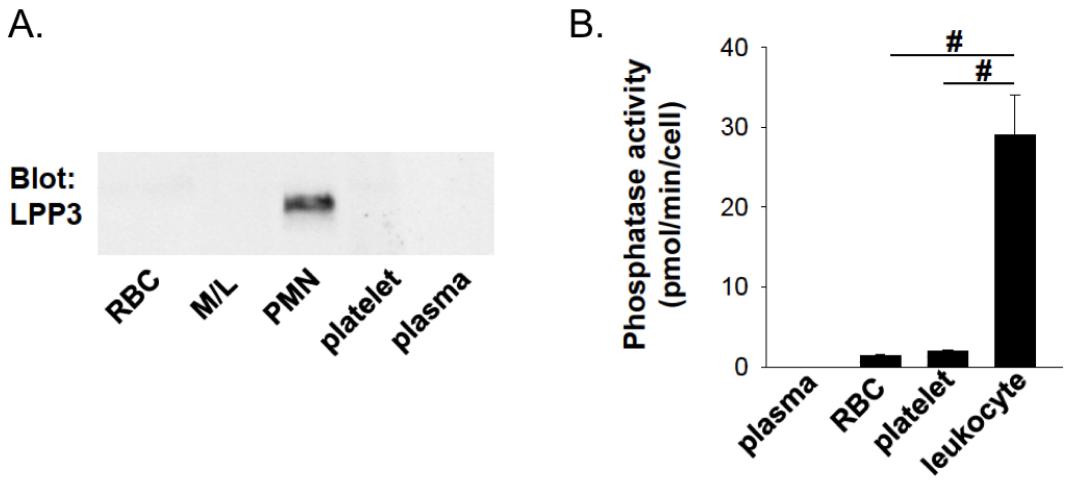

LPP3 is primarily expressed in the neutrophil (PMN) fraction in murine blood. (A) Western blot analysis of LPP3 in lysates containing 40 mg total protein from the indicated cells. M/L = monocyte / lymphocyte fraction. (B) LPA phosphatase activity was measured in plasma and isolated blood cells. Results are presented as mean ± SD from 3 independent experiments. $^{\#}P < 0.001$ by Student's t-test [133].

Figure 3.3

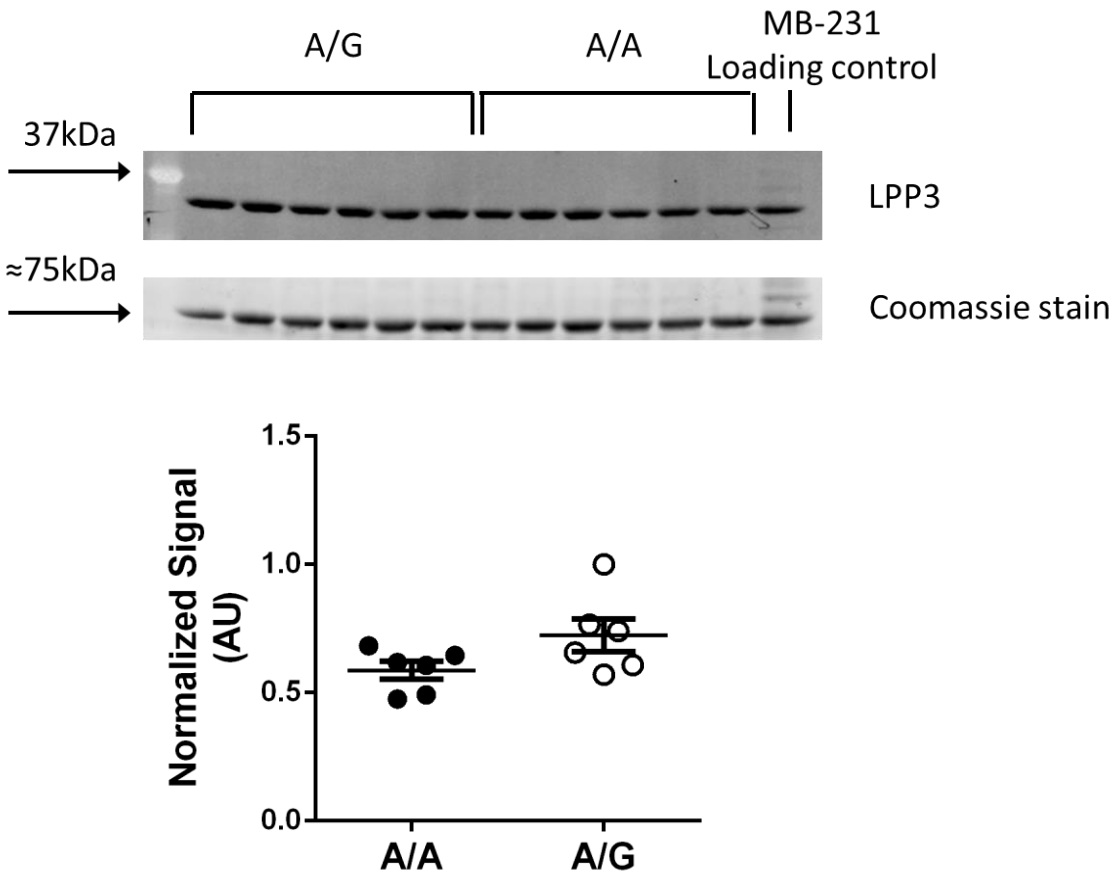

Individuals homozygous for rs17114036 risk allele show no change in neutrophil-specific LPP3. Peripheral blood PMNs were isolated from volunteers and genotyped for rs17114036 as described in materials and methods. (Top) Western blot analysis was performed using antibodies to LPP3 (1:200) and (Bottom) quantified by normalizing to coomassie stained band at ≈75kDa. Data are presented as mean ± SEM.

Figure 3.4

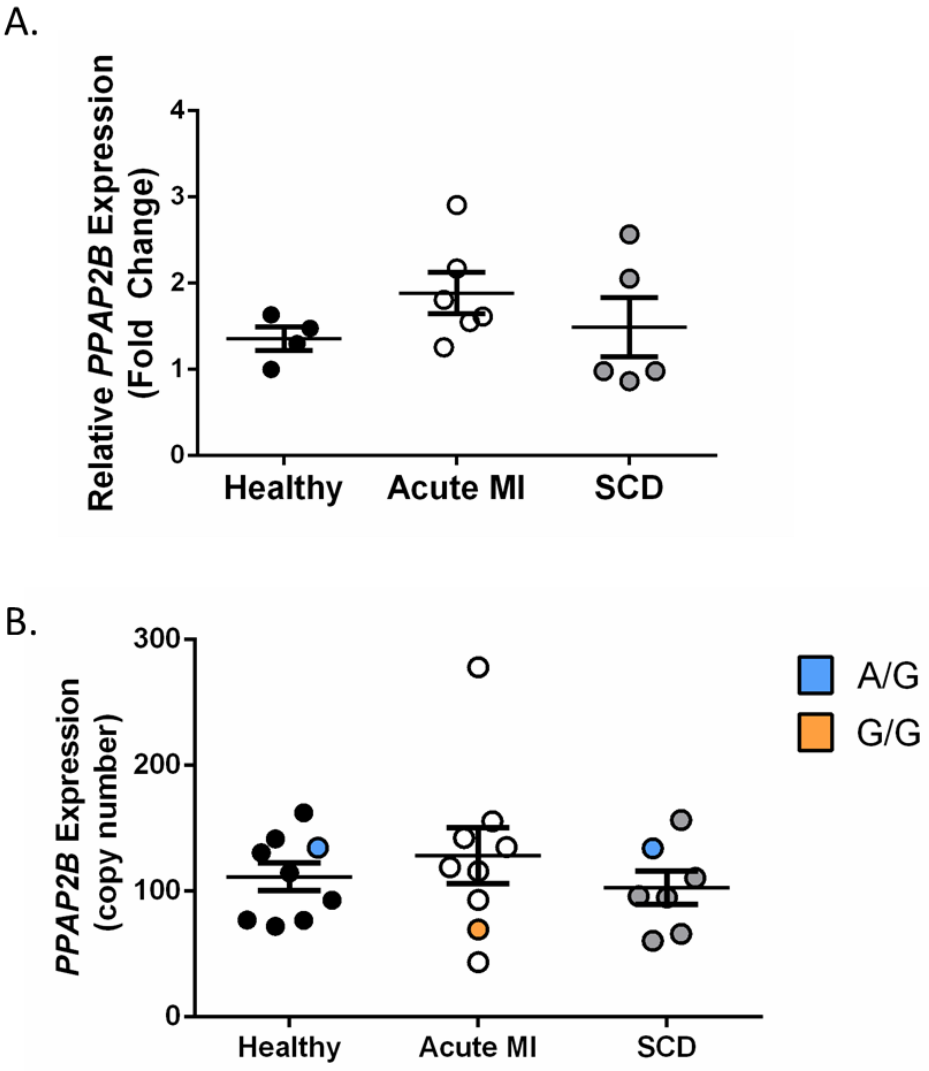

Peripheral blood from patients with acute myocardial infarction does not have upregulated *PPAP2B* expression. RNA was isolated from volunteer peripheral blood as described in materials and methods. **(A)** Comparative qRT-PCR showing relative expression of *PPAP2B* and **(B)** copy number qRT-PCR based on a calibration curve generated from in house *PPAP2B* standards. Blue circles represent samples from volunteers heterozygous for the risk allele and orange circles are from samples from those homozygous to the protective allele. All other circles are samples from volunteers homozygous for the risk allele. Data are presented as mean ± SEM.

Chapter 4: Lysophosphatidic Acid Redistributes to Atherogenic Lipoprotein Fractions in Hyperlipidemic Mice

Introduction

LPA is a potent bioactive lysophospholipid that is found in nearly all eukaryotic tissues and biological fluids including the plasma, ascites and bronchoalveolar lavage fluid. Our lab and others have observed significant accumulation of LPA in both human and mouse atherosclerotic plaques (Figure 4.1). LPA binds to any one of its six known GPCRs (LPA1-6) and elicits a multitude of responses in nearly every cell type studied [10, 11, 21, 24, 26, 84, 151-153]. LPA receptor signaling has been shown to modify vEC barrier function, SMC dedifferentiation, migration and proliferation, and even increase foam cell formation in macrophages *in vitro.* Thus LPA is poised to serve as an important regulator of vascular tissue function. Plasma LPA increases in human disease-states from acute MI to ovarian cancer. Feeding atherosusceptible $Ldlr^{-/-}$ mice chow diet supplemented with unsaturated LPA increases the formation of atherosclerotic lesions compared to saturated LPA or regular chow diet alone.

LPA is carried in plasma bound to proteins, largely albumin, in both human and mice. Recent evidence suggests that LPA could associate with atherogenic LDL-C through the conversion of its precursor LPC into LPA by the actions of the ENPP2 ATX. ATX is a secreted lysophospholipase D found in both human and mouse plasma. Levels of ATX correlate with circulating LPA levels, and genetic deletion or pharmacological inhibition of ATX decreases circulating LPA, indicating that ATX is the primary determinant of plasma LPA levels. LPC has been reported to be a major phospholipid component of LDL-C and enzymatic cleavage of its choline head group by ATX generates LPA. The precursor molecule to LPC is phosphatidylcholine (PC), which is found in abundance in dairy

products as well as red meat. Feeding Western diet significantly increases unsaturated LPA species 20:4 in the plasma of Ldlr$^{-/-}$ mice.

To investigate the dietary contribution to circulating LPA levels, C57BL/6, Apoe$^{-/-}$ and Ldlr$^{-/-}$ mice were fed either chow or Western diet for 3 weeks or 12 weeks. Western diet feeding Apoe and Ldlr mice increased LPA in the plasma fractions containing low-density atherogenic associated VLDL-C and LDL-C which was not observed in C57BL/6 mice. Globally reducing LPP3, the enzyme responsible for hydrolyzing LPA, increases total plasma LPA without altering LPA levels between lipoprotein and protein fractions in the plasma.

Materials and Methods

Animals

All procedures conformed to the recommendations of *Guide for the Care and Use of Laboratory Animals* (Department of Health, Education and Welfare publication number NIH 78-23, 1996), and were approved by the Institutional Animal Care and Use Committee. C57BL/6, *Apoe*$^{-/-}$ and *Ldlr*$^{-/-}$ mice were obtained from The Jackson Laboratory (Bar Harbor, ME). MX-1Δ and fl/fl mice were generated as described in Chapter 3 Materials and Methods. Mice were housed in cages with HEPA-filtered air in rooms on 12-hour light cycles, and fed Chow diet or RD Western Diet (Research Diets Cat#D12079B) ad libitum for specified time points.

Isolating Plasma from Peripheral Blood in Mice

In the morning, peripheral whole blood was collected from mice via the retro-orbital vein while mice were anesthetized with isoflurane. Whole blood was collected in a 1.5 mL

Eppendorf tube containing 10 μL of 0.5 M EDTA and 50 μL CTAD (BD Vacutainer Ref# 367947). Blood samples were centrifuged at 12,000 rpm for 4 minutes and the plasma fraction collected. Samples were placed on dry ice and subsequently stored at -80°C.

Measuring Total Cholesterol and Lipoprotein Cholesterol Distributions in Murine Plasma

Total plasma cholesterol was measured using the Wako Diagnostics Cholesterol E Assay (Wako Diagnostics Cat#439-175001) according to the manufacturer's protocol. Plasma lipoprotein cholesterol distributions were determined via fast-performance liquid chromatography (FPLC). In short, 40μL of plasma from mice, diluted to a concentration of 1μg/μL of total plasma cholesterol, was injected on to a Superose6 FPLC column. Cholesterol concentrations are determined by enzymatic colorimetric assay (Wako Diagnostics) reading at 600nm as the elute flows off of the column.

Measuring Phospholipid Content in Murine Plasma

50 μL of plasma was added to 450 μL of 0.1 M HCl and underwent lipid extraction as previously described in "Lipid extraction for analysis via mass spectroscopy"

FPLC Fractionation of Plasma for Determination of LPA

40μL of plasma from mice was injected into a Superose 6 HPLC column at a flow rate of 0.4mL/minute. Fractions were collected between 18 and 48 minutes and subjected to lipid extraction as described below.

Lipid extraction for analysis via mass spectroscopy

500µL of sample in 0.1M HCl were added to a 12mL glass lipid extraction tube containing 1mL of chloroform, 2mL of methanol, and 50µL of 1µM D7-sphingosine-1-phosphate as an internal standard. Samples in the lipid extraction tubes were vortexed for 5 minutes, and then placed on ice/kept at 4°C for at least 1 hour. 1mL of chloroform and 1.3mL of 0.1M HCl was added to the lipid extraction tubes and vortexed again for 5 minutes. The samples were centrifuged at 3,000rcf for 10 minutes at room temperature, and the lower aqueous phase was transferred to 4mL screw cap glass tube using a Pasteur pipette being careful not to include the protein interphase. Samples were evaporated to dryness using nitrogen in an N-evap under a fume hood. Once the samples were completely dried, 100µL of methanol was added and the tubes were vortexed. Samples sat at room temperature for 10 to 15 minutes and then transferred to an autosampler insert vial for analysis via Agilent Zorbax C8 column and quantified by tandem mass spectrometry using an ABI 4000 QTrap hybrid linear ion trap triple quadrupole mass spectrometer. The mass spectrometer was operated in selective reaction monitoring mode to measure lipid species specific precursor product ion pairs with quantification accomplished by reference to calibration curves generated using synthetic standards obtained from Avanti Polar Lipids that were independently quantitated by phosphorous analysis as described previously.

Statistical Analysis

All data are expressed as mean ± SEM unless otherwise noted. Statistical analysis was performed using an unpaired, two-tailed Student t-test unless otherwise noted. P-value < 0.05 is regarded as significant. Two way ANOVA was used when multiple comparisons were made. Statistical analysis was performed using GraphPad Prism 7.

Results

Cholesterol-rich diet increases circulating LPA in hyperlipidemic mouse models

We placed C57BL/6 wild-type, hyperlipidemic *Apoe*$^{-/-}$ and *Ldlr*$^{-/-}$ mice on normal chow and Western diet for 3 weeks or 12 weeks. As expected, total plasma cholesterol were elevated in the hyperlipidemic Apoe$^{-/-}$ and Ldlr$^{-/-}$ mice and increased upon Western diet feeding for 3 weeks as well as 12 weeks (Figure 4.2a). Total plasma LPA was 75% higher in the hyperlipidemic mice on chow diet and nearly 4-fold in *Apoe*$^{-/-}$ and *Ldlr*$^{-/-}$ on Western diet for 3 weeks compared to levels in C57BL6 wild-type control on the same diet. (Figure 4.2b).

Hyperlipidemia increases unsaturated LPA levels in fractions containing atherogenic lipoproteins in mice

LPA is primarily bound to plasma proteins in mice and humans; however, its precursor LPC is a major phospholipid component of lipoproteins in humans. We investigated whether hyperlipidemia changed the plasma LPA content in the atherogenic-lipoproteins. For the analysis, plasma was separated by size exclusion chromatography and fractions were subjected to LC MS/MS to measure LPA content.

C57BL/6 and *Apoe*$^{-/-}$ mice show LPA content localized primarily in the late fractions 16 to 21 containing HDL-C or plasma proteins whereas *Ldlr*$^{-/-}$ plasma show small increases in fractions 1 to 10 that typically contain LDL-C (Figure 4.3 top). Western diet feeding for 3 weeks results in a dramatic increase in LPA in plasma fractions containing LDL-C in hyperlipidemic mice. The wild-type control plasma looks similar to its chow fed counterpart. *Apoe*$^{-/-}$ and *Ldlr*$^{-/-}$ mouse plasma shows substantial increases in fractions 1 through 6 that contain the atherogenic VLDL-C and LDL-C (Figure 4.3 bottom). C57BL/6 mice fed Western diet for 12 weeks show only modest increases in total cholesterol

compared to 3 weeks or chow diet (Figure 4.2a). Prolonged feeding of Western diet alters the LPA content in the lower density fractions in C57BL/6 mice; specifically the unsaturated LPA content (percent of total). The majority of LPA content in chow fed wild-type mice is found in fractions 18 to 23 but increases in fractions 13 to 18 in mice fed Western diet for 12 weeks (Figure 4.4).

Although LPA increases in fractions typically containing atherogenic-associated LDL-C in hyperlipidemic mice, we cannot say with certainty that these fractions contain their predicted LDL-C. Using size exclusion chromatography we simultaneously measured plasma total cholesterol (mg/dL) as it eluted out of the column with an enzymatic colorimetric assay as described in the Materials and Methods. Overlaying the cholesterol distribution curve with the corresponding time in which each fraction is collected, we see a tight overlap of LPA content with the total plasma cholesterol (Figure 4.5).

Global reduction of LPP3 does not alter plasma-LPA localization

LPP3 is a member of the LPP family of phosphatases who dephosphorylate LPA and limit LPA receptor signaling. Our lab has previously shown that endothelial cell-specific deletion of LPP3 results in a significant LPA-dependent decrease in vEC barrier function [22] suggesting that the phosphatase plays a role in limiting LPA-induced vEC permeability. In Chapter 3 I reported that the global LPP3-deficient MX-1Δ mice fed Western diet have significantly increased lesion formation compared to fl/fl control mice (Figure 211a) that coincides with increased circulating plasma LPA (Figure 2.10d) as well as increased LPA in the proximal aorta (Figure 2.11b). We hypothesized that global reductions in LPP3 would lead to increased LPA content in the plasma fractions containing LDL-C compared to fl/fl controls.

Plasma from MX-1Δ and fl/fl mice was separated by size exclusion chromatography as previously described and LPA content was determined with LC MS/MS. As expected we observed increased total LPA content in plasma from MX-1Δ mice compared to fl/fl controls (Figure 4.6); however, we were unable to detect any differences in the LPA content from fractions containing LDL-C (Figure 4.7).

Discussion

LPA accumulates in human atheroma and hyperlipidemic Apoe and Ldlr mice fed Western diet for weeks (Figure 4.1a). Interestingly, we observed dramatic increases in unsaturated LPA species 18:1, 20:3, 20:4, 20:5, 22:5 and 22:6 in hyperlipidemic mouse atheroma compared to saturated 16:0 and 18:0 species which were still increased but not to the same extent (Figure 4.1b). $ApoE^{-/-}$ and $Ldlr^{-/-}$ mice fed chow diet have increased cholesterol and total LPA compared to C57BL/6 controls fed the same diet (Figure 4.2). Feeding Western diet for 3 weeks dramatically increases plasma cholesterol and total LPA content in hyperlipidemic mice compared to wild-type controls (Figure 4.2b). Plasma LPA from wild-type mice and $Apoe^{-/-}$ fed chow diet was observed in fractions containing HDL-C and plasma proteins (Figure 4.3). *$Ldlr^{-/-}$* mice fed chow diet have LPA content in fractions containing HDL-C and plasma proteins, but also have slight increases fractions 1 through 10 containing LDL-C (Figure 4.3). Feeding Western diet for 3 weeks increases plasma LPA content in fractions 1 through 10 in hyperlipidemic mice but not wild-type mice suggesting increased LPA association with LDL-C. Interestingly, the unsaturated LPA content is markedly increased in hyperlipidemic plasma fractions that contain LDL-C compared to saturated LPA. While wild-type mice show only modestly increased total plasma LPA content and no increase in LPA content in fractions containing LDL-C (Figure 4.3), feeding C57BL/6 mice Western diet for 12 weeks increases the proportion of plasma LPA content in lower density fractions 13 to 18 whereas LPA content is primarily found in

fractions 18 to 23 in chow fed mice. Additionally, we demonstrated that the plasma cholesterol distribution overlaps with the collected fractions used for determined LPA and increased LPA content in fractions 1 through 10 of hyperlipidemic mice correlates with sharp increases in plasma cholesterol (Figure 4.5). Finally, we show that while global reductions in LPP3 increases total plasma LPA it does not increase LPA content in fractions containing LDL-C relative to control mice.

The Increased accumulation of unsaturated LPA in fractions containing LDL-C in hyperlipidemic mice (Figure 4.3) is interesting in the context of atherosclerosis. Navab et al., demonstrates that intestinally-derived unsaturated, but not saturated, LPA increases atherosclerotic lesion formation in *Ldlr*$^{-/-}$ mice [123]. Navab et al.'s observations are also supported in a study published by Zhou et al., where i.v. administration of 20:4 unsaturated LPA, but not 18:0 saturated LPA, increased atherosclerotic lesion formation in *Ldlr*$^{-/-}$ mice, which could be inhibited with LPA1/3 antagonist Ki16425 [14]. In the latter study, unsaturated LPA administration coincided with increased CD68 positive staining in atheromas and upregulation of vEC adhesion molecule CXCL1. Wild-type mice fed Western diet for 12 weeks resulted in an increase in LPA content, specifically the unsaturated species, into the lower density plasma fractions 13 to 18 suggesting that LPA's association with fractions containing LDL-C in the plasma can be affected by diet and not solely through hyperlipidemia. In either case, it is feasible that a cholesterol-enriched diet leads to increases in unsaturated LPA accumulation in circulating LDL-C that is deposited within the vessel wall and propagates LPA receptor signaling to drive multi-tissue dysfunction and lesion formation.

Limitations of this study heed further investigation and lacks some important physiological read-outs. For instance total triglyceride measurements would be helpful in the interpretation of Figure 4.4 in which C57BL6 mice were fed Western diet for 12 weeks.

The LPA distribution shifts to the lower density fractions which cannot be attributed to an increase in cholesterol. Perhaps an increase in circulating triglycerides could account for differences between chow and Western diet fed LPA distributions. Likewise I did not perform an analysis of the total LPA in the mice represented in Figure 4.4 that would be useful in determining there was change in absolute LPA between chow diet and prolonged Western diet administration. Lastly, while we are able to demonstrate that the cholesterol distribution in plasma correlates with the fractions we are collecting and associating with LPA we still have not shown physical LPA-LDL-C binding in these fractions. To address this point Dr. Fred Onono has performed immunoprecipitation of ApoB from human plasma and determined LPA content using LC MS/MS. He observed that 10 to 65% of total circulating LPA is physically associated with the LDL-C protein ApoB depending on whether the individual was in a fed or fasted state (Data not shown).

To summarize, Western diet fed hyperlipidemic mice demonstrate dramatic increases in LPA content in the LDL-C plasma fractions relative to their chow fed counterparts and specifically in the unsaturated species suggesting that LPA in hyperlipidemic models may be bound to LDL-C and could elicit a multitude of effects on the vasculature via LPA receptor signaling. Additionally, LDL-C may in fact be a source of not just LPC, but also LPA in atherosclerotic lesions that would be supported by our observation of increased unsaturated LPA species in murine lesions. Aside from models of hyperlipidemia, unsaturated LPA content in the LDL-C plasma fractions are affected by prolonged administration of cholesterol-enriched diet which may be of relevance considering recent investigations by Zhou et al., and Navab et al. demonstrating a role for both circulatory and intestinally-derived unsaturated LPA in increasing atherosclerotic lesion formation in mice.

Acknowledgements

This study was carried out as a joint effort by Dr. Fred Onono and I and could not have been done without the additional help of others including Dr. Ryan Temel and Dr. Joseph Layne in assisting us with the preliminary FPLC fractionation experiments presented in Figures 4.4, 4.5 and 4.6. None of the LPA measurements presented in this chapter would have been generated without the expertise of Manjula Sunkara and Dr. Sony Soman in performing mass spectrometry. Dr. Onono and myself acquired and processed samples for Figures 4.2 and 4.3 and Dr. Andrew Morris and Dr. Onono are credited with the interpretation and generation of Figures 4.2 and 4.3; whereas I carried out the experiments and analysis of Figures 4.4, 4.5, 4.6 and 4.7.

Figure 4.1

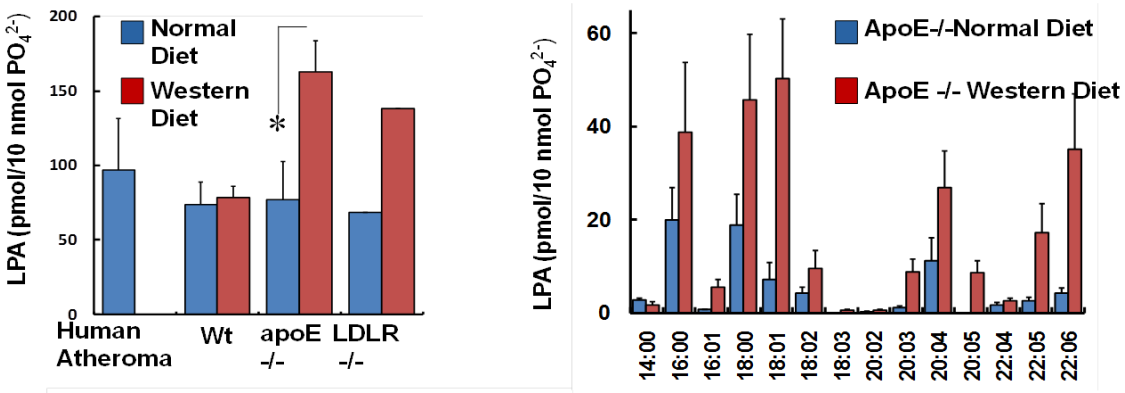

LPA accumulates in human and murine atheroma. Human atheroma and mouse proximal aortas were subjected to lipid extraction to determine LPA concentrations. LPA presented as pmol and normalized to 10 nmol of phosphate calculated using a phosphate binding protein assay (abcam). Human atheroma and chow diet fed mouse samples are represented in blue while Western diet fed mouse samples are represented in red. Data are presented as mean ± SD. *P<0.05

Figure 4.2

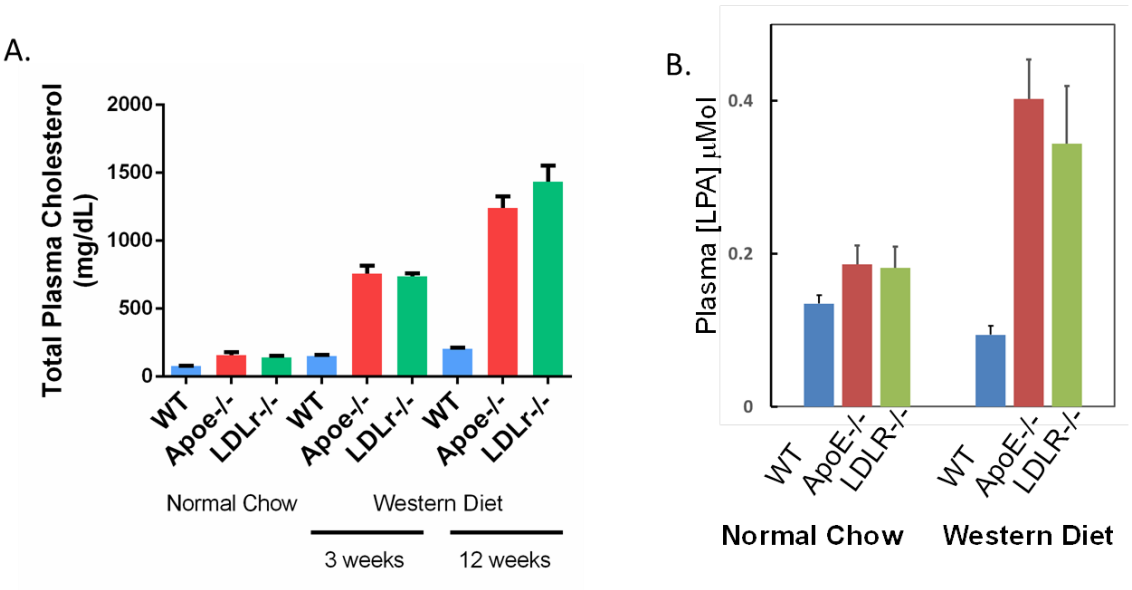

Total plasma LPA increases in hyperlipidemic mice fed Western diet. C57BL/6 (blue), *Apoe*$^{-/-}$ (red), and *Ldlr*$^{-/-}$ (green) mice were fed normal chow or Western diet for 3 or 12 weeks. **(A)** Total plasma cholesterol (mg/dL) from three cohorts (n=5 for each genotype). **(B)** Total plasma LPA (µmols) determined with HPLC MS/MS from mice fed normal chow and Western diet for 3 weeks (n=5 for each genotype). Data are presented as mean ± SEM.

Figure 4.3

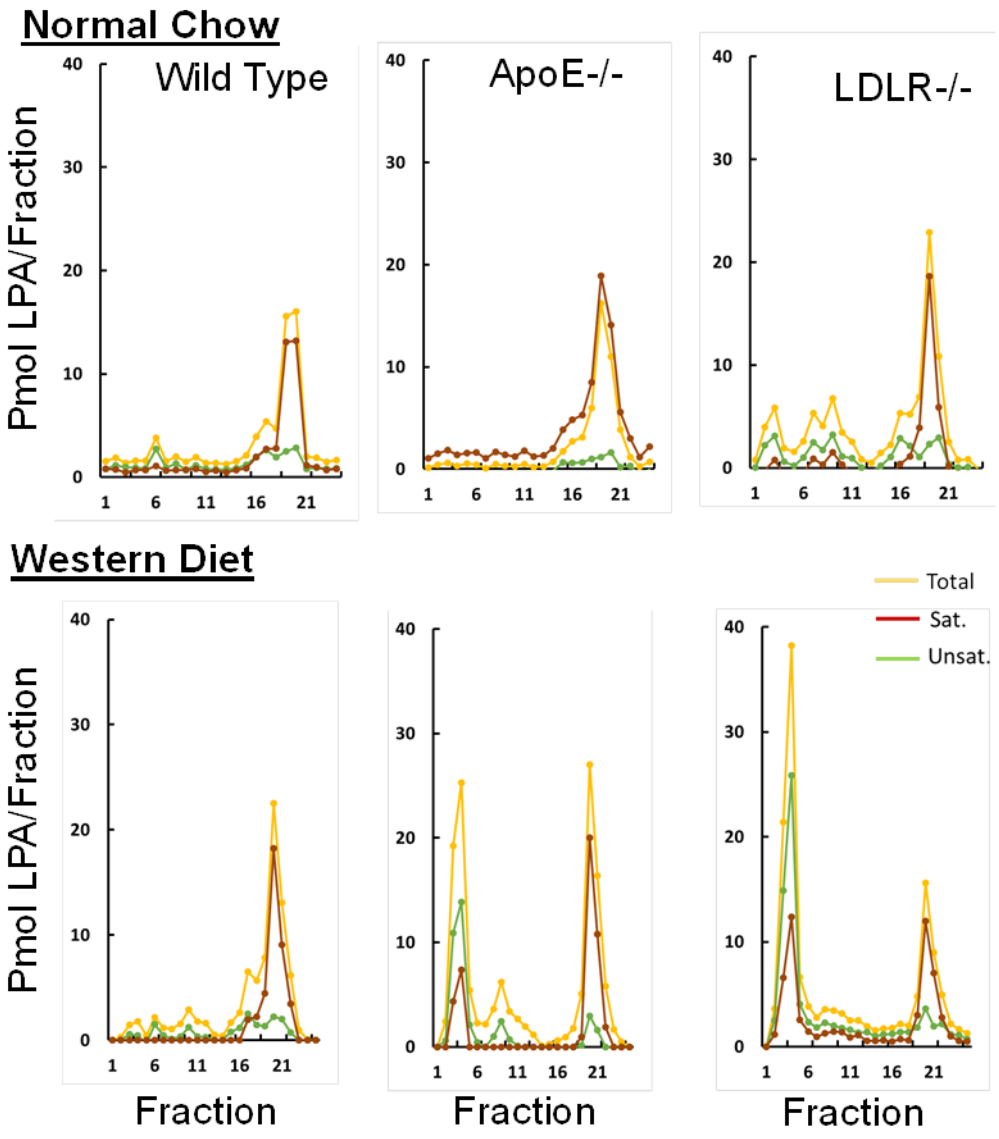

Western diet induces the redistribution of LPA in plasma of hyperlipidemic mice. C57BL/6, *Apoe*$^{-/-}$, and *Ldlr*$^{-/-}$ mice were fed **(Top)** normal chow or **(Bottom)** Western diet for 3 weeks. Plasma was injected into a FPLC column and fractionated as described in methods and materials. Plasma LPA (pmol/Fraction) is presented as total LPA (yellow), saturated LPA (red) and unsaturated LPA (green).

Figure 4.4

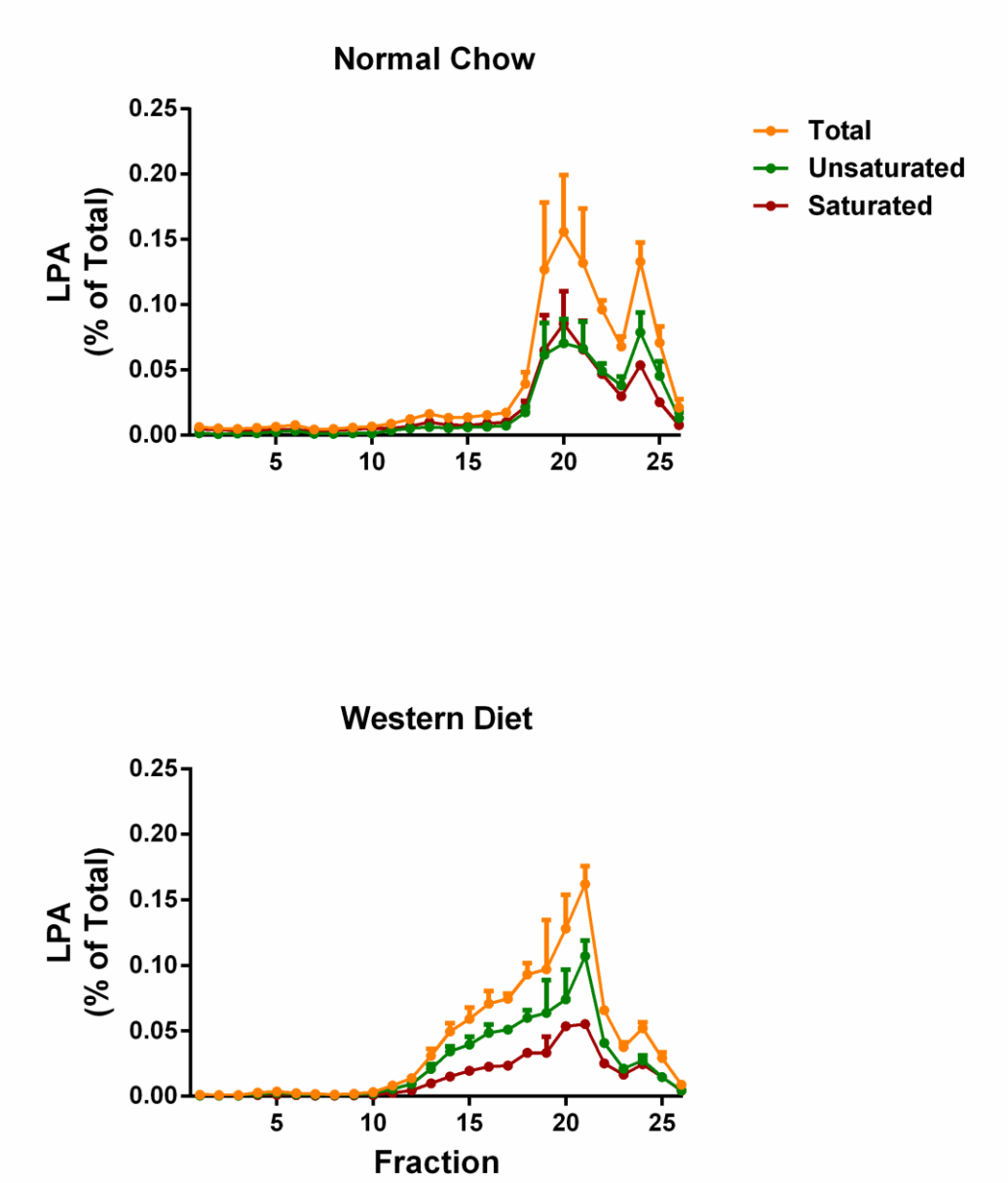

Prolonged Western diet feeding shifts plasma LPA to lower density fractions in wild-type mice. C57BL/6 mice were fed **(Top)** normal chow (n=3) or **(Bottom)** Western diet (n=3) for 12 weeks. Plasma was injected into a FPLC column and fractionated as described in Methods and Materials. Plasma LPA (% of total) is represented as total LPA (yellow), saturated LPA (red) and unsaturated LPA (green). Data are presented as mean ± SEM.

Figure 4.5

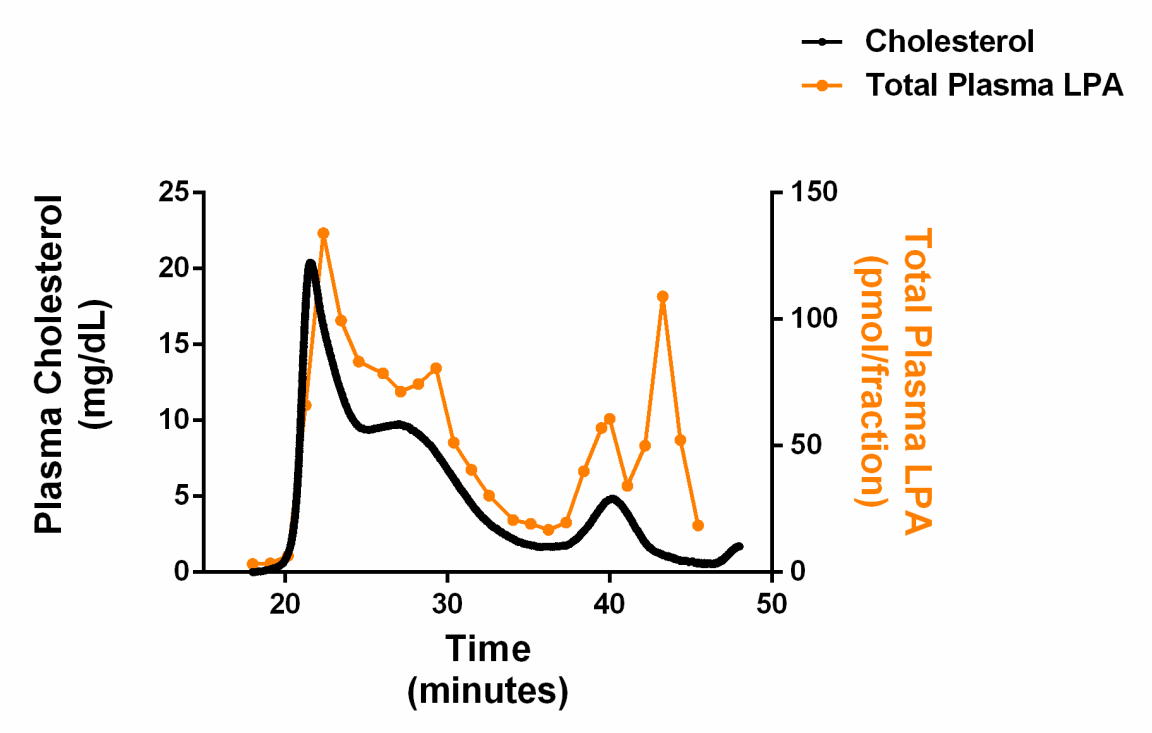

Plasma LPA fractions correlate with total cholesterol curves. Representative image of LPA (pmol/fraction) and plasma cholesterol (mg/dL) from MX-1Δ mouse plasma. Plasma was injected into a FPLC column and fractionated as described in Methods and Materials. Cholesterol concentration was determined using enzymatic colorimetric assay reading at 600nm as the elute flows off of the column. LPA fractions are given at their respective time of collection during the fractionation process.

Figure 4.6

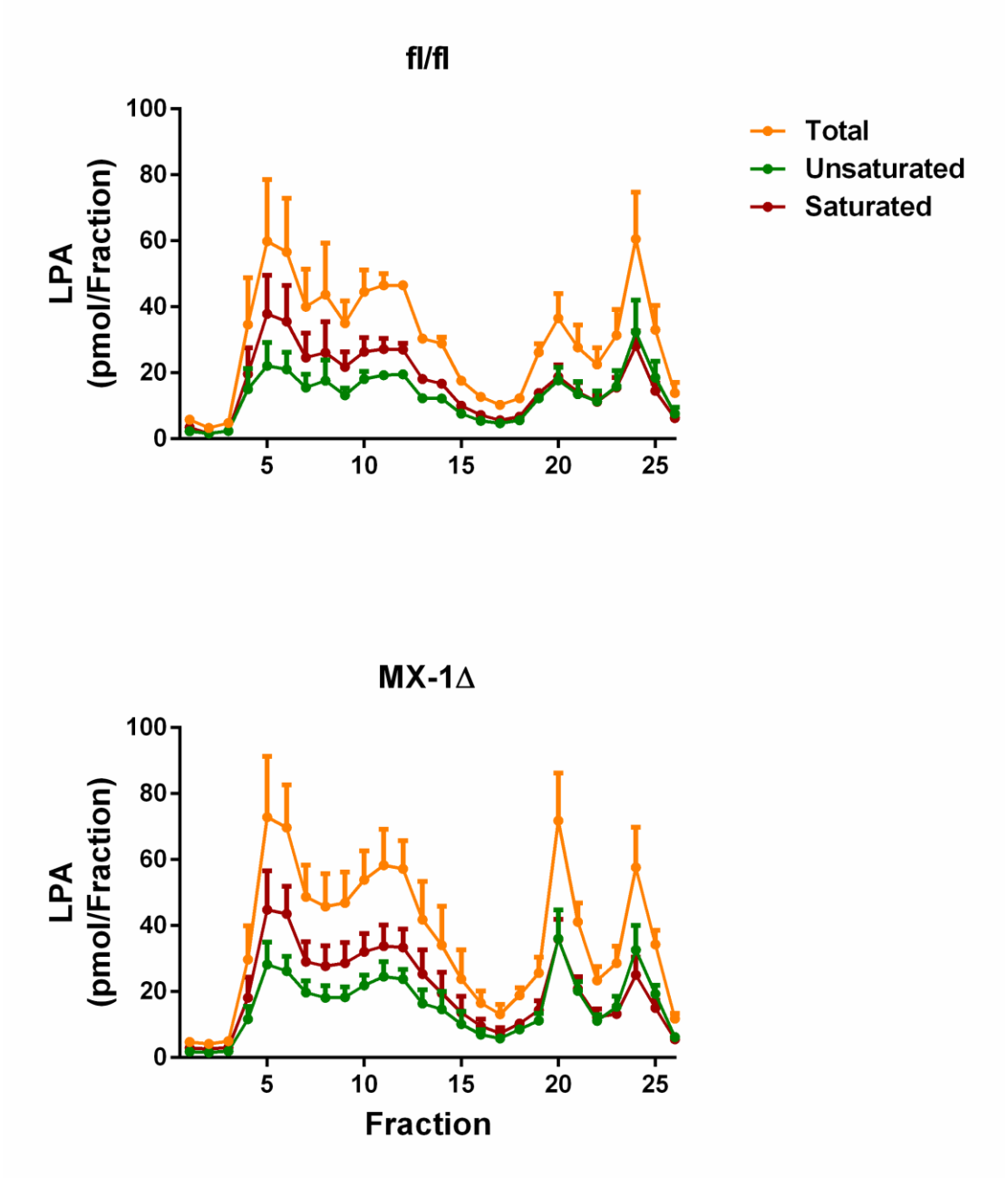

Global reduction of LPP3 does not alter plasma LPA distribution. (Top) fl/fl (n=2) and **(Bottom)** MX-1Δ (n=5) mice were fed Western diet for 12 weeks. Plasma was injected into a FPLC column and fractionated as described in methods and materials. Plasma LPA (pmol/Fraction) is represented as total LPA (yellow), saturated LPA (red) and unsaturated LPA (green). Data are presented as mean ± SEM.

Figure 4.7

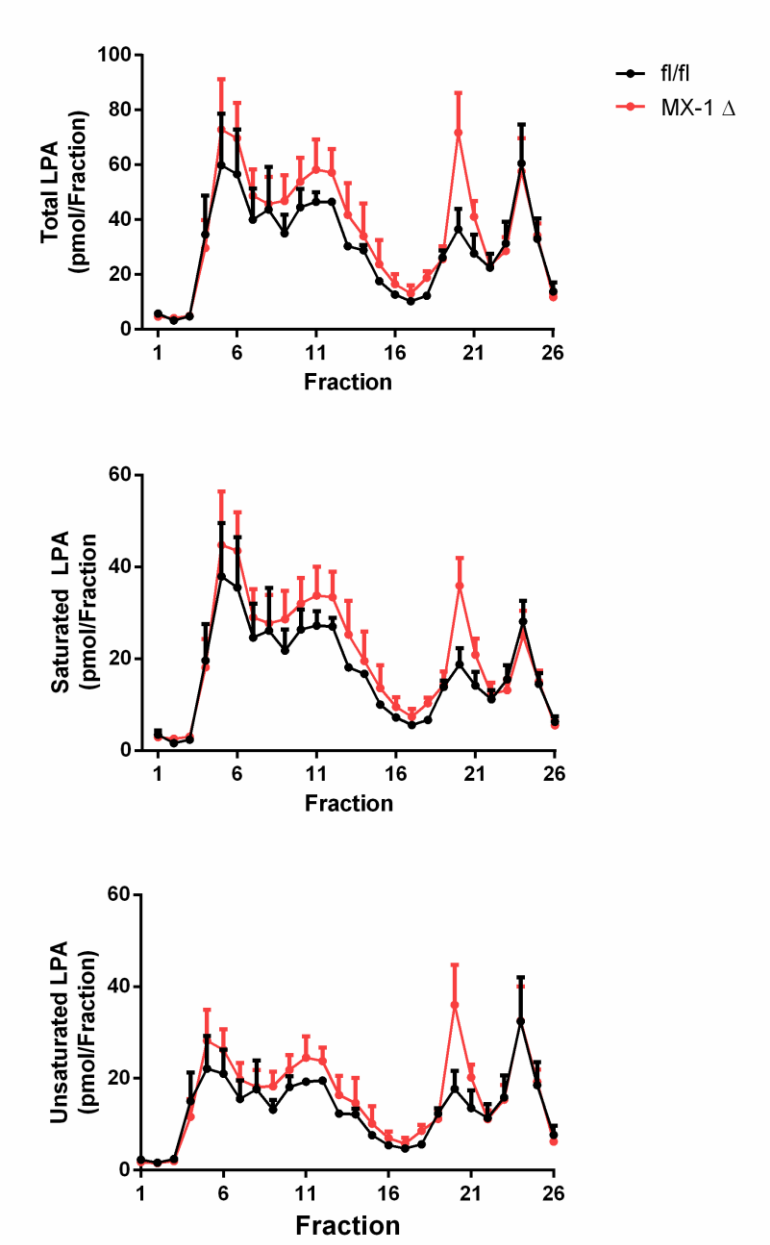

LPA species subtype does not change with global reductions in LPP3.) MX-1Δ (n=5) mice were fed Western diet for 12 weeks. Plasma was injected into a FPLC column and fractionated as described in methods and materials. LPA (pmol/Fraction) from MX-1Δ (red) and fl/fl (black) mice was compared based on species: **(Top)** Total LPA, **(Middle)** saturated LPA and **(Bottom)** unsaturated LPA. Data are presented as mean ± SEM.

Chapter 5: Discussion

So far this dissertation has provided a detailed discussion on mechanisms of atherosclerosis and proposes a role for the ATX-LPA-LPP3 signaling axis in the development and regulation of disease. I provide evidence that LPP3 expression limits lesion formation in murine models of atherosclerosis and that CAD-associated risk loci within *PPAP2B* decrease its expression in a *cis*-manner. Finally, I demonstrate LPA content increases in plasma fractions containing LDL-C in hyperlipidemic mice on a cholesterol-enriched diet. In this chapter I will review data presented in this dissertation and discuss the overarching potential for CAD-associated risk alleles to limit *PPAP2B* expression in atherosclerosis driving local increases in LPA signaling that may be exacerbated based on a diet.

CAD-associated risk loci decrease PPAP2B expression in a cis-manner

In Chapter 2 I present data that our lab generated in collaboration with Reschen et al. that demonstrates upregulation of LPP3 protein in human foam cells that is absent in naïve vehicle treated macrophages (Figure 2.1). These data support observations from the Oxford group that the CAD-associated SNP rs72664324 diminishes the ability of macrophages to upregulate *PPAP2B* expression upon exposure to oxLDL by breaking a C/ETPβ binding motif. In fact, when macrophages were treated with oxLDL Reschen et al. observed open chromatin site remodeling in the region of *PPAP2B* that harbors rs72664324 using FAIRE-seq. rs72664324 is a proxySNP in linkage disequilibrium with rs17114036 and is in a C/EBPβ CCAAT binding motif. Presence of the protective allele (A) facilitates the transcription factor binding and subsequent expression of *PPAP2B;* however, presence of the risk allele (G) disrupts this motif resulting in the diminished upregulation of *PPAP2B* as described above. Their study reveals a mechanism for

PPAP2B upregulation in a key cellular process in atherosclerosis that is limited by a *cis*-acting CAD-associated risk allele in rs72664324.

I present additional evidence in Chapter 3 that CAD-associated risk alleles are acting in a *cis*-manner on *PPAP2B.* I searched a publically available database for microarray data looking at SNP-mediated effects on gene expression. Table 3.1 contains *PPAP2B* exon probes that displayed significant decreases in expression associated with the risk allele of rs9970807, another proxySNP in linkage disequilibrium with rs17114036. The CAD-associated risk loci are found on chromosome 1; interestingly, *PCSK9* is also found on chromosome 1 and is considered a master regulator of cholesterol and, as such, is highly implicated in the development of CAD. To rule out that risk loci in *PPAP2B* are not conferring increased risk of disease by modifying *PCSK9* transcript levels in a trans-manner, I searched the database for the same SNP-mediated effects on *PCSK9* expression. Table 3.2 contains *PCSK9* exon probes; however, unlike *PPAP2B*, the *PCKS9* exon probes expression were unaffected by the presence of rs9970807. This suggests that CAD-associated risk alleles are, in relation to *PCSK9*, not acting in a trans-manner but do regulate *PPAP2B* expression in *cis*.

It is worth mentioning that a study published by Erbilgin et al. also demonstrates risk allele-dependent decreases in *PPAP2B* expression in HAECs. Taking these data together, CAD-associated risk alleles identified within *PPAP2B* are capable of regulating *PPAP2B's* expression in a cis-manner and demonstrate no trans-mediated effects on *PCSK9* expression.

Ppap2b expression limits lesion formation in murine models of atherosclerosis

In Chapter 2 I provide evidence that LPP3 expression increases in murine models of atherosclerosis that is not observed in healthy vasculature (Figure 2.2 through 2.7). We

also demonstrated the same C/ETPβ binding to rs72664324 in a macrophage mouse line RAW264.7 that was observed in human macrophages by Reschen et al. These data suggest that atherosclerotic vessels upregulate LPP3 in response to disease.

We next generated a murine model of atherosclerosis with global leukocyte-specific and SMC-specific reductions in LPP3. Our inducible global *Ppap2b* knockout mice had a 30% increase in atherosclerotic lesion formation compared to fl/fl control mice (Figure 2.11a) despite no differences in plasma cholesterol (Figure 2.10a). Increased atherosclerosis coincided with increased plasma LPA (Figure 2.10d) as well as an accumulation of LPA within the proximal aortas of MX-1Δ mice compared to their controls (Figure 2.11b). Interestingly, increased *Cd68* expression was observed in the proximal aortas determined by qRT-PCR (Figure 2.11c) that is supported by increased positive CD68 staining in aortic root lesions (Figure 2.11d). ICAM-1 staining was also dramatically higher in MX-1Δ aortic root lesions compared to fl/fl mice suggesting an increase in the vEC adhesion molecule (Figure 2.12). We detected no differences in lesion formation in the leukocyte-specific deletion of *Ppap2b* (Figure 2.14); however BMDMs from LysM-Δ mice have increased proinflammatory *Il1b* and *Il12b* expression compared to fl/fl control cells (Figure 2.13b). This observation suggests that while leukocyte-derived LPP3 may be insufficient to confer protection against lesion formation, it is important in limiting inflammation. Finally, we observed increased lesion formation in mice deficient in SMC-derived LPP3 (Figure16a) despite, again, no differences in plasma cholesterol (Figure 2.15b). Proximal aortas from mice deficient in LPP3 from SMCs show significantly higher LPA content (Figure 2.16b) as well as Il6 expression (Figure 2.16c) and their aortic root lesions have increased CD68 expression (Figure 2.16d) similar to what was observed in the global LPP3 knockouts.

Chapter 2 provides evidence that SMCs also upregulate PPAP2B in response to cholesterol loading (Figure 2.17b). This is an interesting observation considering data

generated in our collaboration with Reschen et al., that macrophages upregulate LPP3 in response to oxLDL-induced foam cell formation. Recent evidence proposes that SMCs make up nearly 50% of foam cells present in atherosclerotic plaques, and therefore their PPAP2Bs role in their phenotypic conversion may be an interesting cellular mechanism to investigate.

Global reductions in LPP3 in our murine model resulted in increased expression of Cd68 in proximal aortas. CD68 positive staining in the aortic root lesions of MX-1Δ and SM22-Δ mice were also increased compared to their respective controls. This observation can be explained by the simple fact that a larger lesion size suggests more foam cells. Alternatively, as is suggested by the increased ICAM-1 staining in MX-1Δ lesions, there could be an increased propensity for leukocyte infiltration into the vessel wall when LPP3 is absent. This latter hypothesis would have to be investigated with cell sorting using FACS. Liping Yang from our lab has preliminary data that aorta from SM22-Δ mice do have increased CD68 positive cells compared to fl/fl controls but more experiments should be carried out to confirm this observation. Our lab has previously shown that mice with targeted inactivation of LPP3 in their endothelial cells have decreased endothelial barrier function [22] and increased vEC permeability increases leukocyte infiltration into vessels and increases lesion formation [154]. In our model of LPP3-dependent vascular barrier function, the increased endothelial permeability in LPP3-deficient mice could be attenuated with an ATX inhibitor or a LPA receptor pan antagonist suggesting that LPA signaling is regulating the observed phenotype. LPA signaling has been shown to regulate vEC barrier function before and could provide a mechanism for increased atherosclerotic lesion formation in these mice.

Myeloid cell-specific deletion of LPP3 did not increase the development of atherosclerotic lesions in mice suggesting that the phosphatase in macrophages in not important in

protecting mice from disease (Figure 2.14). However, another way to interpret the data is that the expression of LPP3 from macrophages is insufficient to confer protection compared to the overall net expression of the phosphatase in lesion cells. As discussed in “Chapter 1: Structure and Function of the LPPs”, LPP3 homologs are capable of generating phospholipid gradients and thus affecting cells upwards of 33μm away [132]. It is feasible then that LPP3 expressed in SMCs (as well as other lesion cells not of myeloid lineage) in the LysM-Δ mice is capable of conferring protection to lesion development by affecting cell types in a paracrine or non-autonomous manner, possibly through the regulation of LPA or other phospholipid substrates. However, in both the global and the SMC-specific models of LPP3 deficiency, enough of the phosphatase has been knocked out to abrogate the non-autonomous manner of protection.

LPA content increases in plasma fractions containing LDL-C in hyperlipidemic mice

I present preliminary evidence in Chapter 4 that LPA content increases in plasma fractions containing LDL-C in hyperlipidemic mice. Previously, LPA was found primarily bound to plasma proteins; however its precursor molecule, LPC, is known to be a major phospholipid component of plasma lipoproteins [155]. Interestingly, unsaturated LPA content demonstrates large increases in the plasma fractions containing LDL-C from $Apoe^{-/-}$ and $Ldlr^{-/-}$ mice fed Western diet for 3 weeks (Figure 4.3). Unsaturated LPA has been shown to increase atherosclerotic lesion formation in several investigations [14, 123] and its increase in LDL-C would propose a mechanism in which atherogenic LPA species are introduced into the vessel wall with LDL-C deposition.

Overview

In this dissertation I present a model for LPP3 in limiting the lesion formation in murine models of atherosclerosis which supports our hypothesis that CAD-associated risk loci in *PPAP2B* are acting in a cis-mediated fashion to diminish LPP3 expression in individual's homozygous for the risk alleles (Figure 5.1). LPP3 plays a protective role in the development and progression of atherosclerosis by limiting LPA signaling in the vessel wall, resulting from deposition of LDL-C carrying atherogenic unsaturated LPA, and individuals who are unable to upregulate *PPAP2B* in response to atherosclerotic stimuli are at increased risk of CAD.

Figure 5.1

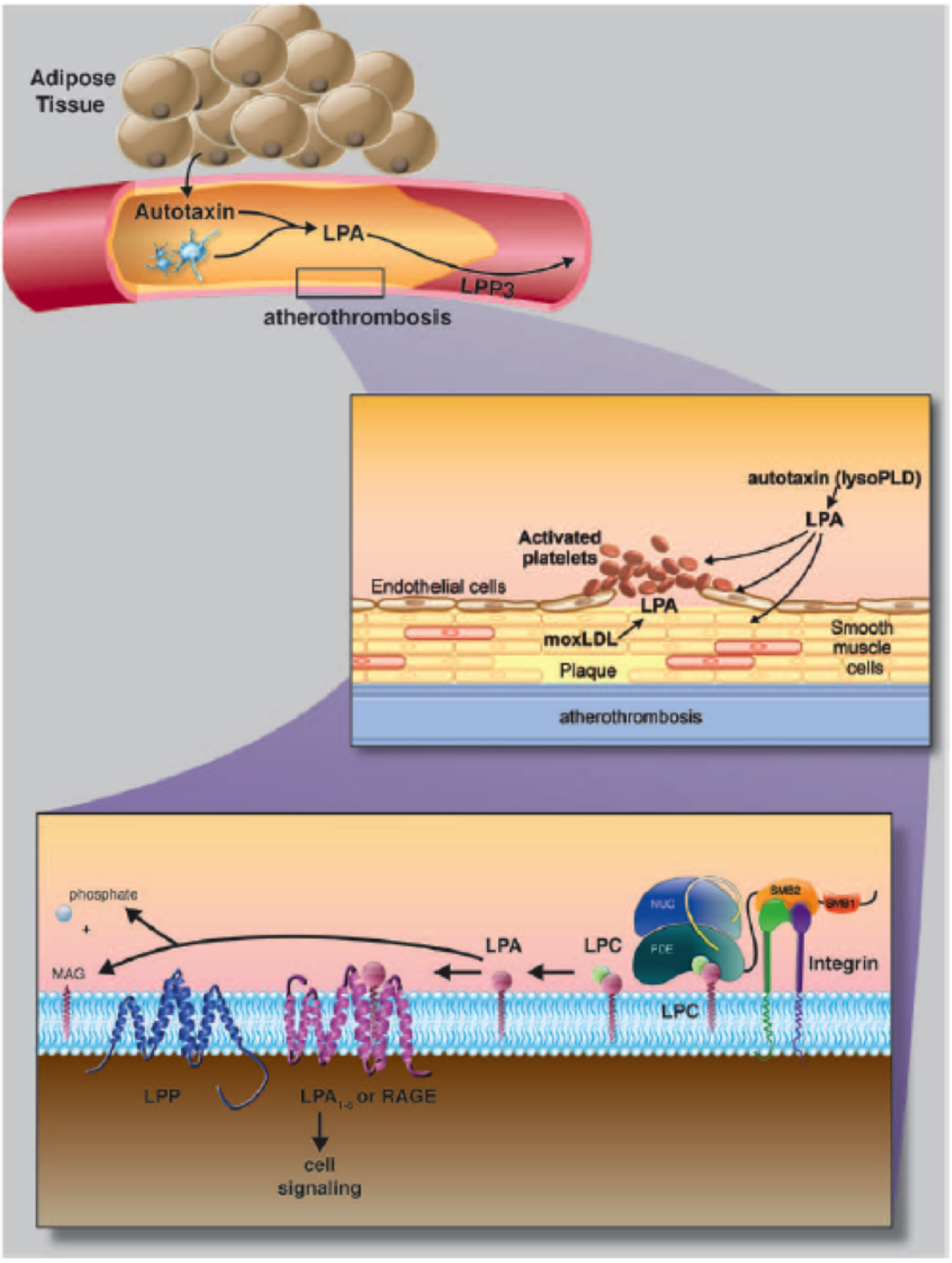
Adipose Tissue
Autotaxin
LPA
LPP3
atherothrombosis
autotaxin (lysoPLD)
LPA
Activated platelets
Endothelial cells
LPA
moxLDL
Plaque
Smooth muscle cells
atherothrombosis
phosphate
+
MAG
LPA
LPC
NUC
PDE
SMB2
SMB1
Integrin
LPC
LPP
LPA1-6 or RAGE
cell signaling

Figure 5.1 (Caption)

Proposed model for ATX –LPA–LPP3 nexus in atherosclerosis and it complications. Top, At least a portion of circulating ATX may derive from adipose tissue. Middle, ATX - derived LPA has potent effects on several blood and vascular cells that could potentially contribute to biological events that underlie atherosclerosis. In addition, atherosclerotic plaque is enriched in LPA. Bottom, Circulating and secreted ATX may interact with integrins and through non–integrin-mediated mechanisms to generate a local gradient of LPA. ATX contains a catalytic phosphodiesterase (PDE) domain, a nuclease like (NUC) domain and integrin binding somatomedin B like (SMB) domains. LPA signaling through G-protein–couple receptors LPA1–6 and possible receptor for advanced glycan end products (RAGE) may be terminated by enzymatic dephosphorylation catalyzed by LPPs. Whether ATX promotes and LPP3 suppresses atherosclerosis remains to be established. Illustration by Matt Hazzard, University of Kentucky, Information Technology. LDL indicates low-density lipoprotein; LPC, lysophophosphatidyl choline; and lyso-PLD, lysophospholipase D [156].

References

1. *Compressed mortality file: underlying cause of death 1999–2013*. 2016, Centers for Disease Control and Prevention: Atlanta, GA: Centers for Disease Control and Prevention.
2. Mozaffarian, D., et al., *Heart Disease and Stroke Statistics-2016 Update: A Report From the American Heart Association.* Circulation, 2016. **133**(4): p. e38-e360.
3. Mozaffarian D, B.E., Go AS, Arnett DK, Blaha MJ, Cushman M, Das SR, de Ferranti S, Després J-P, Fullerton HJ, Howard VJ, Huffman MD, Isasi CR, Jiménez MC, Judd SE, Kissela BM, Lichtman JH, Lisabeth LD, Liu S, Mackey RH, Magid DJ, McGuire DK, Mohler ER III, Moy CS, Muntner P, Mussolino ME, Nasir K, Neumar RW, Nichol G, Palaniappan L, Pandey DK, Reeves MJ, Rodriguez CJ, Rosamond W, Sorlie PD, Stein J, Towfighi A, Turan TN, Virani SS, Woo D, Yeh RW, Turner MB, *Heart Disease and Stroke Statistics -- 2016 Update: a report from the American Heart Association.* Circulation, 2016. **133**(4): p. e38-e360.
4. Schunkert, H., et al., *Large-scale association analysis identifies 13 new susceptibility loci for coronary artery disease.* Nat Genet, 2011. **43**(4): p. 333-8.
5. Choi, J.W., et al., *LPA receptors: subtypes and biological actions.* Annu Rev Pharmacol Toxicol, 2010. **50**: p. 157-86.
6. Blaho, V.A. and T. Hla, *Regulation of mammalian physiology, development, and disease by the sphingosine 1-phosphate and lysophosphatidic acid receptors.* Chem Rev, 2011. **111**(10): p. 6299-320.
7. Moolenaar, W.H. and T. Hla, *SnapShot: Bioactive lysophospholipids.* Cell, 2012. **148**(1-2): p. 378-378.e2.
8. Tigyi, G., *Physiological responses to lysophosphatidic acid and related glycero-phospholipids.* Prostaglandins Other Lipid Mediat, 2001. **64**(1-4): p. 47-62.
9. Tigyi, G., *Preface to the special issue: Lysophospholipids in health and disease.* Biochim Biophys Acta, 2008. **1781**(9): p. 423.
10. Panchatcharam, M., et al., *Lysophosphatidic acid receptors 1 and 2 play roles in regulation of vascular injury responses but not blood pressure.* Circ Res, 2008. **103**(6): p. 662-70.
11. Subramanian, P., et al., *Lysophosphatidic Acid Receptors LPA1 and LPA3 Promote CXCL12-Mediated Smooth Muscle Progenitor Cell Recruitment in Neointima Formation.* Circulation Research, 2010. **107**(1): p. 96-105.
12. Pamuklar, Z., et al., *Individual heterogeneity in platelet response to lysophosphatidic acid: evidence for a novel inhibitory pathway.* Arterioscler Thromb Vasc Biol, 2008. **28**(3): p. 555-61.
13. Haseruck, N., et al., *The plaque lipid lysophosphatidic acid stimulates platelet activation and platelet-monocyte aggregate formation in whole blood: involvement of P2Y1 and P2Y12 receptors.* Blood, 2004. **103**(7): p. 2585-92.
14. Zhou, Z., et al., *Lipoprotein-derived lysophosphatidic acid promotes atherosclerosis by releasing CXCL1 from the endothelium.* Cell Metab, 2011. **13**(5): p. 592-600.
15. Mueller, P., et al., *Lysophospholipid mediators in the vasculature.* Exp Cell Res, 2015. **333**(2): p. 190-4.
16. Sen, S., R.R. Smeby, and F.M. Bumpus, *Antihypertensive effect of an isolated phospholipid.* Am J Physiol, 1968. **214**(2): p. 337-41.
17. Vogt, W., *Pharamacologically active acidic phospholipids and glycolipids.* Biochem Pharmacol, 1963. **12**: p. 415-20.

18. Aoki, J., A. Inoue, and S. Okudaira, *Two pathways for lysophosphatidic acid production.* Biochim Biophys Acta, 2008. **1781**(9): p. 513-8.
19. Contos, J.J., et al., *Requirement for the lpA1 lysophosphatidic acid receptor gene in normal suckling behavior.* Proc Natl Acad Sci U S A, 2000. **97**(24): p. 13384-9.
20. Althoff, T.F., et al., *Procontractile G protein-mediated signaling pathways antagonistically regulate smooth muscle differentiation in vascular remodeling.* J Exp Med, 2012. **209**(12): p. 2277-90.
21. Tager, A.M., et al., *The lysophosphatidic acid receptor LPA1 links pulmonary fibrosis to lung injury by mediating fibroblast recruitment and vascular leak.* Nat Med, 2008. **14**(1): p. 45-54.
22. Panchatcharam, M., et al., *Mice with targeted inactivation of ppap2b in endothelial and hematopoietic cells display enhanced vascular inflammation and permeability.* Arterioscler Thromb Vasc Biol, 2014. **34**(4): p. 837-45.
23. Zhao, J., et al., *Lysophosphatidic acid receptor 1 antagonist ki16425 blunts abdominal and systemic inflammation in a mouse model of peritoneal sepsis.* Transl Res, 2015. **166**(1): p. 80-8.
24. Contos, J.J.A., et al., *Characterization of lpa2 (Edg4) and lpa1/lpa2 (Edg2/Edg4) Lysophosphatidic Acid Receptor Knockout Mice: Signaling Deficits without Obvious Phenotypic Abnormality Attributable to lpa2.* Molecular and Cellular Biology, 2002. **22**(19): p. 6921-6929.
25. Cheng, H.-Y., et al., *Lysophosphatidic Acid Signaling Protects Pulmonary Vasculature From Hypoxia-Induced Remodeling.* Arteriosclerosis, Thrombosis, and Vascular Biology, 2012. **32**(1): p. 24-32.
26. Sumida, H., et al., *LPA4 regulates blood and lymphatic vessel formation during mouse embryogenesis.* Blood, 2010. **116**(23): p. 5060-5070.
27. Rai, V., et al., *Lysophosphatidic acid targets vascular and oncogenic pathways via RAGE signaling.* The Journal of Experimental Medicine, 2012. **209**(13): p. 2339-2350.
28. Albers, H.M.H.G., et al., *Boronic acid-based inhibitor of autotaxin reveals rapid turnover of LPA in the circulation.* Proceedings of the National Academy of Sciences, 2010. **107**(16): p. 7257-7262.
29. Kurano, M., et al., *Possible Involvement of Minor Lysophospholipids in the Increase in Plasma Lysophosphatidic Acid in Acute Coronary Syndrome.* Arteriosclerosis, Thrombosis, and Vascular Biology, 2015. **35**(2): p. 463-470.
30. Dohi, T., et al., *Increased lysophosphatidic acid levels in culprit coronary arteries of patients with acute coronary syndrome.* Atherosclerosis. **229**(1): p. 192-197.
31. Watanabe, N., et al., *Both plasma lysophosphatidic acid and serum autotaxin levels are increased in chronic hepatitis C.* J Clin Gastroenterol, 2007. **41**(6): p. 616-23.
32. Moolenaar, W.H. and A. Perrakis, *Insights into autotaxin: how to produce and present a lipid mediator.* Nat Rev Mol Cell Biol, 2011. **12**(10): p. 674-679.
33. Hausmann, J., et al., *Structural basis of substrate discrimination and integrin binding by autotaxin.* Nat Struct Mol Biol, 2011. **18**(2): p. 198-204.
34. Pamuklar, Z., et al., *Autotaxin/lysopholipase D and lysophosphatidic acid regulate murine hemostasis and thrombosis.* J Biol Chem, 2009. **284**(11): p. 7385-94.
35. Dusaulcy, R., et al., *Adipose-specific disruption of autotaxin enhances nutritional fattening and reduces plasma lysophosphatidic acid.* Journal of Lipid Research, 2011. **52**(6): p. 1247-1255.

36. Leblanc, R., et al., *Interaction of platelet-derived autotaxin with tumor integrin αVβ3 controls metastasis of breast cancer cells to bone.* Blood, 2014. **124**(20): p. 3141-3150.
37. Jansen, S., et al., *Rapid clearance of the circulating metastatic factor autotaxin by the scavenger receptors of liver sinusoidal endothelial cells.* Cancer Letters. **284**(2): p. 216-221.
38. Gierse, J., et al., *A Novel Autotaxin Inhibitor Reduces Lysophosphatidic Acid Levels in Plasma and the Site of Inflammation.* Journal of Pharmacology and Experimental Therapeutics, 2010. **334**(1): p. 310-317.
39. Chen, X., et al., *Serum lysophosphatidic acid concentrations measured by dot immunogold filtration assay in patients with acute myocardial infarction.* Scand J Clin Lab Invest, 2003. **63**(7-8): p. 497-503.
40. van Meeteren, L.A., et al., *Autotaxin, a Secreted Lysophospholipase D, Is Essential for Blood Vessel Formation during Development.* Molecular and Cellular Biology, 2006. **26**(13): p. 5015-5022.
41. Tanaka, M., et al., *Autotaxin Stabilizes Blood Vessels and Is Required for Embryonic Vasculature by Producing Lysophosphatidic Acid.* Journal of Biological Chemistry, 2006. **281**(35): p. 25822-25830.
42. Ferry, G., et al., *Functional invalidation of the autotaxin gene by a single amino acid mutation in mouse is lethal.* FEBS Lett, 2007. **581**(18): p. 3572-8.
43. Yukiura, H., et al., *Autotaxin regulates vascular development via multiple lysophosphatidic acid (LPA) receptors in zebrafish.* J Biol Chem, 2011. **286**(51): p. 43972-83.
44. Siess, W., et al., *Lysophosphatidic acid mediates the rapid activation of platelets and endothelial cells by mildly oxidized low density lipoprotein and accumulates in human atherosclerotic lesions.* Proceedings of the National Academy of Sciences, 1999. **96**(12): p. 6931-6936.
45. Siess, W., *Athero- and thrombogenic actions of lysophosphatidic acid and sphingosine-1-phosphate.* Biochim Biophys Acta, 2002. **1582**(1-3): p. 204-15.
46. Bot, M., et al., *Atherosclerotic Lesion Progression Changes Lysophosphatidic Acid Homeostasis to Favor its Accumulation.* The American Journal of Pathology. **176**(6): p. 3073-3084.
47. Tokumura, A., et al., *Increased formation of lysophosphatidic acids by lysophospholipase D in serum of hypercholesterolemic rabbits.* J Lipid Res, 2002. **43**(2): p. 307-15.
48. Navab, M., et al., *Transgenic 6F tomatoes act on the small intestine to prevent systemic inflammation and dyslipidemia caused by Western diet and intestinally derived lysophosphatidic acid.* J Lipid Res, 2013. **54**(12): p. 3403-18.
49. Dawber, T.R., F.E. Moore, and G.V. Mann, *Coronary heart disease in the Framingham study.* Am J Public Health Nations Health, 1957. **47**(4 Pt 2): p. 4-24.
50. Dawber, T.R., G.F. Meadors, and F.E. Moore, Jr., *Epidemiological approaches to heart disease: the Framingham Study.* Am J Public Health Nations Health, 1951. **41**(3): p. 279-81.
51. Stary, H.C., et al., *A Definition of Advanced Types of Atherosclerotic Lesions and a Histological Classification of Atherosclerosis: A Report From the Committee on Vascular Lesions of the Council on Arteriosclerosis, American Heart Association.* Circulation, 1995. **92**(5): p. 1355-1374.
52. Stary, H.C., et al., *A definition of initial, fatty streak, and intermediate lesions of atherosclerosis. A report from the Committee on Vascular Lesions of the Council on Arteriosclerosis, American Heart Association.* Arterioscler Thromb, 1994. **14**(5): p. 840-56.

53. Stary, H.C., et al., *A definition of the intima of human arteries and of its atherosclerosis-prone regions. A report from the Committee on Vascular Lesions of the Council on Arteriosclerosis, American Heart Association.* Circulation, 1992. **85**(1): p. 391-405.
54. Orr, A.W., et al., *The subendothelial extracellular matrix modulates NF-kappaB activation by flow: a potential role in atherosclerosis.* J Cell Biol, 2005. **169**(1): p. 191-202.
55. Libby, P., *Inflammation in atherosclerosis.* Nature, 2002. **420**(6917): p. 868-74.
56. Buja, L.M., and Jagdish Butany, *Cardiovascular Pathology 4th Edition*. 4 ed, ed. L.M.B.a.J. Butany. 2016, London, UK: Academic Press in an imprint of Elsevier.
57. Kellner-Weibel, G., et al., *Crystallization of free cholesterol in model macrophage foam cells.* Arterioscler Thromb Vasc Biol, 1999. **19**(8): p. 1891-8.
58. Thorp, E., et al., *Mertk receptor mutation reduces efferocytosis efficiency and promotes apoptotic cell accumulation and plaque necrosis in atherosclerotic lesions of apoe-/- mice.* Arterioscler Thromb Vasc Biol, 2008. **28**(8): p. 1421-8.
59. Orr, A.W., Yurdagul Jr A., Patel B., *Pathogenesis of Atherosclerosis: From Cell Biology to Therapeutics*. Integrated Systems Physiology: From Molecule to Function to Disease, ed. a.G.J. Granger D. 2014: Morgan & Claypool Life Sciences.
60. Taubman, M.B., et al., *Tissue factor in the pathogenesis of atherosclerosis.* Thromb Haemost, 1997. **78**(1): p. 200-4.
61. Goncharov, N.V., et al., *Reactive oxygen species in pathogenesis of atherosclerosis.* Curr Pharm Des, 2015. **21**(9): p. 1134-46.
62. Maseri, A. and T. Sanna, *The role of plaque fissures in unstable angina: fact or fiction?* Eur Heart J, 1998. **19 Suppl K**: p. K2-4.
63. Li, Z.Y., et al., *The mechanical triggers of plaque rupture: shear stress vs pressure gradient.* Br J Radiol, 2009. **82 Spec No 1**: p. S39-45.
64. van Dijk, A.C., et al., *Intraplaque Hemorrhage and the Plaque Surface in Carotid Atherosclerosis: The Plaque At RISK Study (PARISK).* 2015. **36**(11): p. 2127-33.
65. Mayranpaa, M.I., et al., *Improved identification of endothelial erosion by simultaneous detection of endothelial cells (CD31/CD34) and platelets (CD42b).* Endothelium, 2007. **14**(2): p. 81-7.
66. Inaba, M. and M. Ueda, *[Vascular Calcification - Pathological Mechanism and Clinical Application - . The significance of arterial calcification in unstable plaques].* Clin Calcium, 2015. **25**(5): p. 679-86.
67. Eisenmenger, L.B. and B.W. Aldred, *Prediction of Carotid Intraplaque Hemorrhage Using Adventitial Calcification and Plaque Thickness on CTA.* 2016.
68. McNamara, D.J., et al., *Heterogeneity of cholesterol homeostasis in man. Response to changes in dietary fat quality and cholesterol quantity.* J Clin Invest, 1987. **79**(6): p. 1729-39.
69. Carter, C.P., P.N. Howles, and D.Y. Hui, *Genetic variation in cholesterol absorption efficiency among inbred strains of mice.* J Nutr, 1997. **127**(7): p. 1344-8.
70. Zhang, S.H., et al., *Spontaneous hypercholesterolemia and arterial lesions in mice lacking apolipoprotein E.* Science, 1992. **258**(5081): p. 468-71.
71. Plump, A.S., et al., *Severe hypercholesterolemia and atherosclerosis in apolipoprotein E-deficient mice created by homologous recombination in ES cells.* Cell, 1992. **71**(2): p. 343-53.
72. Ishibashi, S., et al., *Hypercholesterolemia in low density lipoprotein receptor knockout mice and its reversal by adenovirus-mediated gene delivery.* J Clin Invest, 1993. **92**(2): p. 883-93.

73. Maeda, N., *History of Discovery: Development of Apolipoprotein E-Deficient Mice.* Arteriosclerosis, Thrombosis, and Vascular Biology, 2011. **31**(9): p. 1957-1962.
74. Chen, Y.C., et al., *A novel mouse model of atherosclerotic plaque instability for drug testing and mechanistic/therapeutic discoveries using gene and microRNA expression profiling.* Circ Res, 2013. **113**(3): p. 252-65.
75. von der Thusen, J.H., et al., *Induction of atherosclerotic plaque rupture in apolipoprotein E-/- mice after adenovirus-mediated transfer of p53.* Circulation, 2002. **105**(17): p. 2064-70.
76. Rosenfeld, M.E., et al., *Advanced atherosclerotic lesions in the innominate artery of the ApoE knockout mouse.* Arterioscler Thromb Vasc Biol, 2000. **20**(12): p. 2587-92.
77. Whitman, S.C., *A Practical Approach to Using Mice in Atherosclerosis Research.* Clin Biochem Rev, 2004. **25**(1): p. 81-93.
78. Raslan, Z., et al., *Targeting of type I protein kinase A to lipid rafts is required for platelet inhibition by the 3',5'-cyclic adenosine monophosphate-signaling pathway.* J Thromb Haemost, 2015. **13**(9): p. 1721-34.
79. Chan, M.V., et al., *P2Y12 receptor blockade synergizes strongly with nitric oxide and prostacyclin to inhibit platelet activation.* Br J Clin Pharmacol, 2016. **81**(4): p. 621-33.
80. Macdonald, P.S., M.A. Read, and G.J. Dusting, *Synergistic inhibition of platelet aggregation by endothelium-derived relaxing factor and prostacyclin.* Thromb Res, 1988. **49**(5): p. 437-49.
81. Moncada, S., R.M. Palmer, and E.A. Higgs, *The discovery of nitric oxide as the endogenous nitrovasodilator.* Hypertension, 1988. **12**(4): p. 365-72.
82. Vanhoutte, P.M., et al., *Endothelial Dysfunction and Vascular Disease - A Thirthieth Anniversary Update.* Acta Physiol (Oxf), 2015.
83. Wu, C., et al., *Mechanosensitive PPAP2B Regulates Endothelial Responses to Atherorelevant Hemodynamic Forces.* Circ Res, 2015. **117**(4): p. e41-53.
84. Yukiura, H., et al., *LPP3 localizes LPA6 signalling to non-contact sites in endothelial cells.* J Cell Sci, 2015. **128**(21): p. 3871-7.
85. Hahn, C. and M.A. Schwartz, *Mechanotransduction in vascular physiology and atherogenesis.* Nat Rev Mol Cell Biol, 2009. **10**(1): p. 53-62.
86. Orr, A.W., et al., *p21-activated kinase signaling regulates oxidant-dependent NF-kappa B activation by flow.* Circ Res, 2008. **103**(6): p. 671-9.
87. Rampersad, S.N., et al., *EPAC1 promotes adaptive responses in human arterial endothelial cells subjected to low levels of laminar fluid shear stress: Implications in flow-related endothelial dysfunction.* Cell Signal, 2016. **28**(6): p. 606-19.
88. Tzima, E., et al., *Localized cdc42 activation, detected using a novel assay, mediates microtubule organizing center positioning in endothelial cells in response to fluid shear stress.* J Biol Chem, 2003. **278**(33): p. 31020-3.
89. Tzima, E., et al., *Activation of Rac1 by shear stress in endothelial cells mediates both cytoskeletal reorganization and effects on gene expression.* Embo j, 2002. **21**(24): p. 6791-800.
90. Tzima, E., et al., *Activation of integrins in endothelial cells by fluid shear stress mediates Rho-dependent cytoskeletal alignment.* Embo j, 2001. **20**(17): p. 4639-47.
91. Syvaranta, S., et al., *Potential pathological roles for oxidized low-density lipoprotein and scavenger receptors SR-AI, CD36, and LOX-1 in aortic valve stenosis.* Atherosclerosis, 2014. **235**(2): p. 398-407.
92. Stewart, B.W. and S. Nagarajan, *Recombinant CD36 inhibits oxLDL-induced ICAM-1-dependent monocyte adhesion.* Mol Immunol, 2006. **43**(3): p. 255-67.

93. Bourdillon, M.C., et al., *ICAM-1 deficiency reduces atherosclerotic lesions in double-knockout mice (ApoE(-/-)/ICAM-1(-/-)) fed a fat or a chow diet.* Arterioscler Thromb Vasc Biol, 2000. **20**(12): p. 2630-5.
94. Zernecke, A., E. Shagdarsuren, and C. Weber, *Chemokines in atherosclerosis: an update.* Arterioscler Thromb Vasc Biol, 2008. **28**(11): p. 1897-908.
95. Murray, P.J. and T.A. Wynn, *Protective and pathogenic functions of macrophage subsets.* Nat Rev Immunol, 2011. **11**(11): p. 723-37.
96. Dunay, I.R., et al., *Gr1(+) inflammatory monocytes are required for mucosal resistance to the pathogen Toxoplasma gondii.* Immunity, 2008. **29**(2): p. 306-17.
97. Orihuela, R., C.A. McPherson, and G.J. Harry, *Microglial M1/M2 polarization and metabolic states.* Br J Pharmacol, 2016. **173**(4): p. 649-65.
98. Zhu, L., et al., *Cellular metabolism and macrophage functional polarization.* Int Rev Immunol, 2015. **34**(1): p. 82-100.
99. Colin, S., G. Chinetti-Gbaguidi, and B. Staels, *Macrophage phenotypes in atherosclerosis.* Immunol Rev, 2014. **262**(1): p. 153-66.
100. Chen, F.Y., et al., *Curcumin retunes cholesterol transport homeostasis and inflammation response in M1 macrophage to prevent atherosclerosis.* Biochem Biophys Res Commun, 2015. **467**(4): p. 872-8.
101. Oberoi, R., et al., *Lipocalin (LCN) 2 Mediates Pro-Atherosclerotic Processes and Is Elevated in Patients with Coronary Artery Disease.* PLoS One, 2015. **10**(9): p. e0137924.
102. Chistiakov, D.A., Y.V. Bobryshev, and A.N. Orekhov, *Macrophage-mediated cholesterol handling in atherosclerosis.* J Cell Mol Med, 2016. **20**(1): p. 17-28.
103. Horiuchi, S., Y. Sakamoto, and M. Sakai, *Scavenger receptors for oxidized and glycated proteins.* Amino Acids, 2003. **25**(3-4): p. 283-92.
104. Bishop-Bailey, D., *Peroxisome proliferator-activated receptors in the cardiovascular system.* Br J Pharmacol, 2000. **129**(5): p. 823-34.
105. Nicholson, A.C., et al., *CD36 in atherosclerosis. The role of a class B macrophage scavenger receptor.* Ann N Y Acad Sci, 2000. **902**: p. 128-31; discussion 131-3.
106. Wang, S., et al., *Wnt1 positively regulates CD36 expression via TCF4 and PPAR-gamma in macrophages.* Cell Physiol Biochem, 2015. **35**(4): p. 1289-302.
107. Kotla, S. and G.N. Rao, *Reactive Oxygen Species (ROS) Mediate p300-dependent STAT1 Protein Interaction with Peroxisome Proliferator-activated Receptor (PPAR)-gamma in CD36 Protein Expression and Foam Cell Formation.* J Biol Chem, 2015. **290**(51): p. 30306-20.
108. Kuchibhotla, S., et al., *Absence of CD36 protects against atherosclerosis in ApoE knock-out mice with no additional protection provided by absence of scavenger receptor A I/II.* Cardiovascular research, 2008. **78**(1): p. 185-196.
109. Qu, S.L., et al., *Mipu1 overexpression protects macrophages from oxLDL-induced foam cell formation and cell apoptosis.* DNA Cell Biol, 2014. **33**(12): p. 839-46.
110. Thomsen, J.H., et al., *The haptoglobin-CD163-heme oxygenase-1 pathway for hemoglobin scavenging.* Oxid Med Cell Longev, 2013. **2013**: p. 523652.
111. Boyle, J.J., *Heme and haemoglobin direct macrophage Mhem phenotype and counter foam cell formation in areas of intraplaque haemorrhage.* Curr Opin Lipidol, 2012. **23**(5): p. 453-61.
112. Gomez, D. and G.K. Owens, *Smooth muscle cell phenotypic switching in atherosclerosis.* Cardiovasc Res, 2012. **95**(2): p. 156-64.
113. Moncada, S., et al., *A lipid peroxide inhibits the enzyme in blood vessel microsomes that generates from prostaglandin endoperoxides the substance (prostaglandin X) which prevents platelet aggregation.* Prostaglandins, 1976. **12**(5): p. 715-37.

114. Palmer, R.M., A.G. Ferrige, and S. Moncada, *Nitric oxide release accounts for the biological activity of endothelium-derived relaxing factor.* Nature, 1987. **327**(6122): p. 524-6.
115. Schror, K., et al., *Thrombin receptors in vascular smooth muscle cells - function and regulation by vasodilatory prostaglandins.* Thromb Haemost, 2010. **103**(5): p. 884-90.
116. Schror, K. and A.A. Weber, *Roles of vasodilatory prostaglandins in mitogenesis of vascular smooth muscle cells.* Agents Actions Suppl, 1997. **48**: p. 63-91.
117. Tousoulis, D., et al., *The role of nitric oxide on endothelial function.* Curr Vasc Pharmacol, 2012. **10**(1): p. 4-18.
118. Qiu, J., et al., *Biomechanical regulation of vascular smooth muscle cell functions: from in vitro to in vivo understanding.* J R Soc Interface, 2014. **11**(90): p. 20130852.
119. Owens, G.K., *Regulation of differentiation of vascular smooth muscle cells.* Physiol Rev, 1995. **75**(3): p. 487-517.
120. Allahverdian, S., et al., *Contribution of intimal smooth muscle cells to cholesterol accumulation and macrophage-like cells in human atherosclerosis.* Circulation, 2014. **129**(15): p. 1551-9.
121. Cherepanova, O.A., et al., *Oxidized phospholipids induce type VIII collagen expression and vascular smooth muscle cell migration.* Circ Res, 2009. **104**(5): p. 609-18.
122. Pidkovka, N.A., et al., *Oxidized phospholipids induce phenotypic switching of vascular smooth muscle cells in vivo and in vitro.* Circ Res, 2007. **101**(8): p. 792-801.
123. Navab, M., et al., *Source and role of intestinally derived lysophosphatidic acid in dyslipidemia and atherosclerosis.* J Lipid Res, 2015. **56**(4): p. 871-87.
124. McIntyre, T.M., et al., *Identification of an intracellular receptor for lysophosphatidic acid (LPA): LPA is a transcellular PPARγ agonist.* Proceedings of the National Academy of Sciences, 2003. **100**(1): p. 131-136.
125. *What are single nucleotide polymorphisms (SNPs)?* 2016 March 15, 2016]; Available from: https://ghr.nlm.nih.gov/primer/genomicresearch/snp.
126. Erbilgin, A., et al., *Identification of CAD candidate genes in GWAS loci and their expression in vascular cells.* Journal of Lipid Research, 2013. **54**(7): p. 1894-1905.
127. Sigal, Y.J., M.I. McDermott, and A.J. Morris, *Integral membrane lipid phosphatases/phosphotransferases: common structure and diverse functions.* Biochem J, 2005. **387**(Pt 2): p. 281-93.
128. Long, J.S., N.J. Pyne, and S. Pyne, *Lipid phosphate phosphatases form homo- and hetero-oligomers: catalytic competency, subcellular distribution and function.* Biochem J, 2008. **411**(2): p. 371-7.
129. Tomsig, J.L., et al., *Lipid phosphate phosphohydrolase type 1 (LPP1) degrades extracellular lysophosphatidic acid in vivo.* Biochem J, 2009. **419**(3): p. 611-8.
130. Morris, A.J., et al., *Lipid phosphate phosphatases: Recent progress and assay methods*, in *Lysophospholipid Receptors: Signaling and Biochemistry*. 2012, John Wiley.
131. Escalante-Alcalde, D., et al., *The lipid phosphatase LPP3 regulates extra-embryonic vasculogenesis and axis patterning.* Development, 2003. **130**(19): p. 4623-37.
132. Mukherjee, A., R.A. Neher, and A.D. Renault, *Quantifying the range of a lipid phosphate signal in vivo.* J Cell Sci, 2013. **126**(Pt 23): p. 5453-64.
133. Panchatcharam, M., et al., *Lipid phosphate phosphatase 3 negatively regulates smooth muscle cell phenotypic modulation to limit intimal hyperplasia.* Arterioscler Thromb Vasc Biol, 2013. **33**(1): p. 52-9.

134. The, C.D.C., *Large-scale association analysis identifies new risk loci for coronary artery disease.* Nature genetics, 2013. **45**(1): p. 25-33.
135. Reschen, M.E., et al., *Lipid-induced epigenomic changes in human macrophages identify a coronary artery disease-associated variant that regulates PPAP2B Expression through Altered C/EBP-beta binding.* PLoS Genet, 2015. **11**(4): p. e1005061.
136. Tang, X., M.G. Benesch, and D.N. Brindley, *Lipid phosphate phosphatases and their roles in mammalian physiology and pathology.* J Lipid Res, 2015. **56**(11): p. 2048-60.
137. Escalante-Alcalde, D., R. Sanchez-Sanchez, and C.L. Stewart, *Generation of a conditional Ppap2b/Lpp3 null allele.* Genesis, 2007. **45**(7): p. 465-9.
138. Tomsig, J.L., et al., *LIPID PHOSPHATE PHOSPHOHYDROLASE TYPE 1 (LPP1) DEGRADES EXTRACELLULAR LYSOPHOSPHATIDIC ACID IN VIVO.* The Biochemical journal, 2009. **419**(3): p. 611-618.
139. Escalante-Alcalde, D., S.L. Morales, and C.L. Stewart, *Generation of a reporter-null allele of Ppap2b/Lpp3and its expression during embryogenesis.* Int J Dev Biol, 2009. **53**(1): p. 139-47.
140. Daugherty, A. and D.L. Rateri, *Development of experimental designs for atherosclerosis studies in mice.* Methods, 2005. **36**(2): p. 129-38.
141. Paigen, B., et al., *Quantitative assessment of atherosclerotic lesions in mice.* Atherosclerosis, 1987. **68**(3): p. 231-40.
142. Goldstein, D.G.D.B., *SNPExpress*.
143. Albert, F.W. and L. Kruglyak, *The role of regulatory variation in complex traits and disease.* Nat Rev Genet, 2015. **16**(4): p. 197-212.
144. Lagace, T.A., *PCSK9 and LDLR degradation: regulatory mechanisms in circulation and in cells.* Curr Opin Lipidol, 2014. **25**(5): p. 387-93.
145. Mabuchi, H., et al., *Genotypic and phenotypic features in homozygous familial hypercholesterolemia caused by proprotein convertase subtilisin/kexin type 9 (PCSK9) gain-of-function mutation.* Atherosclerosis, 2014. **236**(1): p. 54-61.
146. Schneider, A., et al., *Differential, inducible gene targeting in renal epithelia, vascular endothelium, and viscera of Mx1Cre mice.* Am J Physiol Renal Physiol, 2003. **284**(2): p. F411-7.
147. Alpert, J.S., *The pathophysiology of acute myocardial infarction.* Cardiology, 1989. **76**(2): p. 85-95.
148. Heinzen, E.L., et al., *Tissue-specific genetic control of splicing: implications for the study of complex traits.* PLoS Biol, 2008. **6**(12): p. e1.
149. Bentzon, J.F., et al., *Mechanisms of Plaque Formation and Rupture.* Circulation Research, 2014. **114**(12): p. 1852-1866.
150. Mozaffarian, D., et al., *Heart Disease and Stroke Statistics—2016 Update: A Report From the American Heart Association.* Circulation, 2015.
151. Hata, E., et al., *Lysophosphatidic acid receptors LPA4 and LPA6 differentially promote lymphocyte transmigration across high endothelial venules in lymph nodes.* Int Immunol, 2015.
152. Igarashi, H., et al., *The lysophosphatidic acid receptor LPA4 regulates hematopoiesis-supporting activity of bone marrow stromal cells.* Sci Rep, 2015. **5**: p. 11410.
153. Knowlden, S.A., et al., *Regulation of T cell motility in vitro and in vivo by LPA and LPA2.* PLoS One, 2014. **9**(7): p. e101655.
154. Ponnuchamy, B. and R.A. Khalil, *Role of ADAMs in Endothelial Cell Permeability. Cadherin Shedding and Leukocyte Rolling.* Circulation research, 2008. **102**(10): p. 1139-1142.

155. Nilsson, J., et al., *Lipoprotein-like phospholipid particles inhibit the smooth muscle cell cytotoxicity of lysophosphatidylcholine and platelet-activating factor.* Arterioscler Thromb Vasc Biol, 1998. **18**(1): p. 13-9.
156. Smyth, S.S., et al., *Arguing the case for the autotaxin-lysophosphatidic acid-lipid phosphate phosphatase 3-signaling nexus in the development and complications of atherosclerosis.* Arterioscler Thromb Vasc Biol, 2014. **34**(3): p. 479-86.

Vita

PERSONAL

Place of Birth: Lexington, KY
Nationality: United States

EDUCATION

Institution	Dates	Degree	Subject
University of Kentucky	2005 – 2009	B. Sc.	Biology

ACADEMIC AND PROFESSIONAL HONORS

Certificates:
Graduate Certificate in Clinical and Translational Science 2015

Research Support:
2009 – 2010 ARRA Award: Integrin Signaling in Vascular Cells (3048105950).

2011 – 2013 NIH "Interdisciplinary Cardiovascular Training Grant" (T32 HL072743).

2013 – 2015 NIH "Clinical and Translational Science Training Grant" (TL1RR033172).

Invited Speaker Engagements:

Mueller, P., Smyth, S. Functional Validation of Polymorphisms in *PPAP2B* that Associates with Coronary Artery Disease. T32 Scholar Presentation Gill Heart Institute Cardiovascular Research Day, Lexington KY – 2011

Mueller, P., Smyth, S. Functional Validation of Polymorphisms in *PPAP2B* that Associates with Coronary Artery Disease T32 Scholar Presentation Gill Heart Institute Cardiovascular Research Day, Lexington KY – 2012

Mueller, P., Smyth S. Functional Validation of Polymorphisms in *PPAP2B* that Associates with Coronary Artery Disease 48th Southeastern Regional Lipid Conference, Cashiers NC – 2013

Mueller, P., Smyth S. Functional Validation of Polymorphisms in *PPAP2B* that Associates with Coronary Artery Disease. CCTS Spring Conference, Lexington KY – March 2014

Mueller, P., Smyth S. *PPAP2B* Expression Regulates the Development of Atherosclerosis" Translational Science Conference 2015, Washington DC – April 2015

Poster Presentations:

Mueller, P., Smyth S. **"**Functional Validation of Polymorphisms in *PPAP2B* that Associates with Coronary Artery Disease". Translational Science Conference, Washington DC – 2014

Mueller, P., Smyth S. "*PPAP2B* Expression Regulates the Development of Atherosclerosis". Scientific Sessions, Chicago IL – 2014

Mueller, P., Smyth S. "*PPAP2B* Expression Regulates the Development of Atherosclerosis". 9th Platelet Colloquium, Lexington KY – 2015

Mueller, P., Smyth S. "*PPAP2B* Expression Regulates the Development of Atherosclerosis". CCTS Spring Conference, Lexington KY – 2015

Mueller, P., Smyth S. "*PPAP2B* Expression Regulates the Development of Atherosclerosis" Translational Science Conference, Washington DC – 2015

Mueller, P., Smyth S. "*PPAP2B* Expression Regulates the Development of Atherosclerosis" ATVB|PVD 2015 Scientific Sessions, San Francisco CA -- 2015

Mueller, P., Smyth S. "*PPAP2B* Expression Regulates the Development of Atherosclerosis" AHA 2015 Scientific Sessions, Orlando FL – 2015
*Invited to re-present the in the **Best of AHA Specialty Conferences: ATVB 2015**

AWARDS

2014 – Travel Support, University of Kentucky Graduate School. Abstract: "Functional Validation of Polymorphisms in *PPAP2B* that Associates with Coronary Artery Disease". Translational Science Conference 2014, Washington DC – April 2014

2014 – ATVB Travel Award for Young Investigators. Abstract: "*PPAP2B* Expression Regulates the Development of Atherosclerosis" Scientific Sessions 2014

2015 – ATVB Travel Award for Young Investigators. Abstract: "*PPAP2B* Expression Regulates the Development of Atherosclerosis" ATVB|PVD 2015 Scientific Sessions

2015 – Invitation to re-present abstract: "*PPAP2B* Expression Regulates the Development of Atherosclerosis" in the **Best of AHA Specialty Conferences: ATVB 2015** at AHA Scientific Sessions, Orlando FL.

PUBLICATIONS

Manuscripts:

1. Dong A, Caicedo J, Han SG, **Mueller P**, Saha S, Smyth SS, Gairola CG. Enhanced platelet reactivity and thrombosis in Apoe-/- mice exposed to cigarette smoke is attenuated by P2Y12 antagonism. *Thromb Res*. 2010 Oct;126(4): e312-7. (PMID 2921009)

2. Cheng HY, Dong A, Panchatcharam M, **Mueller P**, Yang F, Li Z, Mills G, Chun J, Morris AJ, Smyth SS. Lysophosphatidic acid signaling protects pulmonary vasculature from hypoxia-induced remodeling. *Arterioscler Thromb Vasc Biol.* 2012 Jan;32(1):24-32. (PMID 3241874)

3. Federico L, Ren H, **Mueller PA**, Wu T, Liu S, Popovic J, Blalock EM, Sunkara M, Ovaa H, Albers HM, Mills GB, Morris AJ, Smyth SS. Autotaxin and its product lysophosphatidic acid suppress brown adipose differentiation and promote diet-induced obesity in mice. *Mol Endocrinol.* 2012 May;26(5):786-97. (PMID 3355557)

4. Yang F, Dong A, **Mueller P**, Caicedo J, Sutton AM, Odetunde J, Barrick CJ, Klyachkin YM, Abdel-Latif A, Smyth SS. Coronary artery remodeling in a model of left ventricular pressure overload is influenced by platelets and inflammatory cells. *PLoS One*. 2012 August;7(8):e40196. (PMID 3423413)

5. Panchatcharam M, Miriyala S, Salous A, Wheeler J, Dong A, **Mueller P**, Sunkara M, Escalante-Alcalde D, Morris AJ, Smyth SS. Lipid phosphate phosphatase 3 negatively regulates smooth muscle cell phenotypic modulation to limit intimal hyperplasia. *Arterioscler Thromb Vasc Biol***.** 2013 Jan;33(1):52-9. (PMID 3524385)

6. Salous AK, Panchatcharam M, Sunkara M, **Mueller P**, Dong A, Wang Y, Graf G, Smyth S, Morris A. Mechanism of rapid elimination of lysophosphatidic acid and related lipids from the circulation of mice. *J Lipid Res.* 2013 Oct; 54(10): 2775 – 2784. PMC3770090.

Reviews:

1. Ren H, Panchatcharam M, **Mueller P**, Escalante-Alcalde D, Morris AJ, Smyth SS. Lipid phosphate phosphatase (LPP3) and vascular development. *Biochim Biophys Acta*. 2013 Jan;1831(1):126-32. (PMID 3683602)

2. Smyth S, **Mueller P**, Yang F, Brandon JA, Morris A. The case for autotaxin – lysophosphatidic acid – lipid phosphate phosphatase 3 (ATX/LPA/LPP3) signaling nexus in the development and complications of atherosclerosis. *Arterioscler Thromb Vasc Bio.* 2014 Mar;34(3): 479-486. PMC3944085.

3. **Mueller P**, Ye S, Morris A, Smyth S. Lysophospholipid mediators in the vasculature. *Experimental Cell Research*. (Accepted March 2015 – PMC In Process).

TEACHING EXPERIENCE

Center for Academic Resources and Enrichment Services (CARES). University of Kentucky. Tutor in General Chemistry (CHE 105). Fall 2006.

Case Studies in Physiology (PGY 207). Department of Physiology, University of Kentucky. Teaching Assistant. Spring 2012, Fall 2012, Spring 2014.

Human Anatomy and Physiology II (Bio 139). Department of Biological Sciences, Bluegrass Community and Technical College. Adjunct Faculty/Lecturer. Spring 2015.